University of Nevada, Reno

Studies of the Cardiolipin Interactome

A dissertation submitted in partial fulfillment of the requirements for the degree of Doctor of Philosophy in Biochemistry

by

Colin A. Fox

Robert O. Ryan / Dissertation Advisor

December, 2021

THE GRADUATE SCHOOL

We recommend that the dissertation
prepared under our supervision by

COLIN A. FOX

entitled

Studies of the Cardiolipin Interactome

be accepted in partial fulfillment of the
requirements for the degree of

Doctor of Philosophy

Robert O. Ryan, Ph.D.
Advisor

Claus Tittiger, Ph.D.
Committee Member

Patricia Ellison, Ph.D.
Committee Member

Dylan Kosma, Ph.D.
Committee Member

Ruben K. Dagda, Ph.D.
Committee Member

Bradley Ferguson, Ph.D.
Graduate School Representative

David W. Zeh, Ph.D., Dean
Graduate School

December, 2021

Abstract

Nanodisks comprised solely of the anionic glyerophospholipid cardiolipin and an apolipoprotein have been formulated and characterized. Cardiolipin nanodisks (CL ND) are composed of a planar lipid bilayer comprised solely of cardiolipin and an apolipoprotein scaffold, which circumscribes the unstable edge of the bilayer, conferring stability and complete aqueous solubility. These nanoparticles were used in a variety of experiments to better understand the interactions between cardiolipin and several members of its interactome.

Calcium has previously been shown to induce a bilayer to non-bilayer transition when added to liposomes containing cardiolipin, but not in liposomes with a similar lipid composition in the absence of cardiolipin. This phenomenon was evaluated using ND technology. CL ND were found to be a homogenous population of completely aqueous soluble nanoparticles of approximately 200-300 kDa in size. CL ND undergo a bilayer to non-bilayer transformation following addition of sufficient $CaCl_2$, similarly to liposomes and vesicles. This phenomenon is specific to divalent cations, as tested by addition of $CaCl_2$, $MgCl_2$, $SrCl_2$. Addition of NaCl and KCl did not elicit a similar response. This phenomenon is also related to cardiolipin concentration as a component of the lipid bilayer, and decreasing the cardiolipin content results in increased resistance to calcium induced transformation. Ultimately, a novel molecular mechanism was put forth wherein cardiolipin molecules, upon addition of a divalent cation, reposition to allow the phosphate moieties to better bind. This

repositioning increases the strain on the fatty acyl chains, forcing them to reposition and further increase the “cone” shape of the cardiolipin molecule. This interaction reduces the ability of the cardiolipin to reside stably in a planar bilayer. Once a sufficient number of molecules undergo this change, the constraining force on the nanodisk imposed by the apolipoprotein scaffold is exceeded, resulting in a transition to a non-bilayer state.

CL ND were then used to investigate the interactions between cardiolipin, calcium and cytochrome c. Cytochrome c was found to stably bind to CL ND, resulting in co-elution following size exclusion chromatography. Pre-incubation of cytochrome c with CL ND increased susceptibility of CL ND to calcium induced bilayer to non-bilayer transformation, as compared to empty cardiolipin nanodisks. However, following this transformation, ~ 30% of the cytochrome c remained bound to the insoluble lipid-containing pellet. Addition of calcium insufficient to induce this transformation was found to lead to complete dissociation of cytochrome c. CL ND pre-incubated with a similar concentration of calcium no longer bind cytochrome c, suggesting competition for a specific binding site. This revelation may play an important role in furthering our understanding of cytochrome c’s release from the mitochondria during cell mediated apoptosis.

Doxorubicin (DOX) is a clinically important anti-cancer drug. However, usage is restricted due to symptoms that have been termed “DOX induced cardiotoxicity”. This condition causes symptoms reminiscent, but distinct from,

cardiomyopathy and often lead to heart failure. CL ND were investigated as a delivery vehicle to potentially reduce DOX induced cardiotoxicity. DOX CL ND were formulated and found to remain bound following dialysis. A novel assay was designed and tested to show that DOX, when given a choice between DNA or cardiolipin, will preferentially bind to DNA.

Further studies showed that DOX CL ND retain a similar anti-cancer effect as free DOX in two different cancer cell lines while being more effective than liposomal DOX. Furthermore, it was found that DOX binding to CL ND increases cell viability as compared to free DOX in a rat cardiomyocyte cell line. Analysis of mitochondrial respiration of treated cells via XF24 Seahorse analysis suggests that binding of DOX to CL ND reduces mitochondrial dysfunction, as is evidenced by an increase in maximal respiration as compared to DOX treated samples.

These data presented in this dissertation illustrates that CL ND are a useful tool to better understand mitochondrial interactions, an area that has proven difficult to study.

Dedication

To my darling wife Sarah and best friend Mike. Without your unflagging support I may never have started on this journey.

Acknowledgements

I would like to thank my advisor, Dr. Robert Ryan, for not only allowing me to work in his laboratory but for treating me as a friend. Your enthusiasm for science is infectious, your knowledge is deep and your willingness to think outside the norm is an inspiration.

I would like to thank the members of the Ryan Lab, notably Dr. Irina Romenskaia and Sharon Young. Your willingness to teach me the basics laid a great foundation that I will continue to draw upon in the future.

I would also like to thank the members of my committee, who never hesitated to help me in learning how to use a new instrument or would take a few moments to discuss my projects, helping me to think as a scientist and help my projects succeed.

I would also like to thank my friends in the BCH program. Knowing others were going through the same as I helped in even the darkest of times.

Table of Contents

List of Figures

Chapter 1: Introduction

Chapter 2: Calcium-Induced Transformation of Cardiolipin Nanodisks

Chapter 3: Calcium-induced release of cytochrome c from cardiolipin nanodisks: implications for apoptosis

Chapter 4: Dye binding assay reveals doxorubicin preference for DNA versus cardiolipin

Chapter 5: Mitigation of doxorubicin-induced mitochondrial dysfunction by cardiolipin nanodisks

List of Abbreviations

Apo = apolipoprotein
apoLp-III = apolipophorin III
BAK = BCL-2 homologous antagonist killer
BAX = BCL-2-associated X protein
CL = cardiolipin
DAPI = 4′,6-diamidino-2-phenylindole
DMEM = Dulbecco’s Modified Eagle Medium
DOX = doxorubicin
ETC = electron transport chain
FPLC = fast phase liquid chromatography
HDL = high density lipoprotein
MEM = Eagle’s Minimal Essential Medium
MICOS = mitochondrial contact site and cristae organizing system
ND = nanodisks
OCR = oxygen consumption rate
PC = phosphatidylcholine
PHB = prohibitin
PC = Dimyristoylphosphatidylcholine
RCT = reverse cholesterol transport
rHDL = reconstituted high density lipoprotein
TL = tetralinoleoyl
TM = tetramyristoyl

Chapter 1

Introduction

Portions of this chapter are based on work published in:

Fox CA, Moschetti A, Ryan RO (2021), Reconstituted HDL as a therapeutic delivery device. Biochim. Biophys. Acta Mol. Cell Biol. Lipids.

1.1 Reconstituted high density lipoprotein

As our understanding of nascent pre-β HDL biogenesis *in vivo* evolved, it was discovered that isolated apolipoprotein A-I (apoA-I) possesses an intrinsic ability to transform aqueous phospholipid dispersions (*e.g.* vesicles) into reconstituted high density lipoprotein (rHDL) *in vitro*. The product particles possess a structural organization reminiscent of pre-β HDL generated *in vivo* and display stability, particle size homogeneity and aqueous solubility. Under appropriate incubation conditions, aqueous mixtures of apoA-I and dimyristoylphosphatidylcholine (DMPC) interact spontaneously to form rHDL [1]. Methods have been developed wherein DMPC is dried onto the walls of a reaction vessel, hydrated by the addition of buffer and dispersed by vortexing. Upon addition of apoA-I to such phospholipid dispersions (lipid:protein ~5:2 *w*/w) and incubation at 23.9 ◦C (the gel–liquid crystalline phase transition temperature of DMPC), the sample transitions from an opaque lipid suspension to a clear solution as a function of time. The rate of reaction is dramatically increased by bath sonication, yielding a solution from which no material pellets upon centrifugation. Characterization of the product particles by electron microscopy revealed disk-shaped complexes ranging from 9 to 20 nm in diameter, depending on the starting phospholipid/apoA-I ratio [2]. Extensive studies have been performed to characterize the organizational state of apoA-I in these particles. Whereas there was some early controversy regarding the manner in which α-helical segments of apoA-I align with respect to the plane of the discoidal bilayer, the preponderance of accumulated evidence has led to the consensus view [3]

that apoA-I aligns in a belt-like manner around the perimeter of these rHDL (**Figure 1.1**). Moreover, it is considered that, in 10 nm particles, two apoA-I molecules align antiparallel to each other in an extended open conformation. Although DMPC containing rHDL have proven very useful for characterization studies, many experimental strategies benefit from using rHDL that possess naturally occurring phospholipids. Such particles are preferred for cell culture experiments as well as *in vivo* investigations. Methods to generate rHDL with phospholipids such as palmitoyloleoylphosphatidylcholine (POPC), for example, have been developed that rely on the use of a detergent [4]. Known as the "cholate dialysis" method, well defined rHDL are produced by recombining POPC, cholic acid (or deoxycholic acid) and apoA-I. Subsequent exhaustive dialysis of the sample leads to removal of the detergent, while POPC and apoA-I organize into discoidal rHDL. This facile method to generate POPC rHDL has led to myriad cell culture-based studies that validate many aspects of the reverse cholesterol transport (RCT) pathway. Indeed, the realization that POPC rHDL are highly effective acceptors of cell-associated cholesterol has led to a novel therapeutic intervention strategy to treat atherosclerotic heart disease. In this approach discoidal rHDL is administered to human subjects as a means to enhance RCT capacity [5]. Studies have shown that infusion of apoA-I rHDL promotes cholesterol efflux *in vivo* [6]. Several pharmaceutical/biotechnology companies are currently exploiting this technology to develop rHDL-based therapeutics, although clinical trials conducted to date have shown mixed results [7,8].

1.2 Nanodisks

As the effort to harness rHDL to promote RCT and regression of atherosclerotic lesions continues, a parallel application of rHDL technology has also undergone considerable growth in recent years. Rather than serving as an acceptor of cellular cholesterol, a major thrust of “nanodisk” (ND) technology involves formulation of discoidal rHDL that harbor hydrophobic bioactive compounds for purposes of delivery. The term ND refers to a subset of discoidal rHDL that contain extraneous hydrophobic bioactive molecules (*i.e.*, drugs, pesticides, hormones, *etc.*) that are not a natural component of HDL. Whereas discoidal particles prepared *in vitro* containing phospholipid and apoA-I only are referred to as rHDL, particles formulated to possess an additional distinct hydrophobic bioactive molecule (*e.g.* the polyphenolic phytochemical, curcumin) are referred to as ND. Thus, ND are *rHDL formulated to possess a hydrophobic compound(s) that integrates into the lipid milieu of the disk-shaped bilayer, thereby conferring unique biological properties*. When correctly formulated, ND display the same aqueous solubility, structural organization and stability as classical rHDL. At the same time, ND possess unique properties owing to the presence of one or more components that are unrelated to the normal function of HDL. Given the broad range of materials used in ND formulation and characterization studies, some latitude with regard to this definition is appropriate. For example, ND have been formulated with apoA-I and the unique

anionic diphosphoglycerolipid, CL, as the sole bilayer forming phospholipid. Because these particles are conferred with unique and distinctive properties, they have been referred to as CL ND [9]. When the hydrophobic polyene antibiotic, amphotericin B (ampB), is formulated with apoA-I and a 7:3 (*w*/w) mixture of DMPC and dimyristoylphosphatidylglycerol (DMPG), the product particles are referred to as ampB ND [10]. Although apoA-I is the prototypical apolipoprotein employed in ND formulation studies, other apolipoproteins, including apoE [11], apolipophorin III [12,13], apolipoprotein chimeras [14] and synthetic amphipathic peptides [15] have been successfully used to formulate ND. Just as a variety of unique scaffold components have been employed, several different phospholipids have been used to formulate ND, including DMPC, DMPG, CL and egg PC. Thus, ND can be created using an interchangeable collection of protein/peptide scaffolds, bilayer forming lipids and hydrophobic bioactive molecules (**Figure 1.2**), with each of these component parts capable of conferring distinctive properties to the product particle.

1.3 Cardiolipin

CL is an anionic phospholipid localized exclusively to the inner mitochondrial membrane. A CL molecule, unlike other phospholipids, is comprised of two phosphate moieties, three glycerols and four fatty acyl chains. This atypical structure of a small polar head and bulky fatty acid tails results in CL forming a “cone shape”, as opposed to the “rod shape” of other phospholipids. As a result, CL exerts negative curvature pressure when present

in a bilayer [16]. This unusual characteristic is likely why CL has been shown to be integral to the maintenance of mitochondrial structure, notably the highly curved inner mitochondrial membrane and cristae junctions. In addition to its structural role, CL is required for the proper function of Complexes I, III, IV and V of the electron transport chain [17]. CL is also reported to have an important role in the binding and stabilization of cytochrome c, an important component in the electron transport chain (ETC) that is responsible for ferrying electrons between Complexes III and IV of the ETC. Release of cytochrome c from CL and its subsequent escape from the mitochondria is a key step in cell mediated apoptosis [18]. However, the molecular mechanism underlying cytochrome c release from CL remains enigmatic [19].

1.4 Cardiolipin and Calcium

The relatively small polar head group and bulky tails of CL result in the assumption of a cone-like shape in a 3D space. This characteristic shape, as previously mentioned, is what allows CL to play such an important role in maintenance of mitochondrial structure, as it exerts negative curvature pressure when present in a bilayer. This characteristic trait, however, negatively affects its ability to reside stably in a planar bilayer. As a result, liposomes containing CL are prone to light scattering, are not completely aqueous soluble, and CL content likely cluster towards the aqueous interior, potentially limiting their usefulness in certain applications [20,21].

An interesting phenomenon was observed wherein liposomes containing CL undergo a bilayer to non-bilayer transformation following addition of sufficient calcium [22, 23]. Liposomes with similar lipid composition that lack CL do not undergo this same transformation. The ability of calcium to induce this bilayer to non-bilayer transformation has been hypothesized to be related to cytochrome c escape from the mitochondria during cell mediated apoptosis, although direct experimental evidence remains difficult to acquire [24,25].

1.5 Cardiolipin, calcium and cytochrome c

Cytochrome c is a protein known for its role in ferrying electrons between Complexes III and IV of the electron transport chain. However, cytochrome c has another important role in cell mediated apoptosis. Under normal circumstances cytochrome c is kept within the mitochondrial cristae, where it is either tightly or loosely bound to endogenous CL molecules present in the inner leaflet [26,27]. Following induction of apoptosis, cytochrome c is released from both binding interactions. Cytochrome c then escapes the mitochondrial cristae and leaves the mitochondria through pores in the outer mitochondrial membrane. Following its escape to the cytosol, cytochrome c recruits caspases and facilitates formation of apoptosomes, a key, irreversible step in the cell mediated apoptosis pathway [28]. Apoptosome formation and recruitment of caspases is a highly studied area. In contrast, the mechanisms by which cytochrome c is released from CL, as well as its escape from the mitochondrial cristae, remains relatively unstudied [19].

1.6 Doxorubicin and DOX induced cardiotoxicity

Doxorubicin is an anthracycline anti-cancer drug that functions as an intercalation agent, binding to DNA and thereby reducing replication of rapidly dividing cells [29]. As a result of this non-specific but highly effective mechanism, DOX is used to treat a wide variety of cancer types. However, DOX treatment has been shown to result in a group of symptoms that have been termed “DOX induced cardiotoxicity”. These symptoms, which result in symptoms similar to cardiomyopathy and frequently lead to heart failure, can manifest within days of DOX administration, or even years later [30]. The underlying mechanism for DOX induced cardiotoxicity remains unknown despite decades of study [31].

As a result of DOX induced cardiotoxicity, DOX usage is tightly restricted both in terms of individual dosage as well as a hard limitation in lifetime use. These limitations still result in ~10% of patients who receive DOX suffering from DOX induced cardiotoxicity [30]. Liposomal formulations of DOX, wherein the DOX is encapsulated into the center of a liposome, have increased targeting of DOX to cancerous masses and thereby reduced off target effects. DOX liposomes have not, however, allowed for increased individual or lifetime dosages [32, 33]. As a result, there is a need for a better delivery vehicle for DOX as well as additional study into the underlying mechanism into how an intercalation based anti-cancer drug induces heart failure.

1.7 Summary of presented work

Nanodisks comprised of CL and members of the exchangeable apolipoprotein family have been formulated and characterized. The resultant

nanoparticles, termed CL ND, were used to conduct experiments detailed in the subsequent chapters presented in this dissertation. CL ND were used successfully as a model membrane for studies of the interaction between CL and calcium as well as interactions between cytochrome c, CL and calcium.

In addition to model membrane studies, these CL containing nanoparticles were studied as a potential delivery vehicle for DOX. Initially, a novel assay was formulated to investigate DOX preference for DNA versus CL. The results suggest that there is a clear preference for DNA as compared to CL.

Following development of this assay, the ability of DOX CL ND to function as an anti-cancer agent was evaluated and compared to free DOX and DOX liposomes. Lastly, experiments were conducted to determine whether DOX CL ND have a protective effect on cardiomyocyte cell viability and mitochondrial respiration.

In conclusion, ND present an opportunity to study CL and its interactome in a way not previously possible. The study of calcium, cytochrome c and DOX through the use of CL ND presents an opportunity to understand mitochondria in a new and exciting way. Meanwhile, CL ND present a novel means by which to both deliver and better understand the molecular mechanism underlying DOX induced cardiotoxicity.

1.8 References

[1] D. Atkinson, D.M. Small, Recombinant lipoproteins: implications for structure and assembly of native lipoproteins, Annu. Rev. Biophys. Biophys. Chem. 15 (1986) 403–456.

[2] C.G. Brouillette, J.L. Jones, T.C. Ng, H. Kercret, B.H. Chung, J.P. Segrest, Structural studies of apolipoprotein AI/phosphatidylcholine recombinants by high-field proton NMR, nondenaturing gradient gel electrophoresis, and electron microscopy, Biochemistry 23 (1984) 359–367.

[3] W.S. Davidson, T.B. Thompson, The structure of apolipoprotein A-I in high density lipoproteins, J. Biol. Chem. 282 (2007) 22249–22253.

[4] A. Jonas, Reconstitution of high-density lipoproteins, Methods Enzymol. 128 (1986) 553–582.

[5] B.A. Kingwell, M.J. Chapman, A. Kontush, N.E. Miller, HDL-targeted therapies: progress, failures and future, Nat. Rev. Drug Discov. 13 (2014) 445–464.

[6] P. Tricoci, D.M. D'Andrea, P.A. Gurbel, Z. Yao, M. Cuchel, B. Winston, R. Schott, R. Weiss, M.A. Blazing, L. Cannon, A. Bailey, D.J. Angiolillo, A. Gille, C.L. Shear, S. D. Wright, J.H. Alexander, Infusion of reconstituted high-density

lipoprotein, CSL112, in patients with atherosclerosis: safety and pharmacokinetic results from a phase 2a randomized clinical trial, J. Am. Heart Assoc. 4 (2015), e002171.

[7] Y. Kataoka, J. Andrews, M. Duong, T. Nguyen, N. Schwarz, J. Fendler, R. Puri, J. Butters, C. Keyserling, J.F. Paolini, J.L. Dasseux, S.J. Nicholls, Regression of coronary atherosclerosis with infusions of the high-density lipoprotein mimetic CER-001 in patients with more extensive plaque burden, Cardiovasc. Diagn. Ther. 7 (2017) 252–263.

[8] S.J. Nicholls, J. Andrews, J.J.P. Kastelein, B. Merkely, S.E. Nissen, K.K. Ray, G. G. Schwartz, S.G. Worthley, C. Keyserling, J.L. Dasseux, L. Griffith, S.W. Kim, A. Janssan, G. Di Giovanni, A.D. Pisaniello, D.J. Scherer, P.J. Psaltis, J. Butters, Effect of serial infusions of CER-001, a pre-β high-density lipoprotein mimetic, on coronary atherosclerosis in patients following acute coronary syndromes in the CER-001 Atherosclerosis Regression Acute Coronary Syndrome Trial: a randomized clinical trial, JAMA Cardiol. 3 (2018) 815–822.

[9] N. Ikon, B. Su, F.F. Hsu, T.M. Forte, R.O. Ryan, Exogenous cardiolipin localizes to mitochondria and prevents TAZ knockdown-induced apoptosis in myeloid progenitor cells, Biochem. Biophys. Res. Commun. 464 (2015) 580–585.

[10] M.N. Oda, P.L. Hargreaves, J.A. Beckstead, K.A. Redmond, R. van Antwerpen, R. O. Ryan, Reconstituted high density lipoprotein enriched with the polyene antibiotic amphotericin B, J. Lipid Res. 47 (2006) 260–267.

[11] M. Ghosh, A.T. Singh, W. Xu, T. Sulchek, L.I. Gordon, R.O. Ryan, Curcumin nanodisks: formulation and characterization, Nanomedicine 7 (2011) 162–167.

[12] N.O. Fischer, C.D. Blanchette, B.W. Segelke, M. Corzett, B.A. Chromy, E.A. Kuhn, G. Bench, P.D. Hoeprich, Isolation, characterization, and stability of discretelysized nanolipoprotein particles assembled with apolipophorin-III, PLoS One 5 (2010), e11643.

[13] C.P. Wan, M.H. Chiu, X. Wu, S.K. Lee, E.J. Prenner, P.M. Weers, Apolipoprotein induced conversion of phosphatidylcholine bilayer vesicles into nanodisks, Biochim. Biophys. Acta 1808 (2011) 606–613.

[14] D.M. Iovannisci, J.A. Beckstead, R.O. Ryan, Targeting nanodisks via a single chain variable antibody apolipoprotein chimera, Biochem. Biophys. Res. Commun. 379 (2009) 466–469.

[15] M. Tufteland, J.B. Pesavento, R.L. Bermingham, P.D. Hoeprich Jr., R.O. Ryan, Peptide stabilized amphotericin B nanodisks, Peptides 28 (2007) 741–746.

[16] Ikon N, Ryan RO, Cardiolipin and mitochondrial cristae organization. Biochim. Biophys. Acta Biomembr. 1859 (2017) 1156-1163.

[17] Paradies G, Paradies V, De Benedictis V, Ruggiero FM, Petrosillo G, Functional role of cardiolipin in mitochondrial bioenergetics. Biochim. Biophys. Acta Bioenerg. 1837 (2014) 408-417.

[18] Bock FJ, Tait SWG, Mitochondria as multifaceted regulators of cell death. Nat. Rev. Mol. Cell Biol. 21 (2020) 85-100.

[19] Kagan VE, Tyurin VA, Jiang J, Tyurina YY, Ritov VB, Amoscato AA, Osipov AN, Belikova NA, Kapralov AA, Kini V, Vlasova II, Zhao Q, Zou M, Di P, Svistunenko DA, Kurnikov IV, Borisenko GG, Cytochrome c acts as a cardiolipin oxygenase required for release of proapoptotic factors. Nat. Chem. Biol. 1 (2005) 223-232.

[20]. Sharma A, Sharma US (1997) Liposomes in drug delivery: progress and limitations. Int J Pharmaceut. 154, 123–140.

[21]. Bozzuto F, Molinari A (2015) Liposomes as nanomedical devices. Int J Nanomedicine. 10, 975–999. [PubMed: 25678787]

[22]. Rand RP, Sengupta S (1972) Cardiolipin forms hexagonal structures with divalent cations. Biochim Biophys Acta. 255, 484–492. [PubMed: 4333431]

[23]. De Kruijff B, Verkleij AJ, Leunissen-Bijvelt J, Van Echteld CJA, Hille J, Rijnbout H (1982) Further aspects of the calcium dependent polymorphism of bovine heart cardiolipin. Biochim Biophys Acta 693, 1–12. [PubMed: 7150583]

[24] Huang Y, Liu L, Shi C, Huang J, Li G, Electrochemical analysis of the effect of Ca^{2+} on cardiolipin-cytochrome c interaction. Biochim. Biophys. Acta. 1760 (2006) 1827-1830.

[25] Hwang MS, Schwall CT, Pazarentzos E, Datler E, Alder NN, Grimm S, Mitochondrial Ca($^{2+}$) influx targets cardiolipin to disintegrate respiratory chain complex II for cell death induction. Cell Death Differ. 21 (2014) 1733-1745.

[26] Gogvadze V, Orrenius S, Zhivotovsky B, Multiple pathways of cytochrome c release from mitochondria in apoptosis. BBA Bioenergetics. 1757 (2006) 639-647.

[27] Gonzalvez F, Gottlieb E, Cardiolipin: setting the beat of apoptosis. Apoptosis. 12 (2007) 877-885.

[28] Elmore S, Apoptosis: A Review of Programmed Cell Death. Toxicol. Pathol. 35 (2007) 495-516.

[29] C.F. Thorn, C. Oshiro, S. Marsh, T. Hernandez-Boussard, H. McLeod, T.E. Klein, R.B. Altman, Doxorubicin pathways: pharmacodynamics and adverse effects, Pharmacogenetics Genom. 21 (2011) 440–446.

[30] Octavia Y, Tochetti CG, Gabrielson KL, Janssens S, Crijns HJ, Moens AL, Doxorubivin-induced cardiomyopathy: From molecular mechanisms to therapeutic strategies. J. Mol. Cell. Cardiol. 52 (2012) 1213-1225.

[31] Kalyanaraman B, Teaching the basics of the mechanism of doxorubicin-induced cardiotoxicity: Have we been barking up the wrong tree? Redox Biol. (2020) doi: 10.1016/j.redox.2019.101394

[32] “Doxorubicin Hydrochloride Injection Label – FDA.” U.S. Food and Drug Administration, May 2010, https://www.accessdata.fda.gov/drugsatfda_docs/label/2010/050467s070lbl.pdf.

[33] “DOXIL Label – FDA.” U.S. Food and Drug Administration, May 2007, www.accessdata.fda.gov/drugsatfda_docs/label/2007/050718s029lbl.pdf.

1.9 Figures and Figure Legends

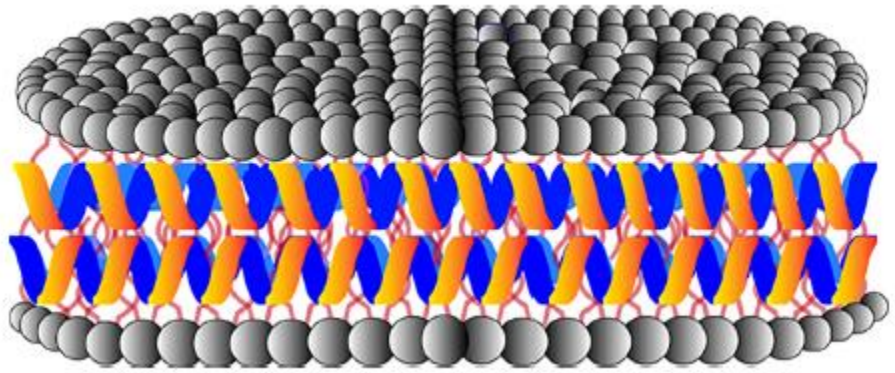

Figure 1.1 Schematic diagram of a discoidal rHDL. The particle depicted has a diameter of 10 nm and is comprised of DMPC as the bilayer forming phospholipid and two copies of an apolipoprotein scaffold that circumscribe the perimeter of the discoidal bilayer.

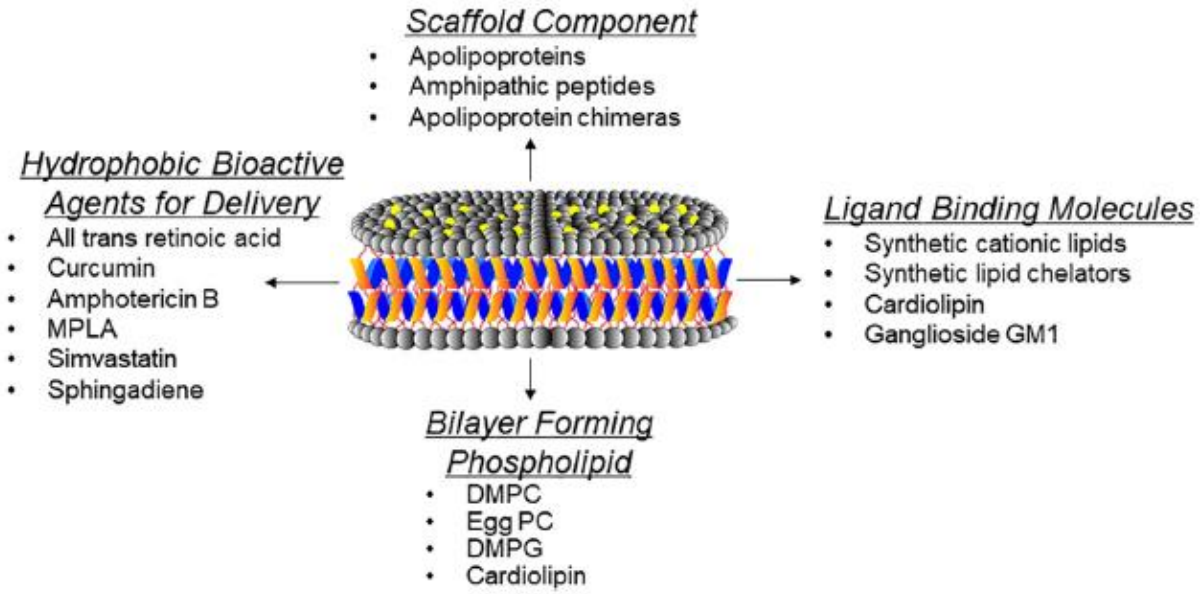

Figure 1.2 Versatility of the ND platform. The ease of rHDL particle formulation *in vitro* permits their assembly with a range of scaffold proteins/peptides and bilayer forming phospholipids. By extension, the basic structure of rHDL can be adapted to create ND that possess a wide range of hydrophobic bioactive agents and/or natural or synthetic ligand binding lipids.

Chapter 2

Calcium-Induced Transformation of Cardiolipin Nanodisks

This chapter is based on work published in:

Fox CA, Ikon N, Ellison P, Ryan RO, Calcium induced transformation of cardiolipin nanodisks. Biochim. Biophys. Acta Biomembr. 1861 (2019) 1030-1036.

2.1 Abstract

Miniature membranes comprised of tetramyristoylcardiolipin (CL) and apolipoprotein (apo) A-I, termed nanodisks (ND), are stable, aqueous soluble, reconstituted high density lipoproteins. When CL ND, but not dimyristoylphosphatidylcholine (PC) ND, were incubated with $CaCl_2$, a concentration dependent increase in sample turbidity occurred, consistent with CL undergoing a bilayer to non-bilayer transition. To assess the cation specificity of this reaction, CL ND were incubated with various mono- and divalent cations. Whereas monovalent cations had no discernable effect, MgCl2 and SrCl2 induced a response similar to $CaCl_2$. When ND were formulated using different weight ratios of CL and PC, those possessing 100% CL or 75% CL remained susceptible to $CaCl_2$ induced sample turbidity development while ND possessing 50% CL displayed reduced susceptibility. ND comprised of 25 % CL and 75 % PC were unaffected by $CaCl_2$ under these conditions. SDS PAGE analysis of insoluble material generated by incubation of CL ND with $CaCl_2$ revealed that nearly all apoA-I was recovered in the insoluble fraction along with CL. One hour after addition of EDTA to $CaCl_2$-treated CL ND, sample clarity was restored. Collectively, these data are consistent with a model wherein Ca^{2+} forms a bidentate interaction with anionic phosphates in the polar head group of CL. As phosphate group repositioning occurs to maximize Ca^{2+} binding, CL acyl chains reposition, accentuating the conical shape of CL to an extent that is incompatible with the ND bilayer structure.

2.2 Introduction

Cardiolipin (CL) is a uniquely structured glycerophospholipid that localizes to the inner membrane of mitochondria [1]. Unlike other phospholipids, cardiolipin possesses two phosphates, three glycerols and four fatty acyl chains. Due to its relatively small polar head group and four esterified fatty acids, CL possesses a “cone-shaped” molecular structure [2,3]. As a result, CL is considered to be a “non-bilayer” phospholipid that, when present in a bilayer setting, exerts negative curvature pressure [4]. Whereas CL is not well accommodated in planar bilayer membranes [5], it is a key component of highly curved bilayers such as the cristae membranes of mitochondria [6].

Calcium plays an important role in mitochondrial signaling and function [7]. Mitochondrial calcium overload is known to induce apoptosis and it is conceivable that interactions between calcium, CL and cytochrome c are involved in molecular events that trigger apoptosis [8,9,10]. Interaction of calcium with CL containing liposomes is known to induce a bilayer to non-bilayer transition, resulting in formation of an inverted hexagonal II lipid phase [11,12,13]. The molecular basis for this phenomenon is not fully understood and, to date, most studies have been performed using liposomes that possess varying percentages (typically ~20%) of their phospholipid mass as CL [14,15,16]. One of the limitations associated with liposomes as a model system is the fact that up to one half of the bilayer phospholipid content resides in the inner monolayer leaflet where it is largely inaccessible to the external environment. In the case of multilamellar vesicles, an even greater proportion of liposomal phospholipid is

inaccessible. Additionally, liposomes often display polydispersity, exhibit limited stability and scatter light to varying degrees, indicating less than complete solubility [17,18,19].

By contrast, recent studies have shown that CL can be fully solubilized in aqueous buffer upon incorporation into nanoscale membrane complexes comprised solely of CL and apolipoprotein (apo) A-I [20]. These complexes, termed nanodisks (ND), exist as disk-shaped phospholipid bilayers whose perimeter is circumscribed by an amphipathic scaffold protein, such as apoA-I [21]. Although CL is generally unstable in a planar bilayer setting, the apolipoprotein scaffold appears to exert a stabilizing force, effectively serving as a “belt” around the perimeter of the discoidal bilayer. Compared to liposomes, CL ND have inherent advantages for studies of molecular interactions, including a uniform nanoscale particle size distribution, complete aqueous solubility, ease of formulation, the absence of an inaccessible bilayer leaflet and, most remarkably, ND can be generated using CL as the sole lipid component. In the present study, CL ND were employed as a model system to investigate the effect of $CaCl_2$ on CL ND structure, stability and aqueous solubility.

2.3 Materials and Methods

Nanodisk formulation

Dimyristoylphosphatidylcholine (PC), tetramyristoyl cardiolipin (CL) and tetralinoleoyl cardiolipin were purchased from Avanti Polar Lipids. Unless

otherwise indicated, studies reported herein employed tetramyristoyl CL. Five mg aliquots were dissolved in 200 µL CHCl3:CH3OH (3:1 v/v), and dried under a stream of N2 gas, creating a thin film on the walls of the vessel. Samples were lyophilized overnight to remove residual solvent. To formulate ND, 750 µL 20 mM HEPES buffer, pH 7.2, was added to a 5 mg aliquot of dried phospholipid. The sample was vortexed to disperse the phospholipid which ultimately appeared as an opaque suspension. Subsequently, 2 mg recombinant human apoA-I [22] in 500 µL HEPES buffer was added to the lipid suspension. The final volume of the mixture was 1.25 ml. PC ND were formulated by bath sonication of the PC/apoA-I mixture at 25 °C until the solution cleared (< 10 min). Tetramyristoyl CL ND (hereafter referred to as CL ND) were formulated in a similar manner, with the exception that bath sonication was performed at 48 °C. Tetralinoleoyl CL ND were formulated by bath sonication at 25 °C under an N2 atmosphere.

Gel filtration chromatography of ND samples

ND samples, formulated as above, were centrifuged at 14,000 × g for 2 min prior to gel permeation chromatography on a Superose 6 Increase 10/300 GL column using a GE AKTA Pure FPLC instrument. Two hundred µL ND (corresponding to 0.8 mg CL), were applied to the column. Samples were chromatographed in 20 mM HEPES at a flow rate of 0.5 ml/min with absorbance monitored at 280 nm and collection of 1.0 ml fractions.

Incubation of ND with cations

Following formulation of ND, 25 µL aliquots (100 µg phospholipid; corresponding to 78 nmol CL or 147 nmol PC) were added to the wells of a UV Star microtiter plate (Greiner Bio-One). Indicated amounts of $CaCl_2$ were added to the wells. The final volume of all wells was maintained at 200 µL through addition of HEPES buffer. After addition of HEPES and $CaCl_2$, samples were incubated for 1 h at 22 °C or 37 °. Sample turbidity was measured as absorbance at 325 nm using a Spectramax M5 microplate reader. Background absorbance at 325 nm, determined in wells containing deionized water, was <0.05. To determine the effect of other cations, ND were added to a microtiter plate as described above. The chloride salts of specified mono- or divalent cations were added to the wells, samples incubated for 1 h at 22 °C and absorbance measured at 325 nm (i.e. turbidity). To assess partitioning of the apoA-I scaffold protein following $CaCl_2$-induced CL ND sample turbidity development, 25 µL CL ND (equivalent to 78 nmol CL) were incubated with 2000 nmol $CaCl_2$ in a final volume of 200 µL for 1 h at 22 °C. The turbid sample was centrifuged at 14,000 × g for 2 min to pellet insoluble material. The supernatant was recovered and the pellet re-suspended in 200 µl HEPES buffer. Ten µL aliquots of the supernatant and resuspended pellet were electrophoresed on a 4–20% SDS PAGE slab gel and stained with GelCode Blue Stain Reagent (Thermo). Gel images were documented on a GE Healthcare Typhoon Trio Variable Mode Imager. To assess the relative distribution of apoA-I in $CaCl_2$ disrupted CL ND supernatant and pellet fractions, densitometric analysis of gel band intensity was performed using ImageJ software [23]. To measure the relative distribution of CL between pellet and

supernatant fractions generated by incubation of CL ND with $CaCl_2$, the CL specific fluorescent dye, 10-N-nonyl acridine orange [24] (Thermo) was employed. Samples were excited at 499 nm and emission monitored from 530 nm to 610 nm on a Spectramax M5 microplate reader in a fluorescence compatible microtiter plate (Greiner Bio-One).

Incubation of mixed phospholipid ND with $CaCl_2$

To assess the effect of $CaCl_2$ on mixed phospholipid ND, different weight ratios of CL and PC were used to formulate “mixed lipid” ND. HEPES buffer (750 µl) was added to separate 5 mg aliquots of CL and PC followed by vortexing to hydrate the lipids. Aliquots of these PC and CL dispersions were combined to achieve the indicated phospholipid weight ratios. ApoA-I was then added to the mixed lipid dispersions at a 5:2 (w/w) lipid:protein ratio. ND formation, as measured by sample clarification, was achieved by bath sonication at 48 °C for 2 min, alternating with bath sonication at 25 °C until sample absorbance was <0.07 at 325 nm (<10 min). For incubations with $CaCl_2$, aliquots of mixed lipid ND, containing 78 nmol CL, were added to the wells of a microtiter plate. Indicated amounts of $CaCl_2$ in HEPES buffer were added to each well (final volume 200 µL) and the plate incubated for 1 h at 22 °C prior to sample absorbance measurements.

CL ND incubation with $CaCl_2$ and EDTA

CL ND were added to the wells of a microtiter plate as above. $CaCl_2$ (0 nmol, 600 nmol or 2000 nmol) was added and the samples incubated at 22 °C for 1 h. Following incubation, a 1:1 molar equivalent of EDTA to $CaCl_2$ was added to each sample. Total sample volumes after EDTA addition were maintained at 300 µL through addition of HEPES buffer. Samples were incubated for a further 1 h at 22 °C followed by absorbance measurement at 325 nm. In other experiments, EDTA-treated, $CaCl_2$-modified CL ND were analyzed by gel filtration chromatography as described above before and after bath sonication at 48 °C for 3 min and centrifugation at 14,000 × g for 2 min.

Statistical Analysis

Statistical analyses were performed by two-way ANOVA followed by Dunnett's test to compare treated samples against control samples (**Figures 2.2, 2.3, 2.4**). Alternatively, the Holm-Sidak multiple t-test was used to compare the absorbance of $CaCl_2$ treated samples to $CaCl_2$ + EDTA treated samples (**Figure 2.5a**). Statistical tests were performed using GraphPad Prism version 8.02 for Windows (GraphPad Software, San Diego, CA)

2.4 Results

Cardiolipin ND formulation and model structure.

When aqueous dispersions of CL are incubated with apoA-I and subjected to bath sonication, lipid nanoparticle complex (i.e. ND) formation is evident by

complete sample clarification [20]. Previous studies, using PC and other glycerophospholipids, revealed that ND exist as disk-shaped phospholipid bilayers whose perimeter is stabilized by interaction with apoA-I, an amphipathic α-helix-rich scaffold protein [21]. Unlike other glycerophospholipids that form ND, CL possesses a relatively small polar head group and four hydrophobic acyl chains, conferring a distinct cone-shaped structure to this lipid. Consistent with this, CL induces negative curvature pressure on bilayer membranes and is prone to adopting a non-bilayer state. With regard to the apparent ability of CL to form ND, it is conceivable that the apoA-I scaffold exerts a belt-like stabilizing force around the ND bilayer perimeter, as depicted in **Figure 2.1A**. In keeping with this model, FPLC gel filtration chromatography of CL ND (**Figure 2.1B**) reveals a homogenous population of particles in a similar size range to well characterized PC ND [25]. Thus, it may be considered that the scaffold function of apoA-I provides an opposing force to CL's tendency to transition to a non-bilayer state, thereby maintaining CL in a soluble bilayer state as ND.

The effect of $CaCl_2$ on ND sample turbidity.

Both CL ND and PC ND are fully soluble in aqueous buffer. Negligible material precipitates upon centrifugation and samples remain stable for 1 week or more when stored at 4 °C. To determine the effect of $CaCl_2$ on ND structural integrity, PC ND and CL ND samples were incubated with increasing quantities of $CaCl_2$ for 1 h (**Figure 2.2**). In control incubations containing HEPES buffer alone, $CaCl_2$ had no effect on sample absorbance at 325 nm. Likewise, when PC ND were

incubated with $CaCl_2$, little or no change in sample absorbance occurred. By contrast, CL ND undergo a marked $CaCl_2$ concentration dependent increase in sample turbidity. The rate of this reaction was temperature dependent, with turbidity development occurring more rapidly at 37 °C than at 22 °C. Moreover, the physiologically relevant CL molecular species, tetralinoleoyl CL is capable for forming ND [20] and is also susceptible to $CaCl_2$ induced ND disruption (data not shown). As seen in **Figure 2.2**, $CaCl_2$ levels below 400 nmol had little or no effect on CL ND sample turbidity. At 400 nmol $CaCl_2$, however, the sample became turbid and absorbance increased. As the amount of $CaCl_2$ was increased further, sample absorbance also increased, plateauing at 1000 nmol $CaCl_2$ / 78 nmol CL.

Effect of alternate cations on CL ND sample turbidity.

To assess the cation specificity of the reaction induced by incubation with $CaCl_2$, CL ND (78 nmol CL) were incubated with increasing amounts of mono- or divalent cations (**Figure 2.3**). CL ND in buffer alone served as control and, in the absence of added cations, remained fully soluble. Addition of $CaCl_2$ induced the expected concentration-dependent increase in CL ND sample absorbance and a similar trend was observed with $MgCl_2$ and $SrCl_2$. The monovalent cations, NaCl and KCl, had no effect on CL ND sample turbidity.

Effect of $CaCl_2$ on mixed phospholipid ND.

To further explore $CaCl_2$ mediated effects on CL ND, different weight ratios of CL and PC were used to formulate ND. The resulting mixed phospholipid ND were

incubated with $CaCl_2$. ND comprised of 100% CL, 75% CL, 50% CL and 25% CL were incubated in the absence or presence of 2 fixed amounts of $CaCl_2$ for 1 h, followed by measurement of sample turbidity (**Figure 2.4**). The final CL content in each incubation was 100 µg (78 nmol). Similar to ND formulated with 100% CL, ND formulated at a 75:25 (w/w) ratio of CL to PC showed a strong $CaCl_2$ concentration-dependent increase in sample turbidity. ND formulated with a 50:50 (w/w) mixture of CL and PC showed a slight, but statistically significant, increase in absorbance at the highest $CaCl_2$ level tested. ND containing 25% CL and 75% PC were unaffected by incubation with $CaCl_2$ under these experimental conditions.

Effect of EDTA on $CaCl_2$-induced CL ND sample turbidity.

To determine whether chelation of added calcium by EDTA is able to reverse $CaCl_2$-mediated effects on CL ND, samples of CL ND were incubated with $CaCl_2$ for 1 h to induce turbidity development. EDTA was then added (1:1 molar equivalence to $CaCl_2$) and the samples incubated for an additional 1 h, followed by absorbance determination at 325 nm (**Figure 2.5A**). CL ND incubated with 600 nmol $CaCl_2$, followed by 600 nmol EDTA, rapidly clarified. Samples treated with 2000 nmol $CaCl_2$ clarified more slowly upon addition of EDTA, returning to near original absorbance by the end of the 1 h incubation period. FPLC gel filtration analysis of $CaCl_2$-treated CL ND samples clarified by incubation with EDTA revealed a slight increase in particle heterogeneity and centrifugation of this sample generated a small but reproducible precipitate (data not shown).

However, bath sonication of EDTA clarified, $CaCl_2$-treated CL ND did not give rise to a precipitate upon centrifugation and FPLC gel filtration chromatography (**Figure 2.5B**) revealed a uniform population of particles whose elution characteristics were nearly indistinguishable from those of CL ND prior to incubation with $CaCl_2$.

Effect of $CaCl_2$ on the interaction of apoA-I with CL.

According to the model presented in **Figure 2.1**, apoA-I is an essential structural component of CL ND. To determine whether apoA-I maintains contact with CL following incubation with $CaCl_2$, insoluble material formed during this reaction was pelleted by centrifugation and the supernatant removed. Following re-suspension of pelleted material in a volume of buffer equal to the reserved supernatant, aliquots of each were subjected to SDS PAGE (**Figure 2.6**). Densitometric scanning of the stained gel indicated >90 % of the apoA-I in the original CL ND sample was recovered in the insoluble fraction generated by incubation of CL ND with $CaCl_2$. Analysis of the relative distribution of CL between the supernatant and pellet fractions using an assay based on binding of 10-N-nonyl acridine orange to CL indicated >70 % of the CL was recovered in the pellet with <30 % in the supernatant. Taken together, these data indicate that, following $CaCl_2$-induced transition of CL to an insoluble, non-bilayer state, apoA-I remains associated with the lipid.

2.5 Discussion

CL is a uniquely structured glycerophospholipid that plays an important role in mitochondrial structure and bioenergetics. CL is a cone-shaped lipid, owing to a relatively small polar head group and four fatty acyl chains. Consistent with this molecular shape, CL exerts negative curvature pressure on membranes and is prone to adopt a nonbilayer, inverted hexagonal II phase. Despite this tendency, CL not only exists stably in mixed lipid membranes but can be induced to form an apparent nanoscale size planar bilayer when an aqueous dispersion of this lipid is bath sonicated in the presence of isolated recombinant human apoA-I. The complexes formed are fully soluble in neutral pH buffer, stable for extended periods when stored at 4 °C and, based on gel filtration chromatography, display a homogeneous particle size distribution. These complexes, comprised solely of CL and apoA-I, termed CL ND, represent a novel miniature membrane system to investigate CL's interactome.

One example of a CL binding partner is calcium. Upon incubation with $CaCl_2$, fully soluble CL ND undergo a marked increase in sample turbidity, consistent with CL undergoing a transition from bilayer to non-bilayer state. This transition does not occur when PC ND are incubated with $CaCl_2$. The reaction is $CaCl_2$ concentration dependent and changes in sample turbidity are detectable at a ~1:5 molar ratio of CL to $CaCl_2$, while maximum sample absorbance values plateau at ã1:12 molar ratio of CL to $CaCl_2$. Mixed lipid ND that contain different ratios of CL and PC respond differently to $CaCl_2$. The response is directly related to the CL content of the ND. Reducing the amount of CL in a given ND by

replacing it with PC confers resistance against $CaCl_2$-induced transformation of ND from a soluble bilayer state to an insoluble non-bilayer state. Overall, these results reveal that decreasing the proportion of CL in ND decreases the absorbance increase induced by incubation with $CaCl_2$. In other words, mixed lipid ND containing a lower proportion of CL per ND require more $CaCl_2$ to induce a bilayer to non-bilayer transition. This trend holds for ND formulated to possess 100%, 75%, 50% and 25% CL content.

The reaction described between CL ND and $CaCl_2$ also occurs when CL ND are incubated with other divalent cations, including $MgCl_2$ and $SrCl_2$. Magnesium, which has the smallest atomic radius of the divalent cations tested, induced a lesser increase in sample absorbance than either calcium or strontium at the lower ion level tested. At higher amounts, however, all three divalent cations induced a similar increase in sample absorbance. On the other hand, incubation with monovalent cations across a wide concentration range had no discernable effect on CL ND. The specificity of this reaction for divalent cations suggests that the two negatively charged phosphate groups in CL's polar head group play a key role. Divalent cations, such as Ca^{2+}, are capable of forming a bidentate binding interaction with these phosphates, as depicted in **Figure 2.7**. Moreover, it is anticipated that, as the two phosphates reposition to increase contact with the Ca^{2+} ion, conformational strain is placed on other parts of the CL molecule. This strain may be relieved by repositioning the hydrocarbon tails of CL in a manner that further accentuates its cone shape. Such a change in the orientation of CL hydrocarbon tails, relative to the polar head group, is postulated

to accentuate the conical shape of CL, decreasing its ability to stably reside in planar bilayer structure of ND. It is likely such a molecular shape change, induced by calcium binding, ultimately leads to disruption of the ND bilayer structure and the transition of CL from a soluble bilayer to an insoluble non-bilayer state that ultimately precipitates from solution. This calcium-induced bilayer disruption may relate to other biological interactions in the CL interactome. In particular, release of cytochrome c from the inner mitochondrial membrane may be related to an influx of calcium into the mitochondria, though the exact mechanism remains under investigation [26, 27]. In any event, CL ND may be a viable model for examining this interaction in a controlled, readily accessible in vitro setting.

Whereas it is considered that the apolipoprotein scaffold surrounding the disk-shaped bilayer of ND exerts a stabilizing force that “holds” CL in a bilayer phase through direct contact of its amphipathic α-helices with otherwise exposed fatty acyl chains around the edge of the discoidal bilayer (see **Figure 2.1**), these data indicate calcium-mediated effects on CL structure exert an opposing force that, above a certain threshold, results in CL ND particle disruption. Based on experiments conducted with mixed phospholipid ND, as the CL content of a given ND formulation is increased, the easier it is for the stabilizing influence of the apolipoprotein to be exceeded by incubation with $CaCl_2$.

Once the scaffold protein’s stabilizing force is exceeded, CL undergoes a bilayer to non-bilayer transition and this process coincides with obvious changes in sample turbidity. Remarkably, however, upon addition of EDTA, which

effectively chelates all calcium present, including that bound to CL, an environment is created wherein apoA-I is capable of re-solubilizing CL, presumably by reconstitution of CL ND. FPLC analysis revealed that bath sonication of EDTA clarified, $CaCl_2$-treated CL ND gives rise to an elution profile that is nearly indistinguishable from that of the starting CL ND. The observation that the reaction induced by $CaCl_2$ can be reversed by the addition of EDTA may be related to the fact that, following $CaCl_2$ mediated disruption of CL ND, apoA-I remains associated with the insoluble CL precipitate. Assuming Ca^{2+} bound CL adopts a hexagonal II phase, then it is likely that apoA-I maintains a binding interaction with exposed hydrocarbon tails at the aqueous interface of this insoluble lipid phase, thereby minimizing contact between hydrophobic CL fatty acyl chains and the aqueous milieu, as depicted in **Figure 2.8**. Maintenance of a binding interaction between apoA-I and CL in the $CaCl_2$ disrupted state is likely a key factor in the ability of EDTA to promote re-formation of intact CL ND. Just as the initial formation of CL ND required bath sonication to generate a uniform homogenous population of CL ND, following EDTA treatment of $CaCl_2$ disrupted CL ND, bath sonication yielded a single major population of CL ND.

It is noteworthy that the major CL molecular species found in mitochondria of heart and muscle tissue is tetralinoleoyl CL. This molecular species is generated by acyl chain remodeling of nascent CL through the action of a transacylase termed tafazzin [28]. Although the potential benefits of establishing a uniform fatty acyl distribution in CL are not known, it has been shown that tafazzin activity in vitro is optimal when CL exists in a non-bilayer state [29].

Insofar as tetralinoleoyl CL is capable of forming ND and is susceptible to $CaCl_2$ mediated conversion to a non-bilayer state, this system may provide a model for understanding the role(s) of calcium in CL remodeling and its role in maintenance of mitochondrial membrane integrity.

2.6 References

[1]. Horvath SE, Daum G (2013) Lipids of mitochondria, Prog. Lipid Res 52, 590–614. [PubMed: 24007978]

[2]. Cullis PR, de Kruijff B (1979) Lipid Polymorphism and the functional roles of lipids in biological membranes. Biochim Biophys Acta 559, 399–420. [PubMed: 391283]

[3]. Stepanyants N, Macdonald PJ, Francy CA, Mears JA, Qi X, Ramachandran R (2015) Cardiolipin's propensity for phase transition and its reorganization by dynamin-related protein 1 form a basis for mitochondrial membrane fission. Mol Biol Cell. 26, 3104–3116. [PubMed: 26157169]

[4]. Renner LD, Weibel DB (2011) Cardiolipin microdomains localize to negatively curved regions of E. coli membranes. Proc. Natl. Acad. Sci. U.S.A 108, 6264–6269. [PubMed: 21444798]

[5]. Lewis R, McElhaney RN (2009) The physicochemical properties of cardiolipin bilayers and cardiolipin-containing lipid membranes. Biochim Biophys Acta 1788, 2069–2079. [PubMed: 19328771]

[6]. Ikon N, Ryan RO (2017) Cardiolipin and mitochondrial cristae organization. Biochim Biophys Acta 1859, 1156–1163.

[7]. Brookes PS, Yoon Y, Robotham JL, Anders MW, Sheu SS (2004) Calcium, ATP, and ROS: a mitochondrial love-hate triangle. Am J Physiol Cell Physiol. 287, C817–C833. [PubMed: 15355853]

[8]. Paradies G, Petrosillo G, Paradies V, Ruggiero FM (2009) Role of cardiolipin peroxidation and Ca^{2+} in mitochondrial dysfunction and disease. Cell Calcium. 45, 643–650. [PubMed: 19368971]

[9]. Celsi F, Pizzo P, Brini M, Leo S, Fotino C, Pinton P, Rizzuto R (2009) Mitochondria, calcium, and cell death: A deadly triad in neurodegeneration. Biochim Biophys Acta Bioenerg. 1787(5), 335–344.

[10]. Peng T, Jou MJ (2010) Oxidative stress caused by mitochondrial calcium overload. Ann N Y Acad Sci. 1201, 183–188. [PubMed: 20649555]

[11]. Rand RP, Sengupta S (1972) Cardiolipin forms hexagonal structures with divalent cations. Biochim Biophys Acta. 255, 484–492. [PubMed: 4333431]

[12]. De Kruijff B, Verkleij AJ, Leunissen-Bijvelt J, Van Echteld CJA, Hille J, Rijnbout H (1982) Further aspects of the calcium dependent polymorphism of bovine heart cardiolipin. Biochim Biophys Acta 693, 1–12. [PubMed: 7150583]

[13]. Kirk GL, Gruner SM, Stein DL (1984) A thermodynamic model of the lamellar to inverse hexagonal phase transition of lipid membrane-water systems. Biochemistry 23 1093–1102.

[14]. Cullis PR, Verkleij AJ, Ververgaert PHJ (1978) Polymorphic phase behaviour of cardiolipin as detected by 31P NMR and freeze-fracture techniques. Effects of calcium, dibucaine and chlorpromazine. Biochim Biophys Acta 513, 11–20. [PubMed: 102344]

[15]. Smaal EB Schreuder C, van Baal JB, Tijburg PNM, Mandersloot JG, Kruijff BD, Gier JD (1987) Calcium-induced changes in permeability of dioleoylphosphatidylcholine model membranes containing bovine heart cardiolipin. Biochim Biophys Acta. 897, 191–196. [PubMed: 3099844]

[16]. Macdonald PM, Seelig J (1987) Calcium binding to mixed cardiolipinphosphatidylcholine bilayers as studied by deuterium nuclear magnetic resonance. Biochemistry. 26, 6292–6298. [PubMed: 3689777]

[17]. Sharma A, Sharma US (1997) Liposomes in drug delivery: progress and limitations. Int J Pharmaceut. 154, 123–140.

[18]. Akbarzadeh A, Rezaei-Sadabady R, Davaran S, Joo SW, Zarghami N, Hanifehpour Y, Samiei M, Kouhi M, Nejati-Koshki K (2013) Liposome: classification, preparation, and applications. Nanoscale Res Lett. 8, 102. [PubMed: 23432972]

[19]. Bozzuto F, Molinari A (2015) Liposomes as nanomedical devices. Int J Nanomedicine. 10, 975–999. [PubMed: 25678787]

[20]. Ikon N, Su B, Hsu F, Forte TM, Ryan RO (2015) Exogenous cardiolipin localizes to mitochondria and prevents TAZ knockdown-induced apoptosis in myeloid progenitor cells. Biochem Biophys Res Comm 464, 580–585. [PubMed: 26164234]

[21]. Ryan RO (2010) Nanobiotechnology applications of reconstituted high density lipoprotein. J. Nanobiotech 8, 8–28.

[22]. Ryan RO, Forte TM, Oda MN (2003) Optimized bacterial expression of human apolipoprotein A-I. Protein Expr Purif. 27, 98–103. [PubMed: 12509990]

[23]. Rueden CT, Schindelin J, Hiner MC, DeZonia BE, Walter AE, Arena ET, Eliceiri KW (2017) ImageJ2: ImageJ for the next generation of scientific image data. BMC Bioinformatics 18, 529. [PubMed: 29187165]

[24]. Garcia Fernandez MI, Ceccarelli D, Muscatello U (2004) Use of the fluorescent dye 10-N-nonyl acridine orange in quantitative and location assays of cardiolipin: a study of different experimental models. Anal Biochem. 328, 174–80. [PubMed: 15113694]

[25]. Wadsater M, Maric S, Simonsen JB, Mortensen K, Cardenas M (2013) The effect of using binary mixtures of zwitterionic and charged lipids on nanodisc formation and stability. Soft Matter. 9, 2329–2337.

[26]. Prudent J, McBride HM (2017) The mitochondria-endoplasmic reticulum contact sites: a signaling platform for cell death. Curr Opin Cell Biol. 47, 52–63. [PubMed: 28391089]

[27]. Giorgi C, Baldassari F, Bononi A, Bonora M, Marchi ED, Marchi S, Missiroli S, Patergnani S, Rimessi A, Suski JM, Wieckowsky MR, Pinton P (2012) Mitochondrial Ca^{2+} and apoptosis. Cell Calcium 52, 36–43. [PubMed: 22480931]

[28]. Schlame M (2013) Cardiolipin remodeling and the function of tafazzin. Biochim Biophys Acta. 1831, 582–588. [PubMed: 23200781]

[29]. Schlame M, Acehan D, Berno B, Xu Y, Valvo S, Ren M, Stokes DL, Epand RM (2012) The physical state of lipid substrates provides transacylation specificity for tafazzin. Nat Chem Biol. 8, 862–869. [PubMed: 22941046]

2.7 Figures and Legends

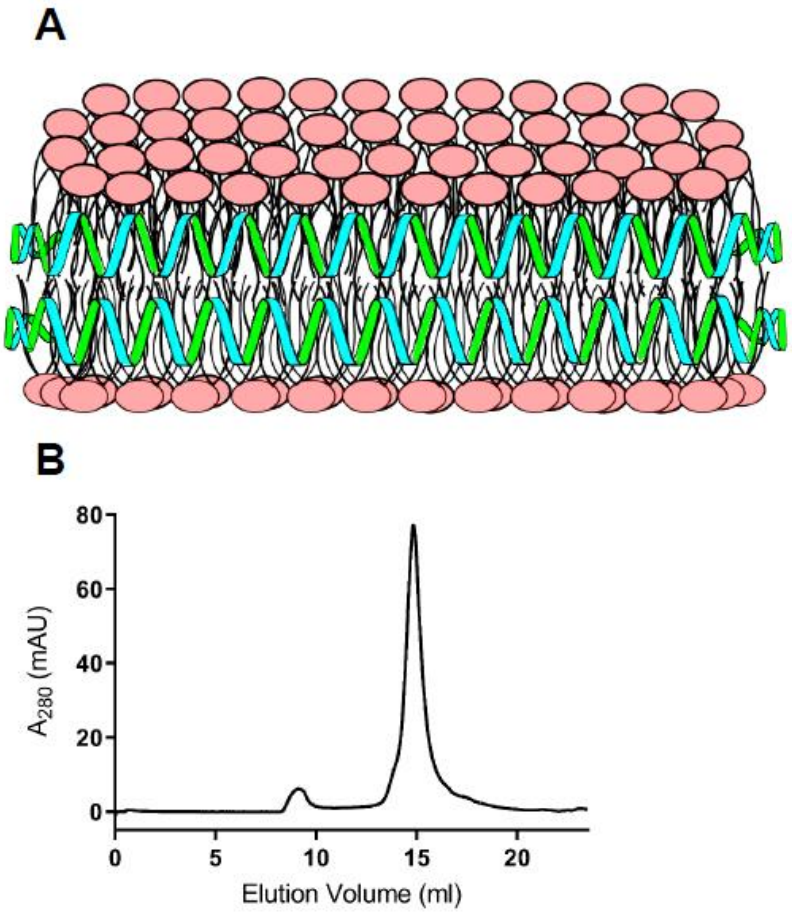

Figure 2.1 Model structure of CL ND. A) In this depiction, CL (polar head groups in pink) is organized as a disk-shaped bilayer whose perimeter is circumscribed and stabilized by apoA-I (green/blue helices), which interacts with CL fatty acyl chains at the edge of the disk. **B**) FPLC size exclusion chromatography profile of CL ND. ND were formulated with apoA-I and CL as described. An aliquot of CL ND (0.32 mg apoA-I / 0.8 mg CL) in 20 mM HEPES buffer, pH 7.2, was applied to a Superose 6 Increase 10/300 GL column and elution monitored at 280 nm.

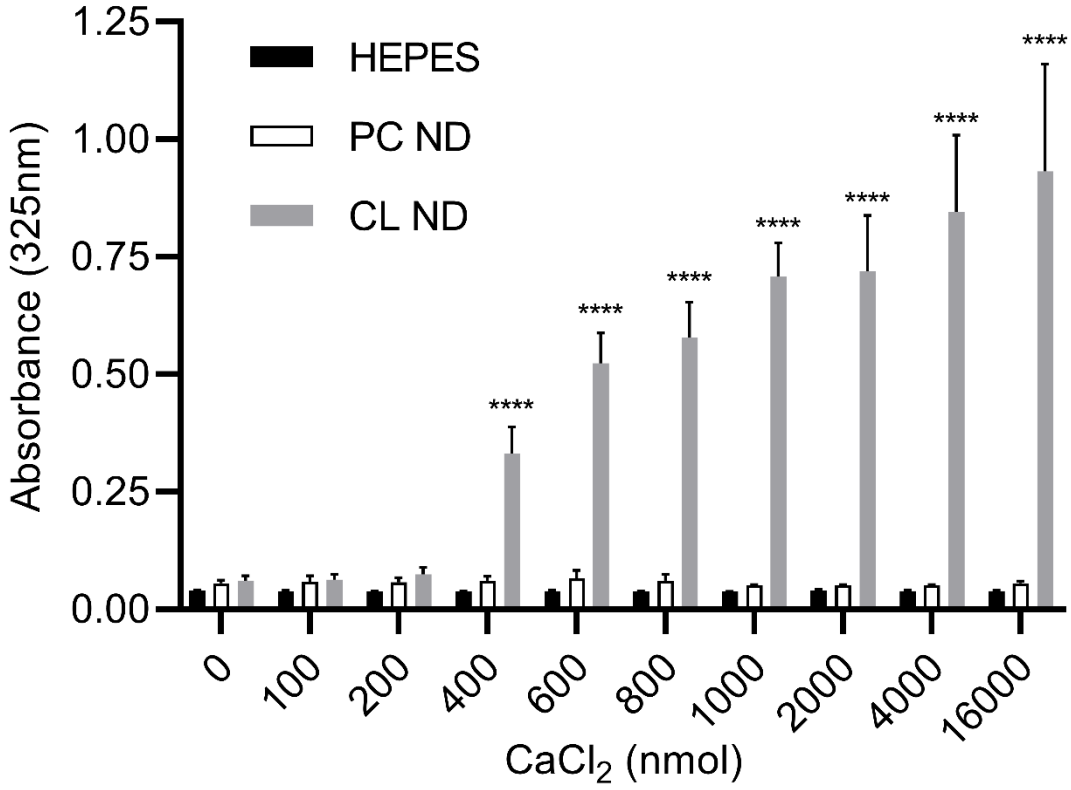

Figure 2.2 Effect of $CaCl_2$ on ND sample integrity. ApoA-I containing PC ND and CL ND were formulated in HEPES buffer as described and aliquots of each (corresponding to 78 nmol CL or 147 nmol PC) were applied to the wells of a 96 well microtiter plate. To each well, indicated amounts of $CaCl_2$ (in HEPES buffer) were added and the volume adjusted to 200 µl with HEPES buffer. The plate was incubated for 1 h at 22 °C and, following incubation, sample absorbance measured at 325 nm on a SpectraMax plater reader. Values reported are the mean ± standard error (n = 9) ****, P<0.0001 versus HEPES control and PC ND.

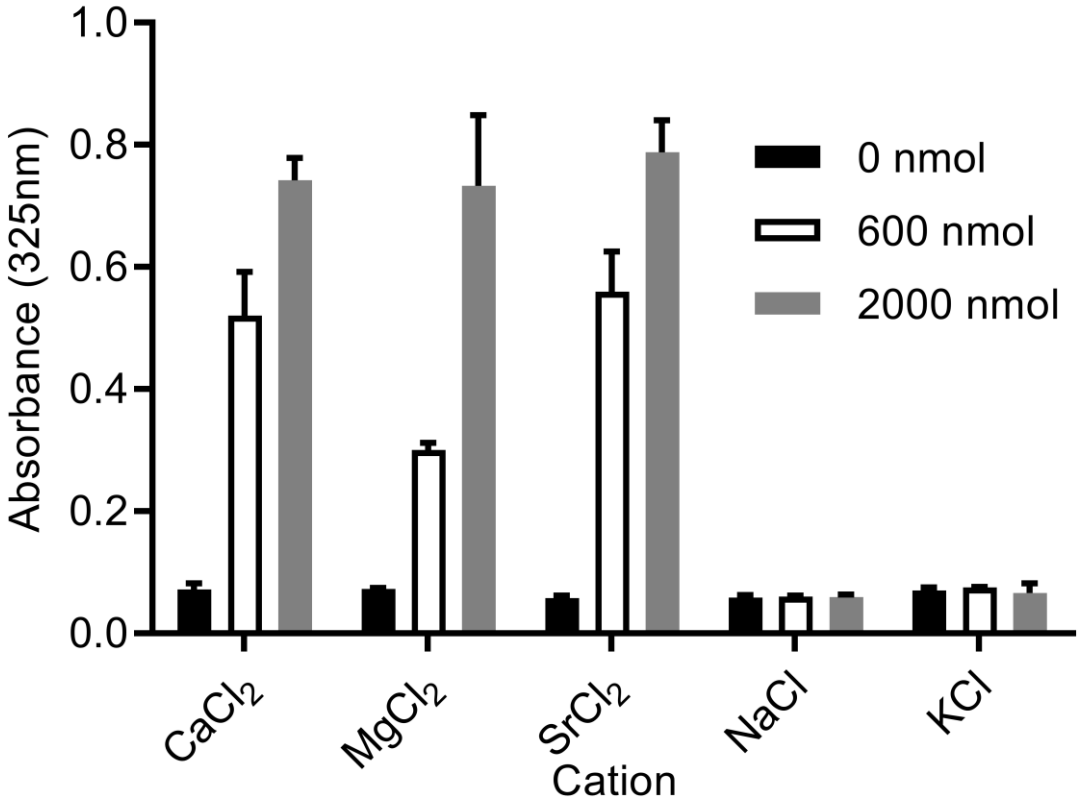

Figure 2.3 Effect of alternate cations on ND sample integrity. Aliquots of CL ND (78 nmol CL), solubilized in HEPES buffer, were applied to the wells of a 96 well microtiter plate. To each well, specified quantities of the chloride salt of mono- or divalent cations was added and the volume adjusted to 200 µl with HEPES buffer. The plate was incubated for 1 h at 22 °C followed by sample absorbance determination at 325 nm. Values reported are the mean ± standard error (n = 3) ****, P<0.0001 versus 0 nmol divalent cation.

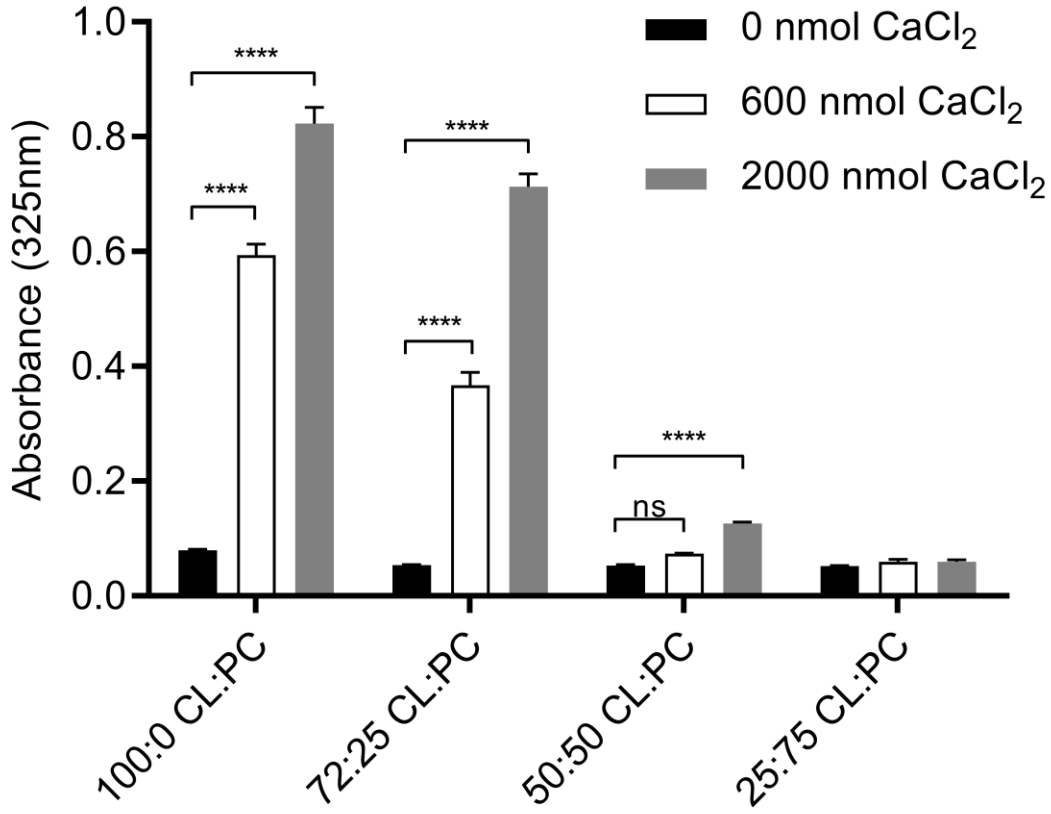

Figure 2.4 Effect of calcium on mixed lipid ND sample integrity. ND containing specified weight ratios of CL and PC were formulated with apoA-I in HEPES buffer. Aliquots of the different ND samples (corresponding to 78 nmol CL), were added to the wells of a 96 well microtiter plate. To each well, indicated amounts of $CaCl_2$ were added and the volume adjusted to 200 µl with HEPES buffer. The plate was incubated for 1 h at 22 °C and, following incubation, sample absorbance at 325 nm was measured. Values reported are the mean ± standard error (n = 3) ****, P<0.0001 versus 0 nmol $CaCl_2$. ns, not significant.

A

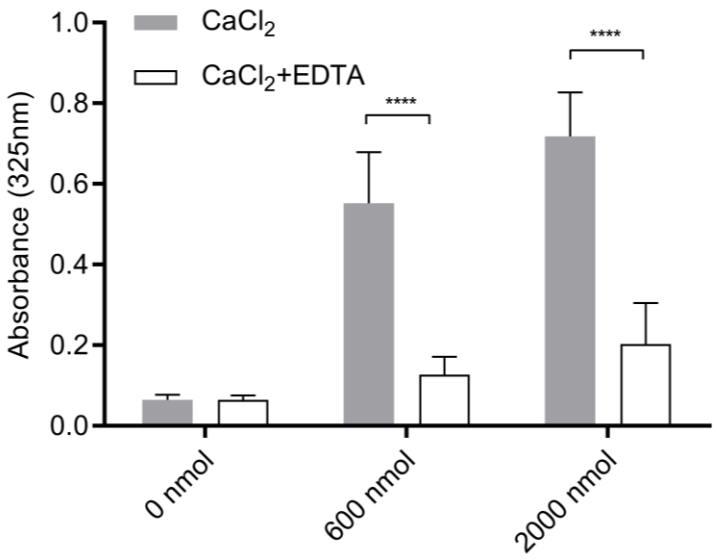

B

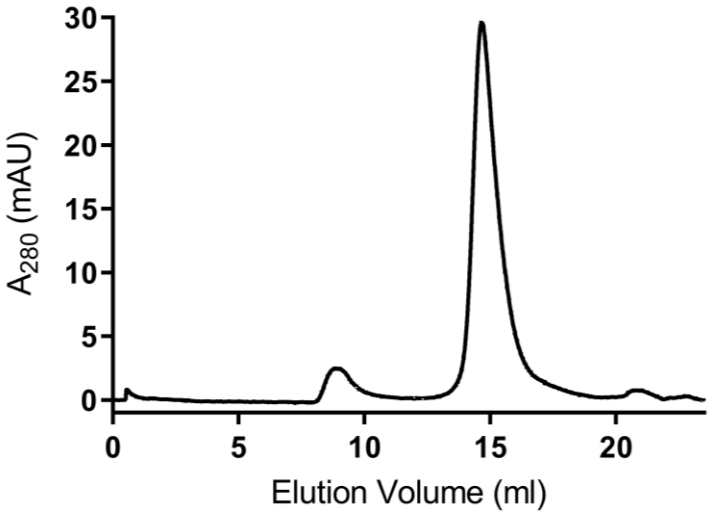

Figure 2.5. Effect of EDTA on $CaCl_2$-disrupted CL ND. A) CL ND were formulated in HEPES buffer with apoA-I and aliquots corresponding to 78 nmol CL applied to the wells of a 96 well microtiter plate. Indicated amounts of $CaCl_2$

were added and the volume adjusted to 200 µl with HEPES buffer. The plate was incubated for 1 h at 22 °C and, following incubation, sample absorbance at 325 nm was measured on a Spectramax plate reader. Subsequently, EDTA, dissolved in HEPES buffer, was added to each well to achieve a concentration equivalent to that of the added $CaCl_2$. The final volume of each well was adjusted to 300 µl and the plate incubated for an additional 1 h at 22 °C. Following incubation, sample absorbance at 325 nm was measured. Values reported are the mean ± standard error (n = 6) ****, P<0.0001 calcium-treated versus EDTA-treated. **B)** FPLC size exclusion chromatography of EDTA-treated, $CaCl_2$-disrupted CL ND. A sample of CL ND (622 nmol CL), solubilized in HEPES buffer, was incubated with 8,000 nmol $CaCl_2$ for 1 h at 22 °C to induce sample turbidity development. To this sample, 8,000 nmol EDTA was added followed by incubation for 1 h at 22 °C to induce sample clarification. The clarified sample was bath sonicated at 48 °C for 2 min followed by chromatography on a Superose 6 Increase 10/300 GL FPLC column with elution monitored at 280 nm.

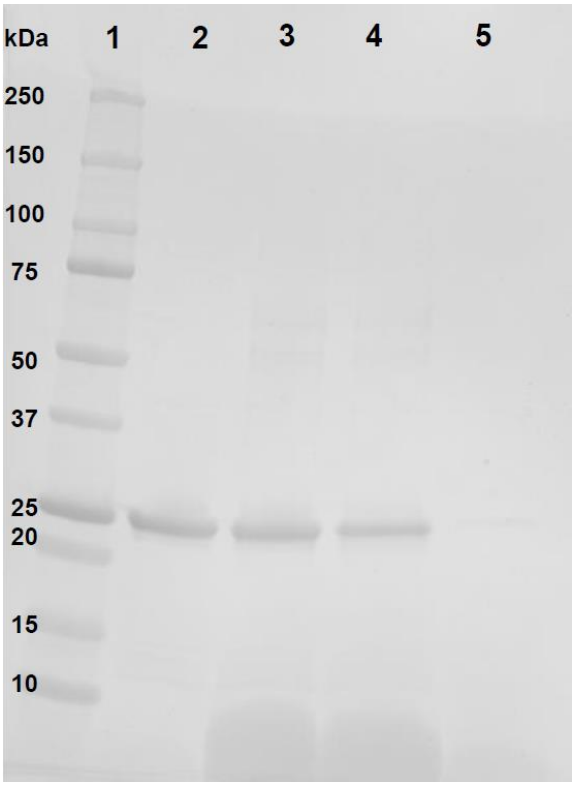

Figure 2.6 Effect of $CaCl_2$-mediated disruption of CL ND on apoA-I solubility. CL ND were formulated with apoA-I in HEPES buffer and an aliquot, corresponding to 78 nmol CL, was incubated with 2000 nmol $CaCl_2$ for 1 h at 22 °C to induce sample turbidity development. Following this, the sample was centrifuged at 14,000 × g for 2 min and the supernatant recovered. The precipitate was re-suspended in a volume of HEPES buffer equal to that of the reserved supernatant. Equivalent aliquots of the resuspended pellet and supernatant were electrophoresed on a 4–20% acrylamide gradient SDS PAGE gel and stained with GelCode Blue. Lane 1) molecular weight markers; Lane 2) apoA-I standard; Lane 3) control CL ND; Lane 4) $CaCl_2$-disrupted CL ND re-suspended pellet; Lane 5) $CaCl_2$-disrupted CL ND supernatant.

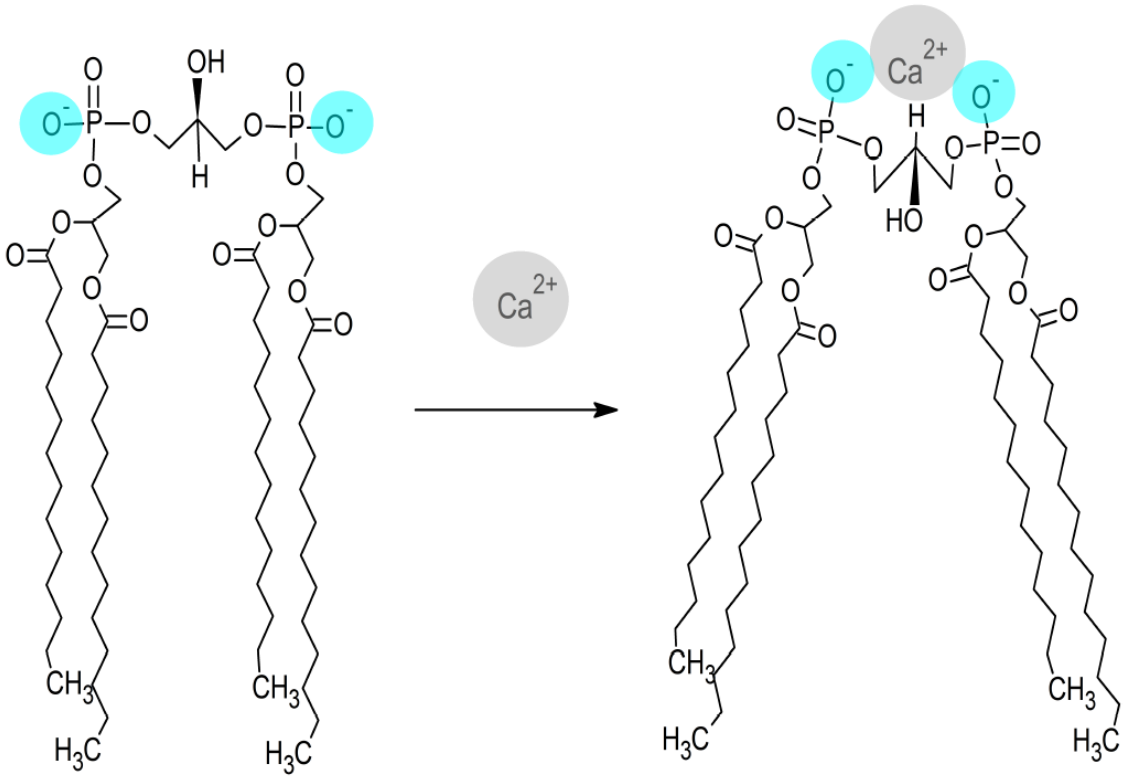

Figure 2.7 Model depicting the effect of calcium binding on CL structure. Divalent cations, such as Ca^{2+}, are attracted to the anionic polar head group of CL, forming a bidentate binding interaction with its two phosphate moieties (blue). A single calcium ion localized between these phosphates induces structural repositioning of CL in order to maximize interaction with calcium. As the phosphate moieties converge toward the calcium ion, conformational strain is relieved by realignment of the CL fatty acyl chains, which results in the adoption of a conformation that is incompatible with a bilayer state.

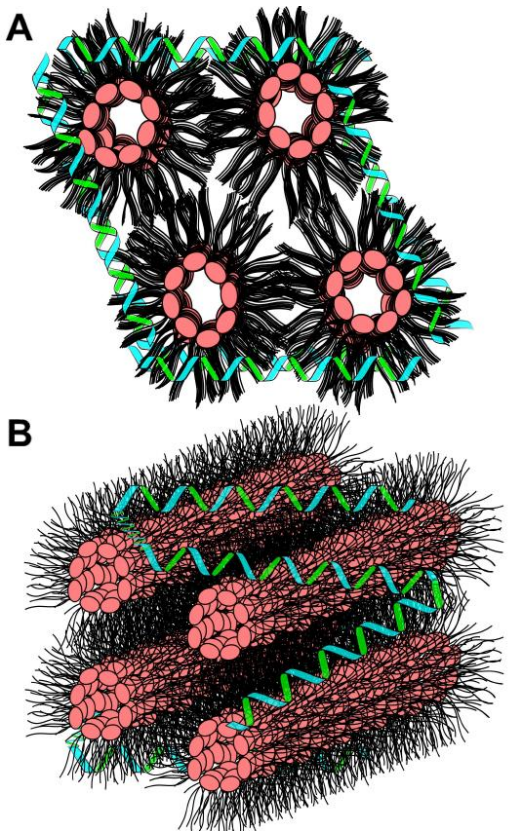

Figure 2.8 Model of $CaCl_2$-disrupted CL ND. After addition of $CaCl_2$ to CL ND, CL molecules transition to a non-bilayer state, presumably an inverted hexagonal II phase. In an inverted hexagonal II phase, the CL polar head groups (pink) align toward the center of lipid cylinders while CL fatty acyl chains (black) project into the aqueous milieu. Data presented indicates apoA-I (green/blue helices) remains associated with CL following $CaCl_2$-mediated CL ND disruption. This association most likely involves apoA-I binding to exposed CL hydrocarbon tails, thereby providing some measure of protection from direct lipid interaction with the aqueous milieu. Upper image) End on depiction of CL in an inverted hexagonal II phase with apoA-I interacting with exposed acyl chains. Lower image) CL hexagonal II phase cylinders with associated apoA-I.

Chapter 3:

Calcium-induced release of cytochrome c from cardiolipin nanodisks: implications for apoptosis

This chapter is based on work published in

Fox CA, Lethcoe K and Ryan RO, Calcium-induced release of cytochrome c from cardiolipin nanodisks: implications for apoptosis. Biochim Biophys Acta Biomembr (2021)

3.1 Abstract

Miniature bilayer membranes comprised of phospholipid and an apolipoprotein scaffold, termed nanodisks (ND), have been used in binding studies. When ND formulated with cardiolipin (CL), but not phosphatidylcholine, were incubated with cytochrome c, FPLC gel filtration chromatography provided evidence of a stable binding interaction. Incubation of CL ND with CaCl2 resulted in a concentration-dependent increase in sample turbidity caused by ND particle disruption. Prior incubation of CL ND with cytochrome c increased CL ND sensitivity to CaCl2-induced effects. Centrifugation of CaCl2-treated CL ND samples yielded pellet and supernatant fractions. Whereas the ND scaffold protein, apolipophorin III, was recovered in the pellet fraction along with CL, the majority of the cytochrome c pool was in the supernatant fraction. Moreover, when cytochrome c CL ND were incubated with CaCl2 at concentrations below the threshold to induce ND particle disruption, FPLC analysis showed that cytochrome c was released. Pre-incubation of CL ND with CaCl2 under conditions that do not disrupt ND particle integrity prevented cytochrome c binding to CL ND. Thus, competition between Ca^{2+} and cytochrome c for a common binding site on CL modulates cytochrome c binding and likely plays a role in its dissociation from CL-rich cristae membranes in response to apoptotic stimuli.

3.2 Introduction

Cytochrome c is a 104 amino acid polypeptide that possesses a covalently bound iron protoporphyrin IX (heme) prosthetic group. In animals and plants, it functions as a mitochondrial redox protein, shuttling electrons from the reducing end of Complex III to the oxidizing end of Complex IV. The function of cytochrome c as a biological electron transporter is facilitated by its heme iron, which alternates between ferrous and ferric states. As such, cytochrome c serves a vital role in cellular respiration, forming an electron bridge between substrates and oxygen. In addition to its role in the electron transport chain (ETC), cytochrome c mobilization from mitochondria to cytosol triggers a cascade of events that culminate in apoptosis [1].

In mitochondria, cytochrome c is known to bind to cardiolipin (CL). This unusual anionic glycerophospholipid possesses a relatively small polar head group and four fatty acyl chains. These structural features are responsible for its ability to exert negative curvature pressure when present in a bilayer setting [2,3]. In mitochondria, CL is enriched in the inner membrane [4], and is proposed to segregate to the inner leaflet of highly curved cristae membranes [5]. Although it is an aqueous soluble protein, cytochrome c interacts with CL in two distinct ways. First, given its basic pI (~10.0–10.5), cytochrome c forms an ionic interaction with the doubly negative charged CL polar head group [6]. In addition, it has been reported that hydrophobic interactions contribute to cytochrome c binding to CL-containing membranes [7]. In this mode of interaction, it is considered that cytochrome c partially inserts between fatty acyl chains of

membrane phospholipids [6]. Thus, under normal circumstances, cytochrome c maintains contact with CL-rich membranes [8,9], although oxidative stress [10] and ionic strength [11] are known to modulate this interaction. In addition, Wilkinson et al [12] report that CL acyl chain length, and degree of unsaturation, affect cytochrome c binding to CL. Upon exposure to various cellular stressors, however, cytochrome c is released from its membrane binding site and exits the mitochondria, an important step in the induction of apoptosis.

It has been reported [13,14] that Ca^{2+} influx into mitochondria precedes cytochrome c release, leading to the concept that this divalent cation plays a role in cytochrome c release [15,16]. The mechanism whereby intra-mitochondrial Ca^{2+} induces cytochrome c release, or its relative importance versus CL oxidation-induced cytochrome c release [17], is not clear. Given the ability of Ca^{2+} to bind CL and induce a bilayer to non-bilayer phase transition [18], it is conceivable that Ca^{2+} infiltration to the inner cristae space functions in release of cytochrome c from CL. Recently, Fox et al [19] studied the interaction of Ca^{2+} with CL-containing miniature bilayer membranes, termed nanodisks (ND). CL ND are comprised of only two components, CL and an amphipathic α-helix containing scaffold protein. Incubation of CL ND with CaCl2 leads to a concentration dependent transformation of ND from a soluble, apolipoprotein-stabilized, discoidal bilayer to an insoluble reversed hexagonal II phase [19].

Building on a recent report that cytochrome c binds to CL ND [20], it was hypothesized that Ca^{2+} can displace cytochrome c from CL. To examine the ability of Ca^{2+} to induce cytochrome c release from CL, cytochrome c CL ND

were employed as a model membrane system. The results obtained indicate that incubation with CaCl2 leads to disruption of this binding interaction, with recovery of cytochrome c as a soluble protein. Taken together, the results obtained provide novel insight into the mechanism underlying cytochrome c release from mitochondria in response to apoptotic stimuli.

3.3 Materials and Methods

Nanodisk formulation

Five mg aliquots of tetramyristoyl-cardiolipin (CL) or dimyristoylphosphatidylcholine (PC) (Avanti Polar Lipids), were dissolved in CHCl3:CH3OH (3:1 v/v) and dried under a stream of N2 gas, creating a thin film on the walls of the vessel. Following the addition of 750 µl 20 mM HEPES, pH 7.4, the sample was vortexed to hydrate and disperse the phospholipid. Two mg recombinant *Locusta migratoria* apolipophorin III (apoLp-III; [21]) in 500 µL HEPES buffer was added, followed by bath sonication at 48 °C for ~10 min. PC ND were formulated similarly, except that bath sonication was conducted at 24 °C. To prepare cytochrome c CL ND, 10 µl of a stock solution (10 mg/ml) of bovine heart cytochrome c (Sigma-Aldrich) in 20 mM HEPES, pH 7.4, was added to a sample (200 µL) of ND (800 µg as CL or PC) and incubated at 37 °C for 30 min. The resultant lipid:protein molar ratio of the cytochrome c + CL ND and cytochrome c + PC ND was 76:1 and 145:1, respectively.

FPLC Gel filtration chromatography

Samples including free cytochrome c, CL ND, PC ND, cytochrome c + PC ND and cytochrome c + CL ND, were centrifuged at 15,000 x g for 10 min. A 200 µL aliquot of each sample was diluted with an equivalent volume of 20 mM HEPES, pH 7.4, 150 mM NaCl and loaded onto a Superdex 200 Increase 10/300 GL column fitted to a GE AKTA Pure FPLC instrument. The column was eluted with 20 mM HEPES, pH 7.4, 75 mM NaCl at a flow rate of 0.75 ml/min with absorbance continuously monitored at 280 nm and collection of 2.0 ml fractions. Following chromatography, fractions corresponding to ND or free cytochrome c, respectively, were pooled and concentrated to ~200 µL using a 3 kDa MWCO centrifugal filtration device. Aliquots of each sample were subjected to SDS-PAGE on “Any kD” Mini PROTEAN precast gel (Bio-Rad) and stained with a solution (90% methanol and 10% glacial acetic acid) containing Amido Black (1 g/L) for 30 min. Gels were de-stained in a solution containing 45% water, 45% methanol, 10% glacial acetic acid. Gel images were obtained on a Bio-Rad ChemiDoc instrument. Densitometric analysis of band intensity was performed using NIH ImageJ software v1.52a [22].

Incubation of ND with CaCl2 in a microplate format

CL ND or cytochrome c CL ND (100 µg as CL; 76:1 CL to cytochrome c molar ratio) were incubated with specified amounts of CaCl2 in wells of a Greiner UV Star half well plate for 1 h at 37°C. Sample volumes were maintained at 100 µL by the addition of 20 mM HEPES, pH 7.4. Following incubation, sample turbidity was measured at 325 nm on a Spectramax plate reader. Each

microplate experiment was performed on three separate occasions with an n = 3 for each condition. The data from each experiment was compiled and statistical significance determined by two-way ANOVA followed by Dunnett's test to compare treated samples against untreated control samples. Statistical tests were performed using GraphPad Prism version 9.0.0 for Windows (GraphPad Software, San Diego, CA).

Incubation of ND with CaCl2 in a microcentrifuge tube format

CL ND or cytochrome c CL ND (equivalent to 100 μg CL) were incubated with 12 mol CaCl2 per mol CL at 37 °C for 1 h in a 1.5 mL microcentrifuge tube to induce ND particle disruption [19]. Following incubation, samples were centrifuged at 2,000 x g for 5 min to pellet insoluble material. The supernatant was reserved and the pellet re-suspended in an equal volume of HEPES buffer. Aliquots of each sample were then analyzed by SDS PAGE. In other experiments, cytochrome c CL ND were incubated with 1 mol CaCl2 per 3 mol CL at 37 °C for 1 h. Following incubation, the sample was subjected to FPLC gel filtration chromatography and aliquots of specified elution fractions analyzed by SDS PAGE.

In a variation of this experiment, CL ND were prepared and incubated with CaCl2(1 mol CaCl2 per 3 mol CL) for 1 h at 37 °C prior to incubation with cytochrome c for an additional 1 h at 37 °C. Following incubation, the sample was subjected to FPLC gel filtration chromatography and aliquots of indicated elution fractions analyzed by SDS PAGE.

3.4 Results

Interaction of cytochrome c with CL ND

To test the hypothesis that CL ND can serve as a water soluble, nanoscale model bilayer membrane for studies of CL - cytochrome c interactions, FPLC gel filtration chromatography experiments were performed. Control CL ND eluted in a single peak (designated Peak I) centered at 8.6 ml (**Figure 3.1A**). When isolated bovine heart cytochrome c (MW = 13 kDa) was subjected to FPLC gel filtration chromatography (**Figure 3.1B**), it eluted as a single peak centered at 19.0 ml (Peak II). Thus, apoLp-III-containing CL ND and free cytochrome c are well separated by this FPLC gel filtration chromatography protocol. When CL ND were incubated with cytochrome c for 30 min prior to FPLC, the absorbance intensity of Peak I increased and shifted slightly toward higher molecular weight (elution volume = 8.2 ml) (**Figure 3.1C**) while no absorbance was detected in the region corresponding to Peak II. SDS-PAGE of material eluting in Peak I revealed that apoLp-III and cytochrome c co-elute in Peak I (**Figure 3.1D**). Based on these results, it is evident that apoLp-III (MW = 17 kDA) and cytochrome c can be distinguished on the basis of their electrophoretic mobility and that cytochrome c forms a binding interaction with CL ND that is stable during FPLC.

To examine the specificity of the binding interaction between cytochrome c and CL ND, PC was used in lieu of CL to formulate ND. When PC ND were subjected to FPLC gel filtration chromatography, the elution pattern was similar to that observed for CL ND, with a single absorbance peak centered at 8.7 ml

(Peak I) (**Figure 3.2A**). When cytochrome c was incubated with PC ND, FPLC analysis revealed two absorbance peaks, one corresponding to CL ND (Peak I) and the other to free cytochrome c (Peak II) **(Figure 3.2B)**. When aliquots of each peak were subjected to SDS PAGE, Peak I was found to contain the ND scaffold protein, apoLp-III, while Peak II contained cytochrome c (**Figure 3.2C**). Thus, it may be concluded that, whereas cytochrome c binds to CL ND, it does not bind to PC ND.

Effect of cytochrome c on CL ND susceptibility to CaCl2-induced particle disruption

In a previous study, Fox et al [19] showed that CaCl2 induces CL ND to undergo a bilayer to non-bilayer phase transition, with CL adopting an insoluble reverse hexagonal II phase. To determine if this reaction is affected by cytochrome c association with ND, control CL ND and cytochrome c CL ND were incubated with increasing amounts of CaCl2 for 1 h, followed by measurement of sample turbidity at 325 nm (**Figure 3.3**). The amount of CaCl2 required to induce a statistically significant increase in ND sample turbidity was 100 nmol (~1.3 mol CaCl2 per 1 mol CL) for control CL ND and 50 nmol (~0.65 mol CaCl2 per 1 mol CL) for cytochrome c CL ND. Thus, cytochrome c binding to CL increases ND particle susceptibility to CaCl2-induced bilayer disruption.

Partitioning of apoLp-III and cytochrome c following CaCl2-induced CL ND particle disruption.

To examine the fate of CL ND-associated proteins following particle disruption, control CL ND and cytochrome c CL ND were incubated with 12 mol CaCl2 per mol CL. This amount of CaCl2 is in excess of that required to induce ND particle disruption, as evidenced visually by near immediate sample turbidity development. Centrifugation of the turbid samples yielded pellet and supernatant fractions, which were then analyzed by SDS-PAGE (**Figure 3.4**). The apoLp-III scaffold protein component of CL ND was recovered exclusively in the pellet fraction following CaCl2-dependent disruption of either CL ND or cytochrome c CL ND. In the latter sample, however, a large portion of the cytochrome c partitioned to the supernatant fraction. Thus, whereas apoLp-III remains bound to CL following CaCl2-induced disruption of cytochrome c CL ND, ~75 % of the cytochrome c was recovered in the supernatant fraction.

CaCl2-induced cytochrome c release in the absence of ND particle disruption

Cytochrome c CL ND were formulated and incubated with CaCl2 at a 1:3 (mol/mol) ratio of Ca^{2+} to CL, a concentration below the threshold for ND particle disruption. Following incubation, the sample remained clear and no material precipitated upon centrifugation. Subsequent analysis by FPLC gel filtration chromatography revealed 2 absorbance peaks (I and II) (**Figure 3.5A**). Analysis of these fractions by SDS-PAGE (**Figure 3.5B**) revealed that Peak I contained apoLp-III, while Peak II contained cytochrome c. Thus, ND membrane disruption is not required for CaCl2 to induce cytochrome c release from CL ND. Moreover,

because a saturated molecules species of CL was used, release of cytochrome c cannot be attributed to oxidation-induced effects [17].

Effect of pre-incubation with CaCl2 on cytochrome c binding to CL ND

To assess whether Ca^{2+} and cytochrome c compete for the same binding site on CL, CL ND were preincubated with CaCl2 at a 1:3 (mol/mol) ratio of Ca^{2+} to CL. Following this, the sample was incubated with cytochrome c. Under these conditions the sample remained clear and no material precipitated upon centrifugation. FPLC analysis (**Figure 3.6A**) revealed the presence of two absorbance peaks (I and II) and SDS-PAGE analysis (**Figure 3.6B**) indicated that Peak I contained apoLp-III, while Peak II contained cytochrome c. Thus, pre-incubation with CaCl2 prevents cytochrome c binding to CL ND, consistent with the conclusion that both ligands are attracted to the same binding site on CL, for which Ca^{2+} has higher affinity.

3.5 Discussion

Cytochrome c plays a fundamental role in aerobic respiration, shuttling electrons from Complex III to Complex IV of the ETC. In so doing, cytochrome c maintains contact with the inner leaflet of cristae membranes by binding to CL. In the present study, nanoscale model membranes (i.e. ND) [23], were used to investigate the interaction between CL and cytochrome c. CL ND provide a novel platform to characterize aspects of this interaction because these water soluble nanoparticles contain only two components: CL and apoLp-III. The apoLp-III

scaffold protein circumscribes the perimeter of a disk-shaped CL bilayer, interacting with CL fatty acyl chains at the edge of the particle. Similar to other members of the class of amphipathic exchangeable apolipoproteins [24], apoLp-III exists as an amphipathic α-helix bundle in the absence of lipid, while, upon interaction with lipid it undergoes a conformational change, adopting an extended open conformation. In this latter state, apoLp-III amphipathic α-helices orient with their hydrophobic faces toward the lipid milieu while their opposing, hydrophilic faces, are directed toward the aqueous environment. In this way, the otherwise exposed edge of this disk-shaped bilayer is stabilized and supported.

Consistent with the findings of Steele et al [20], when these aqueous soluble, CL rich, miniature membranes were incubated with cytochrome c, evidence of a stable binding interaction was obtained. On the other hand, in studies with PC ND, no cytochrome c binding was detected. Thus, as in cristae membranes, cytochrome c binding to ND is dependent upon the presence of CL. Vesicles have been used extensively to study the interaction between cytochrome c and CL. Previous studies have shown that binding occurs anywhere from a 5:1 to 1000:1 CL:cytochrome c, although the ratio used appears to affect the mode of binding [25]. In the present study, a 76:1 molar ratio of CL to cytochrome c was found to be stable and, thus, was used for all experiments. In a previous study [19], CL ND were shown to be susceptible to $CaCl_2$-induced ND particle disruption. A model of the binding interaction between Ca^{2+} and CL was presented that depicts a bidentate interaction between the positively charged Ca^{2+} and the two negatively charged phosphates in the polar head

group of CL. When Ca^{2+} binds, the phosphates pinch in around this divalent cation to optimize the interaction, thereby forcing CL's four fatty acyl chains apart. When a sufficient number of CL molecules adopt this orientation, a bilayer state can no longer be maintained. Counteracting this Ca^{2+}-induced conformational change in ND-associated CL is apoLp-III, which functions in a belt-like manner to maintain particle integrity. As more Ca^{2+} binds to CL ND, however, the ability of apoLp-III to stabilize the ND bilayer is overcome, resulting in particle disruption.

Compared to CL ND, cytochrome c CL ND display increased susceptibility to CaCl2-induced particle disruption. Given this finding, we sought to determine if exposure to Ca^{2+} induces release of cytochrome c. When cytochrome c CL ND were disrupted by incubation with CaCl2, apoLp-III was recovered in the insoluble pellet fraction along with CL, while the bulk of cytochrome c dissociated from CL and was recovered in the soluble supernatant. This result prompted the question whether CaCl2 concentrations below the threshold required to disrupt CL ND can also lead to cytochrome c dissociation. The results obtained showed complete release of cytochrome c from CL ND by CaCl2, despite the fact that ND particle structure was maintained. In addition, when CL ND were preincubated with CaCl2 prior to incubation with cytochrome c, evidence was obtained that cytochrome c and Ca^{2+} compete for the same binding site on CL. Thus, when Ca^{2+} is present, cytochrome c association with CL is prevented.

In an earlier study, de Kruijff and Cullis [26] reported that cytochrome c interaction with CL liposomes induced formation of a non-bilayer, hexagonal II

phase. The mechanism underlying this transition is not known but appears to be related to the ability of cytochrome c to penetrate the liposomal bilayer. Similar results were not observed in the present study and cytochrome c binding had no apparent effect (other than enhanced sensitivity to CaCl2-mediated particle disruption) on the structure or stability of the CL ND particles. It may be that cytochrome c interacts with CL ND in such a manner that it is unable to penetrate the bilayer. The cytochrome c - CL complexes employed in [26] were large particles that could be recovered by low speed centrifugation. By contrast, CL ND represent a discrete, planar nanoscale bilayer wherein the scaffold protein may constrain the ability of cytochrome c to penetrate, and thereby disrupt, ND particle structure. It is clear, however, that Ca^{2+} can overcome the stabilizing effects of the scaffold protein, inducing formation of a non-bilayer phase that is accompanied by ND particle disruption.

The present study represents the first direct demonstration that Ca^{2+} induces cytochrome c release from a CL-rich model bilayer membrane. As such, these findings have implications with respect to release of cytochrome c during apoptosis [27]. Despite the fact that cytochrome c escape from mitochondria is central to intrinsic apoptosis, details of how this occurs remain obscure. It is conceivable that multiple factors modulate cytochrome c dissociation from cardiolipin and subsequent release from the inner cristae space. For example, aside from Ca^{2+} dependent effects, oxidation of CL has been shown to reduce its affinity for cytochrome c [17]. Oxidation can occur through a variety of pathways including production of reactive oxygen species or conformational changes in

cytochrome c [27]. Using isolated permeabilized mitochondria, Uren et al [28] reported that, whereas cytochrome c was not released under low ionic strength conditions, upon transition to 50-80 mM KCl, NaCl or LiCl cytochrome c release occurred.

It is generally accepted that cytochrome c localizes to the inner cristae space of mitochondria, where it maintains contact with this CL-enriched membrane [8, 27]. Cristae membranes exist as narrow (~ 30 nm diameter), extended tubular invaginations of the inner boundary membrane that project into the matrix space (**Figure 3.7A**). Given the high radius of curvature of these cylinder-shaped bilayers, a specialized phospholipid composition is required to maintain cristae membrane structural integrity [5]. As a component of the negatively curved, inner leaflet of cristae membranes, CL plays an important structural role. It is in this environment that ETC complexes reside and where aerobic respiration / oxidative phosphorylation take place. The enclosed inner cristae space is the site of hydrogen ion accumulation, generating the proton motive force that drives ADP phosphorylation. In this confined space, an electrochemical gradient is established despite the apparent confluence of the inner cristae space with the intermembrane space. Indeed, the inner cristae space and cristae membrane can be regarded as “privileged”, such that solutes / lipids / transmembrane proteins from the adjacent intermembrane space / inner boundary membrane cannot freely diffuse from one region to the other. Perhaps the clearest example of this is the proton gradient that drives ATP synthesis. If protons that accumulate in the inner cristae space were able to diffuse into

the inter-membrane space, the gradient would rapidly dissipate, thereby diminishing aerobic ATP production efficiency. Just as it is with protons, the same is true for proteins and ions such as Ca^{2+}. Under normal conditions, cytochrome c remains localized to the inner cristae space while Ca^{2+} is excluded from this space. As reported herein, when Ca^{2+} gains access to CL-bound cytochrome c, competition for their common binding site results in cytochrome c displacement.

Given the need to prevent solute diffusion between the inter-membrane space / inner boundary membrane and the inner cristae space / cristae membrane, several distinct processes likely contribute to this compartmentalization phenomenon. First, the mitochondrial contact site and cristae organizing system (MICOS), a large heterooligomeric protein complex, functions in formation and maintenance of cristae junctions [29]. Cristae junctions are characterized by a 90° turn in the inner boundary membrane, redirecting it into the matrix space. Recall that each cristae invagination is a cylinder shaped membrane that can span nearly the entire width of a mitochondrion. By maintaining cristae junction stability, the MICOS complex exerts influence over the entire length of the cristae membrane. It may also be considered that MICOS represents a physical bottleneck capable of hindering / preventing solute diffusion into, or out of, the inner cristae space.

A second factor involved in cristae structural maintenance and, presumably, its barrier function, is the dynamin-like GTPase, OPA1. Also known to modulate mitochondrial fusion, OPA1 maintains cristae membrane integrity

through formation of oligomeric complexes comprised of the membrane-bound long form, L-OPA1, and the truncated short form, S-OPA1 [30]. In this manner, OPA1 oligomers span the diameter of the cylindrical crista membrane and, thereby, modulate the aperture of the cristae junction. It is likely that OPA1 oligomers stabilize the cylindrical membrane to which they are attached and control the diameter of this tubular membrane structure.

A third component that maintains, and regulates, the structural integrity of cristae are prohibitin (PHB) rings [31]. PHB rings are created by oligomerization of 16-20 copies of alternating PHB1 and PHB2 subunits, wherein each subunit of the ring is embedded in the inner leaflet of the cristae membrane via an N-terminal hydrophobic domain. The barrier function of PHB ring structures (25 nm dimeter) most likely arises from their ability to encircle the circumference of the inner leaflet of cristae membranes (~30 nm) [5]. Since each PHB subunit independently maintains contact with the cristae membrane while interacting with adjacent subunits, PHB rings are well-designed to serve a scaffold function that defines distinct cristae sub-compartments [32]. In this capacity PHB rings can limit diffusion of membrane lipids and solutes throughout the length of tubular cristae structures. Given that PHBs are known to interact with other proteins [33], it is conceivable that members of the PHB interactome function to regulate protein / ion diffusion within the inner cristae space [34].

When these systems are in place and functioning, aerobic respiration can proceed optimally because cytochrome c is free to participate in the ETC, leading to establishment of a proton gradient within the confines of the inner cristae

space. In response to apoptotic stimuli, however, structural changes to mitochondria lead to a breakdown of cristae compartmentalization (**Figure 3.7B**). This includes 1) mitochondrial outer membrane permeabilization; 2) disruption of the diffusion barrier between the inter-membrane space and the inner cristae space; 3) dissipation of the electrochemical gradient across the cristae membrane; 4) breach of the inner cristae space by Ca^{2+} ions; 5) displacement of CL-bound cytochrome c by Ca^{2+}; 6) mobilization of cytochrome c from the inner cristae space into the inter-membrane space and out from mitochondria via pores in the outer membrane and 7) cytochrome c-dependent activation of apoptosis.

When an apoptotic stimulus (e.g. DNA damage) is received, it is followed by permeabilization of the outer mitochondrial membrane. This process, termed mitochondrial outer membrane permeabilization, occurs via controlled interplay between anti-apoptotic BCL-2 protein family members and pro-apoptotic BH3 protein family members, notably BCL-2-associated X protein (BAX) and BCL-2 homologous antagonist killer (BAK) [13,35]. Normally, BAX and BAK are sequestered by anti-apoptotic members of the BCL-2 family. As BCL-2 protein family member binding to BAX and BAK is reduced, BAK-BAX oligomers assemble and, in combination with t-Bid, form pores in the outer mitochondrial membrane [36].

In concert with permeabilization of the outer membrane, the inner cristae space diffusion barrier breaks down, permitting dissipation of the proton gradient and diffusion of Ca^{2+} into the inner cristae space. In a normal functioning mitochondrion, Ca^{2+} concentration is tightly controlled and, although it may be

present in the matrix and intermembrane space at concentrations up to 100 nM [37,38], it is largely excluded from the privileged inner cristae space. The same factors that prevent proton escape from the inner cristae space also prevent Ca^{2+} entry. When systems that regulate cristae integrity / structure / morphology break down, and Ca^{2+} gains entry to the inner cristae space, cytochrome c displacement from the CL-rich inner cristae membrane follows. Consistent with this, unregulated Ca^{2+} entry into mitochondria is a known trigger of apoptosis [39,40].

Upon displacement from its membrane docking site, cytochrome c is free to migrate to the inter-membrane space and out of the organelle through BAX/BAK pores [41-43]. Once it reaches the cytosol, cytochrome c binds to apoptosis-protease activating factor 1 which leads to recruitment of pro-caspase 9 and formation of apoptosomes [44,45]. Within the apoptosome, pro-caspase 9 is converted to caspase-9. Ultimately, apoptosome formation results in the activation of executioner caspases 3 and 7, which cleave proteins required for normal cell function. When this occurs, changes to the plasma membrane and cell morphology ensue, leading to macrophage recognition [35].

In summary, CL ND provide an aqueous soluble miniature membrane that serves as a binding site for cytochrome c. Using this system, it was demonstrated that Ca^{2+} triggers dissociation of cytochrome c from CL ND. This finding has potential implications with respect to the mechanism of cytochrome c mobilization from mitochondria during apoptosis. The concept that Ca^{2+} infiltration to the inner cristae space is sufficient to displace cytochrome c from

membrane association provides an explanation for how cytochrome c mobilization is triggered. Although further investigation is required to extend findings obtained with CL ND, it is clear that interplay between Ca^{2+}, cytochrome c and CL constitutes a nexus for regulation of mitochondrial function.

3.6 References

[1] Bock FJ, Tait SWG, Mitochondria as multifaceted regulators of cell death. Nat. Rev. Mol. Cell Biol. 21 (2020) 85-100.

[2] Renner LD, Weibel DB, Cardiolipin microdomains localize to negatively curved regions of *Escherichia coli* membranes. Proc. Natl. Acad. Sci. USA. 108 (2011) 6264-6269.

[3] Beltran-Heredia E, Tsai FC, Salinas-Almaguer S, Cao FJ, Bassereau P, Monroy F, Membrane curvature induces cardiolipin sorting. Commun. Biol. 20 (2019) 225.

[4] Horvath SE, Daum G, Lipids of mitochondria. Prog. Lipid Res. 52 (2013) 590-614.

[5] Ikon N, Ryan RO, Cardiolipin and mitochondrial cristae organization. Biochim. Biophys. Acta Biomembr. 1859 (2017) 1156-1163.

[6] Hanske J, Toffey JR, Morenz, Bonilla AJ, Schiavonni KH, Pletneva EV, Conformational properties of cardiolipin-bound cytochrome c. Proc. Natl. Acad. Sci. USA. 109 (2012) 125-130.

[7] Bergstrom CL, Beales PA, Lv Y, Vanderlick TK, Groves JT, Cytochrome c causes pore formation in cardiolipin-containing membranes. Proc. Natl. Acad. Sci. USA. 110 (2013) 6269-6274.

[8] Gogvadze V, Orrenius S, Zhivotovsky B, Multiple pathways of cytochrome c release from mitochondria in apoptosis. BBA Bioenergetics. 1757 (2006) 639-647.

[9] Gonzalvez F, Gottlieb E, Cardiolipin: setting the beat of apoptosis. Apoptosis. 12 (2007) 877-885.

[10] Ott M, Zhivotovsky B, Orrenius S, Role of cardiolipin in cytochrome c release from mitochondria. Cell Death Differ. 14 (2007) 1243-1247.

[11] Ott M, Robertson JD, Gogvadze V, Zhivotovsky B, Orrenius S, Cytochrome c release from mitochondria proceeds by a two-step process. Proc. Natl. Acad. Sci. USA. 99 (2002) 1259-1263.

[12] Wilkinson JA, Silvera S, LeBlanc PJ. The effect of cardiolipin side chain composition on cytochrome c protein conformation and peroxidase activity. Physiol Rep. 9 (2021) e14772.

[13] Rizzuto R, Pinton P, Ferrari D, Chami M, Szabadkai G, Megalgaes PJ, Di Virgilio F, Pozzan T, Calcium and apoptosis: facts and hypotheses. Oncogene. 22 (2004) 8619-8627.

[14] Mattson MP, Chan SL, Calcium orchestrates apoptosis. Nat. Cell Biol. 5 (2003) 1041-1043.

[15] Huang Y, Liu L, Shi C, Huang J, Li G, Electrochemical analysis of the effect of Ca^{2+} on cardiolipin-cytochrome c interaction. Biochim. Biophys. Acta. 1760 (2006) 1827-1830.

[16] Hwang MS, Schwall CT, Pazarentzos E, Datler E, Alder NN, Grimm S, Mitochondrial Ca($^{2+}$) influx targets cardiolipin to disintegrate respiratory chain complex II for cell death induction. Cell Death Differ. 21 (2014) 1733-1745.

[17] Kagan VE, Tyurin VA, Jiang J, Tyurina YY, Ritov VB, Amoscato AA, Osipov AN, Belikova NA, Kapralov AA, Kini V, Vlasova II, Zhao Q, Zou M, Di P, Svistunenko DA, Kurnikov IV, Borisenko GG, Cytochrome c acts as a cardiolipin oxygenase required for release of proapoptotic factors. Nat. Chem. Biol. 1 (2005) 223-232.

[18] Rand RP, Sengupta S, Cardiolipin forms hexagonal structures with divalent cations. Biochim. Biophys. Acta 255 (1972) 484-492.

[19] Fox CA, Ikon N, Ellison P, Ryan RO, Calcium induced transformation of cardiolipin nanodisks. Biochim. Biophys. Acta Biomembr. 1861 (2019) 1030-1036.

[20] Steele HBB, Elmer-Dixon MM, Rogan JT, Ross JBA, Bowler BE, The human cytochrome c domain-swapped dimer facilitates tight regulation of intrinsic apoptosis. Biochemistry. 59 (2020) 2055-2068.

[21] Weers PMM, Wang J, Van der Horst DJ, Kay CM, Sykes BD, Ryan RO, Recombinant locust apolipophorin III: characterization and NMR spectroscopy. Biochim. Biophys. Acta. 1393 (1998) 99-107.

[22] Schneider CA, Rasband WS, Eliceiri KW, NIH Image to ImageJ: 25 years of image analysis. Nat. Methods. 9 (2012) 671-675.

[23] Ryan RO, Nanobiotechnology applications of reconstituted high density lipoprotein. J. Nanobiotechnology. 8 (2010) 28.

[24] Narayanaswami V, Ryan RO, Molecular basis of exchangeable apolipoprotein function. Biochim. Biophys. Acta. 1483 (2000) 15-36.

[25] Schweitzer-Stenner R. Relating the multi-functionality of cytochrome c to membrane binding and structural conversion. Biophys Rev. 10, (2018), 1151-1185.

[26] de Kruijff B, Cullis PR, Cytochrome c specifically induces non-bilayer structures in cardiolipin-containing model membranes. Biochim Biophys Acta. 602 (1980) 477-490.

[27] Ow YP, Green DR, Hao Z, Mak TW, Cytochrome c functions beyond respiration. Nat. Rev. Mol. Cell Biol. 9 (2008) 532-542.

[28] Uren RT, Dewson G, Bonzon C, Lithgow T, Newmeyer DD, Kluck RM, Mitochondrial release of pro-apoptotic proteins:electrostatic interactions can hold cytochrome c but not Smac/DIABLO to mitochondrial membranes. J. Biol. Chem. 280 (2005) 2266-2274.

[29] Kondadi AK, Anand R, Reichert AS, Cristae Membrane Dynamics - A Paradigm Change. Trends Cell Biol. 30 (2020) 923-936.

[30] Frezza C, Cipolat S, Martins de Brito O, Micaroni M, Beznoussenko GV, Rudka T, Bartoli D, Polishuck RS, Danial NN, De Strooper B, Scorrano L, OPA1

controls apoptotic cristae remodeling independently from mitochondrial fusion. Cell. 126 (2006) 177-189.

[31] Merkwirth C, Langer T, Prohibitin function within mitochondria: essential roles for cell proliferation and cristae morphogenesis. Biochim. Biophys. Acta. 1793 (2009) 27- 32.

[32] Osman C, Merkwirth C, Langer T, Prohibitins and the functional compartmentalization of mitochondrial membranes. J. Cell Sci. 122 (2009) 3823-30.

[33] Richter-Dennerlein R, Korwitz A, Haag M, Tatsuta T, Dargazanli S, Baker M, Decker T, Lamkemeyer T, Rugarli EI, Langer T, DNAJC19, a mitochondrial cochaperone associated with cardiomyopathy, forms a complex with prohibitins to regulate cardiolipin remodeling. Cell Metab. 20 (2014) 158-171.

[34] Peng TY, Chen P, Ouyang RY, Song L, Multifaceted role of prohibitin in cell survival and apoptosis. Apoptosis. 20 (2015) 1135-1149.

[35] Pfeffer CM, Singh ATK, Apoptosis: a target for anticancer therapy. Int. J. Mol. Sci. 19 (2018) 448.

[36] Orrenius S, Gogzadze V, Zhivotovsky B, Calcium and mitochondria in the regulation of cell death. Biochem. Biophys. Res. Commun. 460 (2015) 72-81.

[37] Giorgi C, Marchi S, Pinton P, The machineries, regulation and cellular functions of mitochondrial calcium. Nat. Rev. Mol. Cell Biol. 19 (2018) 713-730.

[38] Atchison DK, Beierwaltes WH, The influence of extracellular and intracellular calcium on the secretion of renin. Pflugers Arch. 465 (2013) 56-69.

[39] Sattler R, Tymianski M, Molecular mechanisms of calcium-dependent excitotoxicity. J. Mol. Med. 78 (2000) 3-13.

[40] Giorgi C, Baldassari F, Bononi A, Bonora M, De Marchi E, Marchi S, Missiroli S, Patergnani S, Rimessi A, Suski JM, Wieckowski MR, Pinton P, Mitochondrial Ca^{2+} and apoptosis. Cell Calcium. 21 (2012) 36-43.

[41] Green DR, Llambi F, Cell Death Signaling. Cold Spring Harb. Perspect. Biol. 7 (2015) a006080.

[42] Taylor RC, Cullen SP, Martin SJ, Apoptosis: controlled demolition at the cellular level. Nat. Rev. Mol. Cell Biol. 9 (2008) 231-241.

[43] Singh R, Letai A, Sarosiek K, Regulation of apoptosis in health and disease: the balancing act of BCL-2 family proteins. Nat. Rev. Mol. Cell Biol. 20 (2019) 175-193.

[44] Elmore S, Apoptosis: A Review of Programmed Cell Death. Toxicol. Pathol. 35 (2007) 495-516.

[45] Pinton P, Giorgi C, Siviero R, Zecchini E, Rizzuto R, Calcium and apoptosis: ER-mitochondria Ca^{2+} transfer in the control of apoptosis. Oncogene. 27 (2008) 6407-6418.

3.7 Figures and Figure Legends

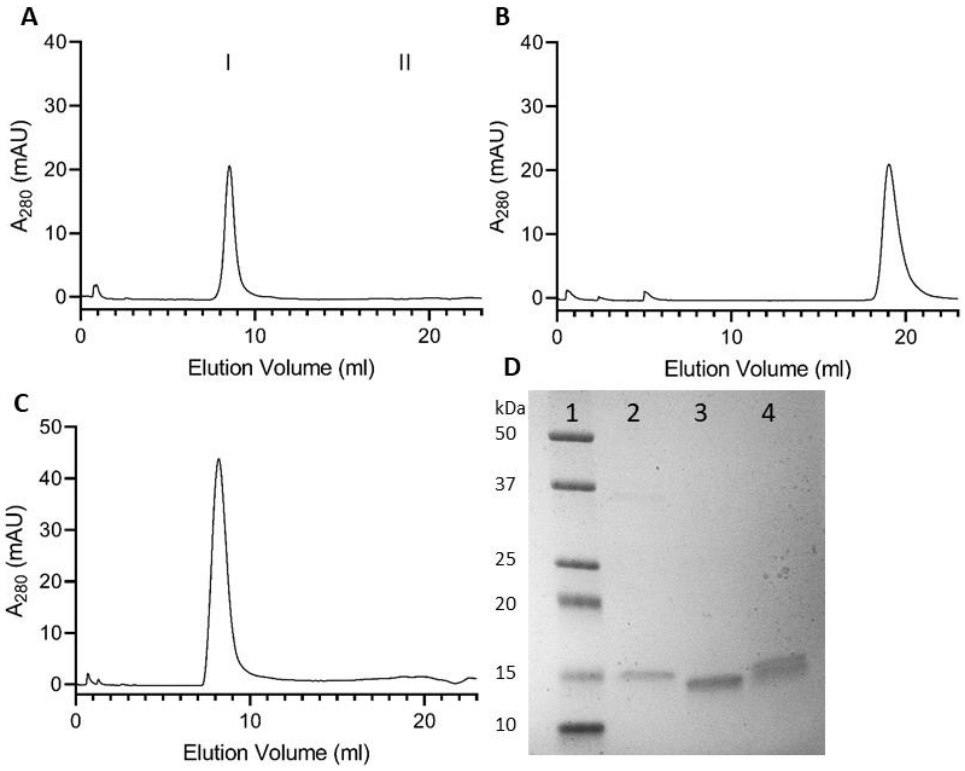

Figure 3.1 Interaction of cytochrome c with CL ND. A) FPLC gel filtration chromatography of CL ND (800 µg as CL); B) FPLC gel filtration chromatography of cytochrome c (100 µg), C) FPLC gel filtration chromatography of CL ND (800 µg) and cytochrome c (100 µg) following 30 min incubation at 37 °C. Samples were applied to a Superdex 200 increase 10/300 column with elution absorbance monitored at 280 nm and collection of 2.0 ml fractions. D) Fractions corresponding to either Peak I (8-10 mL) or Peak II (18-20 mL) were concentrated using a centrifugal filtration device and aliquots analyzed by SDS PAGE. Lane 1) molecular weight markers; Lane 2) Peak I from Panel A; Lane 3) Peak II from Panel B and Lane 4) Peak I from Panel C.

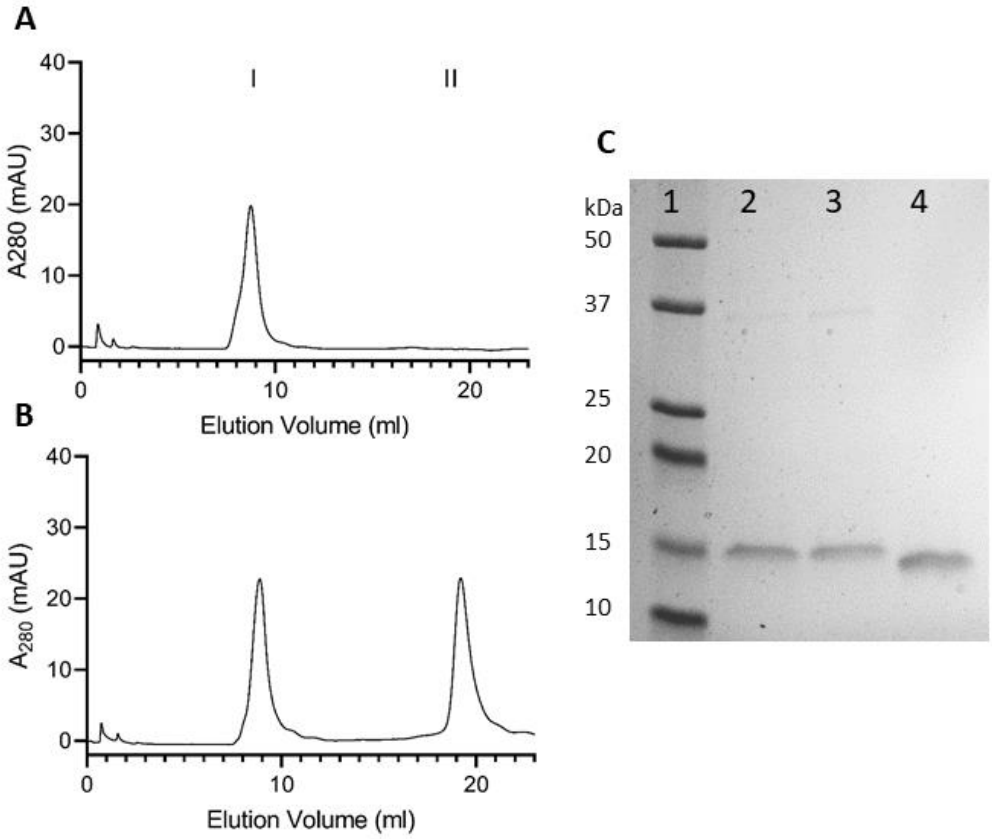

Figure 3.2 Incubation of cytochrome c with PC ND. A) FPLC gel filtration chromatography of PC ND (800 µg as PC); B) FPLC gel filtration chromatography of PC ND (800 µg) and cytochrome c (100 µg) following 30 min incubation at 37 °C. Samples were applied to a Superdex 200 increase 10/300 column with elution absorbance monitored at 280 nm and collection of 2.0 ml fractions. Fractions corresponding to either Peak I (8-10 mL) or Peak II (18-20 mL) were concentrated using a centrifugal filtration device and aliquots analyzed by SDS PAGE (Panel C). Lane 1) Molecular weight markers; Lane 2) Peak I from Panel A; Lane 3) Peak 1 from Panel B and Lane 4) Peak II from Panel B.

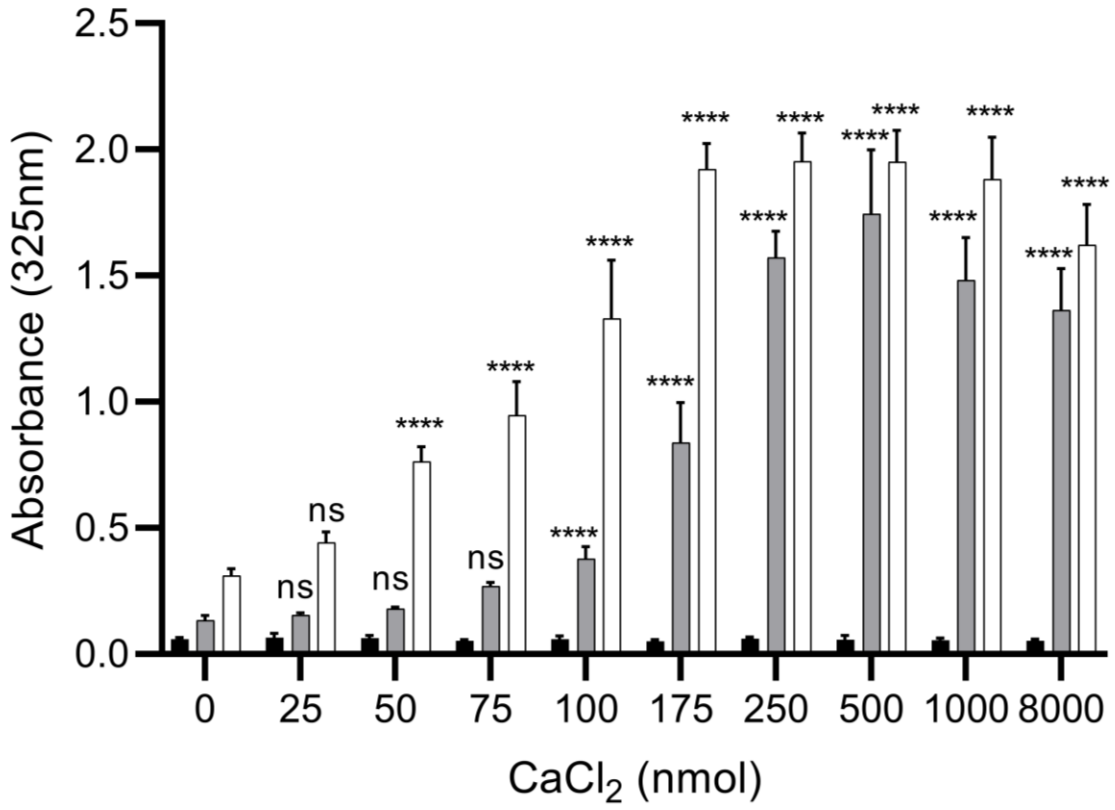

Figure 3.3. Effect of CaCl2 on cytochrome c ND sample integrity. CL ND (100 µg as CL), cytochrome c CL ND (100 µg as CL; 76:1 CL to cytochrome c molar ratio) or buffer alone, were introduced to the wells of a microtiter plate. Subsequently, indicated amounts of CaCl2 were added to each well and the final volume adjusted to 100 µL with 20 mM HEPES, pH 7.4. Following incubation for 1 h at 37°C, sample absorbance was measured at 325 nm on a Spectramax plate reader. Black bars) buffer only; Grey bars) CL ND, and White bars) cytochrome c CL ND. Values reported are the mean ± standard error (n=9). ****, P<0.0001 versus 0 nmol CaCl2 treated controls.

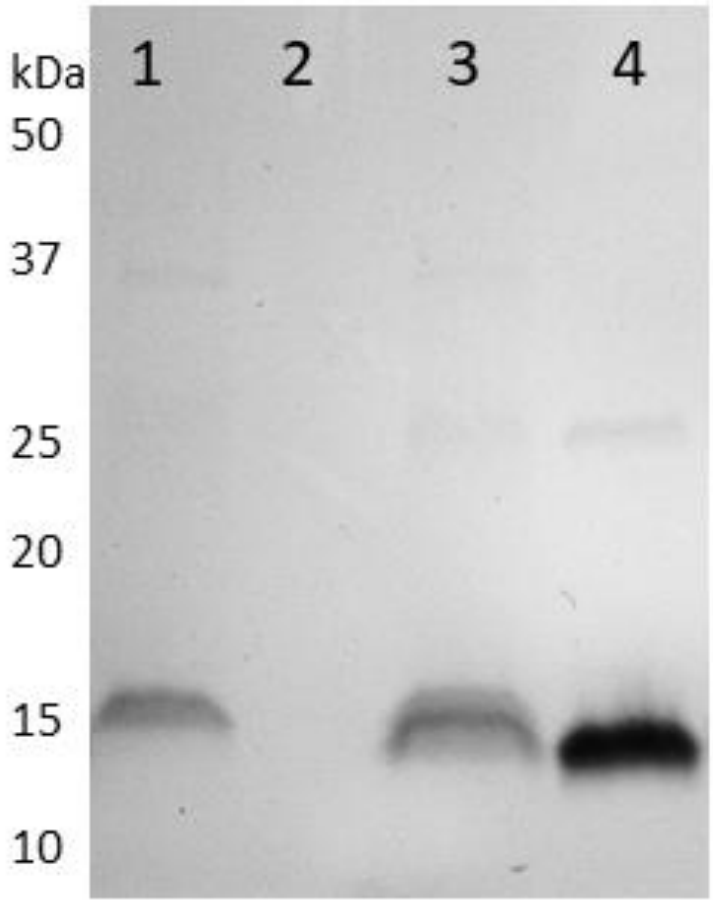

Figure 3.4 Partitioning of apoLp-III and cytochrome c following CaCl2-induced ND disruption. CL ND or cytochrome c CL ND were incubated with CaCl2 at a 12:1 ratio of Ca^{2+}:CL (mol/mol). Following incubation for 1 h at 37°C, the samples were centrifuged at 2,000 x g for 5 min to pellet insoluble material. The supernatant was recovered and the pellet resuspended in an equal volume of HEPES buffer. Aliquots of each sample were then analyzed by SDS PAGE. Lane 1) CL ND pellet fraction; Lane 2) CL ND supernatant; Lane 3) cytochrome c CL ND pellet fraction; Lane 4) cytochrome c CL ND supernatant.

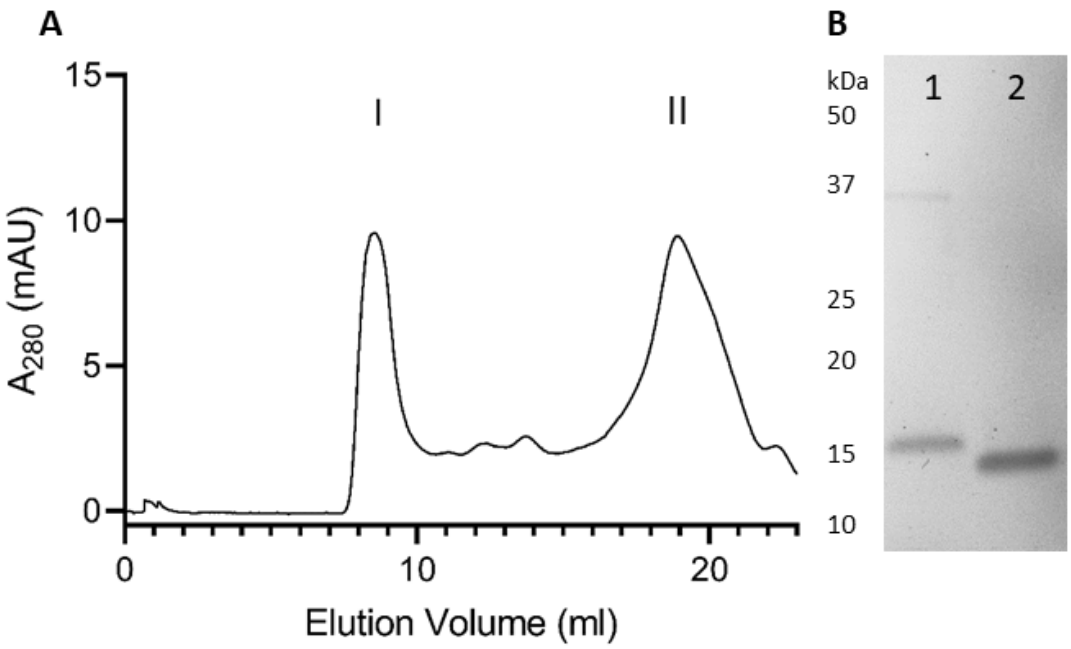

Figure 3.5 Effect of CaCl2 on cytochrome c interaction with CL ND.

Cytochrome c CL ND were prepared and incubated with CaCl2 at a 1:3 ratio of Ca^{2+}:CL (mol/mol) for 1 h at 37 °C. Following incubation, the sample was subjected to FPLC gel filtration chromatography (Panel A) with collection of 2 mL fractions. Elution fractions corresponding to Peak I and Peak II were concentrated and analyzed by SDS PAGE (Panel B); Lane 1) FPLC Peak I and Lane 2) FPLC Peak II.

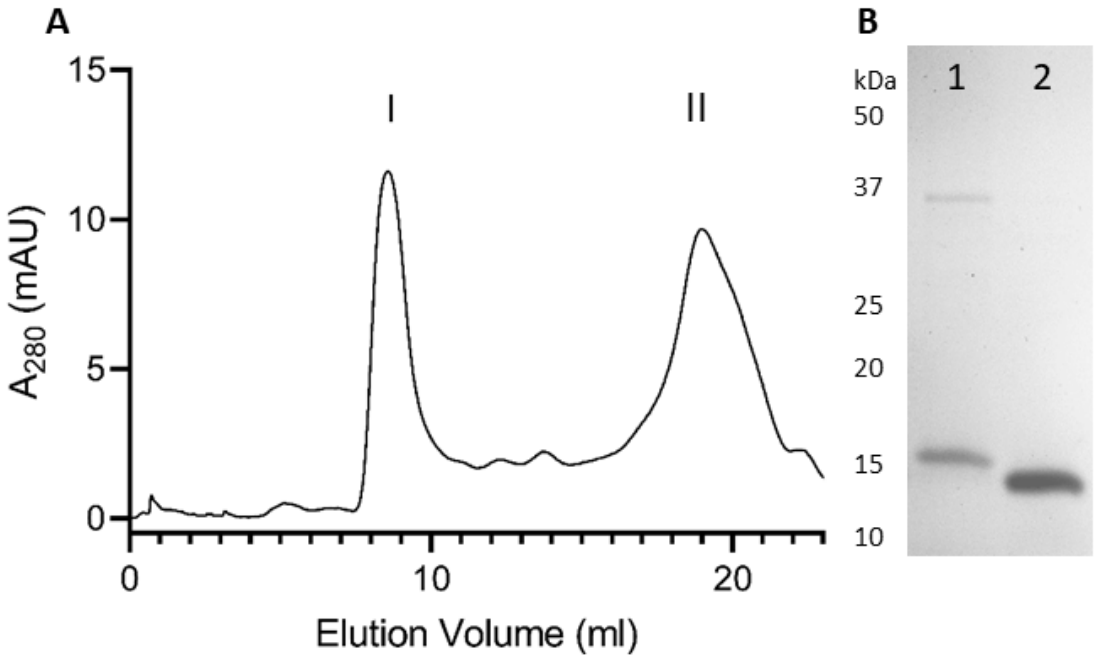

Figure 3.6 Effect of pre-incubation with CaCl2 on cytochrome c binding to CL ND. CL ND were prepared and incubated with CaCl2 at a 1:3 ratio of Ca^{2+}:CL (mol/mol) for 1 h at 37 °C. Following incubation with CaCl2, cytochrome c was added and the incubation continued for an additional 1 h at 37°C. Following incubation, the sample was subjected to FPLC gel filtration chromatography (Panel A) with collection of 2 mL fractions. Elution fractions corresponding to Peak I and Peak II were concentrated and analyzed by SDS PAGE (Panel B); Lane 1) FPLC Peak I and Lane 2) FPLC Peak II.

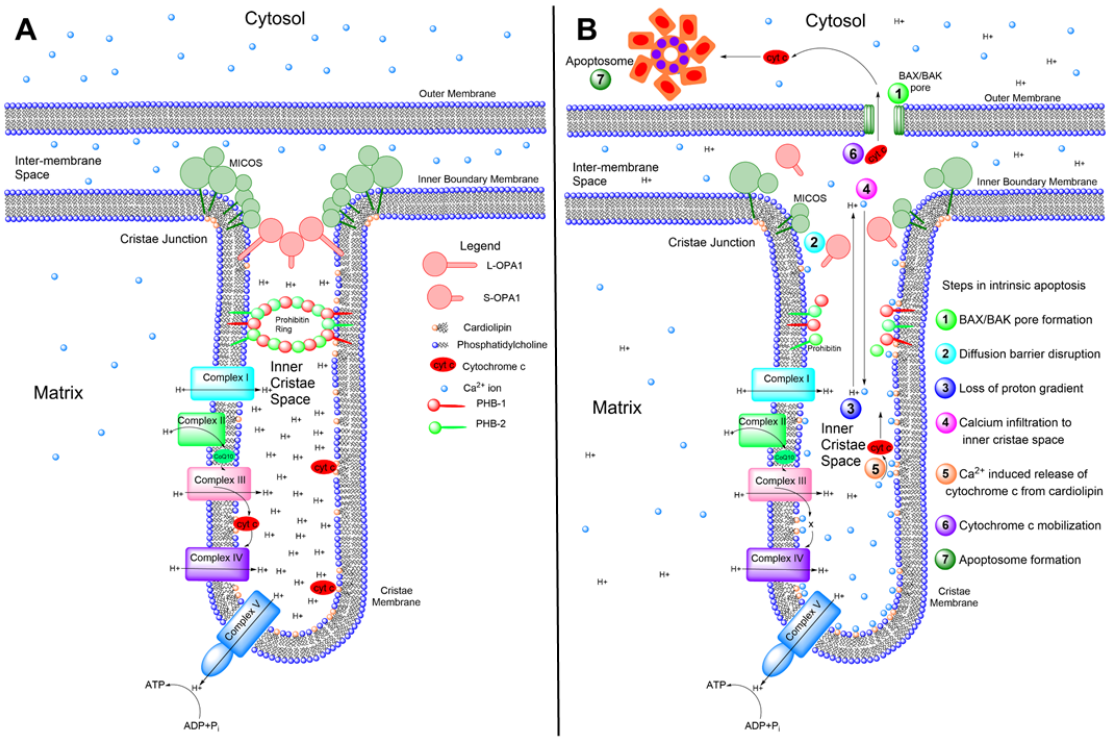

Figure 3.7 Model depiction of the inner cristae membrane of mitochondria.

Panel A) Depiction of the binding interaction between cytochrome c (cyt c) and the CL component of the cristae membrane in a normal functioning mitochondria. Cristae membranes exist as tubular membrane extensions of the inner boundary membrane (90° turn at the cristae junction) that house complexes of the ETC. Oxidative metabolism generates a proton gradient in the inner cristae space that drives ATP production. Maintenance of the inner cristae space as “privileged”, in terms of solute diffusion, is achieved by some combination of the MICOS Complex, OPA1 oligomers and prohibitin ring formation (note that, although not shown in this two dimensional rendering, each PHB subunit in the ring structure depicted is in contact with the inner leaflet of the cylinder-shaed cristae membrane). As a result, components of the inner cristae space / membrane do

not mix with components of the contiguous inter-membrane space / inner boundary membrane. **Panel B)** Induction of intrinsic apoptosis leads to sequence of events, labeled 1 – 7, that culminate in apoptosis.

Chapter 4

Dye binding assay reveals doxorubicin preference for DNA versus cardiolipin

This chapter is based on a manuscript published in:

Fox CA, Ryan, RO (2020) Dye binding assay reveals doxorubicin preference for DNA versus cardiolipin. *Anal. Biochem*. **594**, 113617.

4.1 Abstract

Doxorubicin (DOX) is a potent anticancer agent that binds both DNA and cardiolipin (CL). To investigate DOX binding to CL versus DNA, aqueous soluble, CL-enriched nanoparticles, termed nanodisks (ND), were employed. Upon incubation with CL-ND, but not with phosphatidylcholine ND, DOX binding was detected. DOX binding to CL-ND was sensitive to buffer pH and ionic strength. To investigate if a DOX binding preference for DNA versus CL-ND exists, an agarose gel-based dye binding assay was developed. Under conditions wherein the commercial fluorescent dye, GelRed, detects a 636 bp DNA template following electrophoresis, DOX staining failed to visualize this DNA band. Incubation of the template DNA with DOX prior to electrophoresis resulted in a DOX concentration-dependent attenuation of GelRed staining intensity. When the template DNA was pre-incubated with equivalent amounts of free DOX or DOX-CL-ND, no differences in the extent of GelRed staining intensity attenuation were noted. When DOX was incubated with DNA alone, or a mixture of DNA and CL-ND, the extent of DOX-induced GelRed staining intensity attenuation was equivalent. Thus, DOX has a binding preference for DNA versus CL and, moreover, DOX-CL-ND offer a potential strategy to prevent DOX-induced cardiotoxicity while not affecting its affinity for DNA.

4.2 Introduction

Doxorubicin (DOX) is an aqueous soluble anthracycline known for its bright red color and potent anti-tumor properties [1]. Anti-cancer properties of DOX manifest through intercalation of nuclear DNA, inhibiting topoisomerase II function and DNA replication [2]. While DOX is one of the most effective anti-cancer pharmaceuticals currently available, many patients suffer from a potentially lethal side effect referred to as 'DOX-induced cardiotoxicity' [3,4]. Evidence indicates that DOX-induced cardiotoxicity is unrelated to its ability to intercalate DNA but, rather, arises from a secondary DOX-induced phenomenon [5–8]. A prominent mechanism proposed to explain DOX-induced cardiotoxicity involves conversion of DOX's anthraquinone moiety (**Figure 4.1A**) to a reactive semiquinone free radical, which induces oxidative stress via generation of reactive oxygen species [7]. Subsequent lipid peroxidation leads to membrane defects, alterations in molecular signaling pathways and, ultimately, cardiac cell death.

Cardiolipin (CL) is an anionic phospholipid that localizes exclusively to the inner mitochondrial membrane where it plays important roles in cristae structure and bioenergetics [9,10]. Despite the fact that DOX is water soluble, it displays a binding affinity for CL containing membranes [11,12]. Although the binding interaction between DOX and CL is unrelated to its DNA intercalation activity, it is plausible to consider that CL is involved in DOX-induced cardiotoxicity. With regard to the nature of the interaction between DOX and CL, it has been shown that the positively charged amino group on DOX's carbohydrate constituent (**Figure 4.1A**) forms an electrostatic interaction with negatively charged

phosphate groups on CL [13]. Others have proposed that, following an initial electrostatic attraction, DOX's aromatic anthraquinone moiety intercalates between phospholipid fatty acyl chains in bilayer membranes [12, 14–16]. It is conceivable that the interaction between membrane localized DOX and CL leads to oxidative damage, initiating molecular events that lead to cardiotoxicity [17–19]. Toward the goal of developing strategies that minimize negative side effects of DOX, while retaining its beneficial anticancer effects, it is important to characterize the relative affinity of DOX for DNA versus CL.

To characterize this affinity, water soluble CL-enriched nanoparticles, termed CL nanodisks (CL-ND), were used. These self-assembled nanoscale complexes are comprised solely of cardiolipin and recombinant human apolipoprotein (apo) A-I [20]. The particles adopt a discoidal structure in which CL adopts a bilayer state while apoA-I molecules circumscribe the disk perimeter, creating a stable, water soluble complex [21]. In binding assays, DOX is shown to associate with CL-ND comprised of either tetramyristoyl (TM)- or tetralinoleoyl (TL)-CL. Subsequently, the relative affinity of DOX for DNA versus CL was investigated using a competitive agarose gel-based dye binding assay. Experiments employing this assay provide evidence that the affinity of DOX for DNA is greater than that for CL.

4.3 Materials and Methods

ND formulation

Nanodisks (ND) were formulated as described previously [20]. Briefly, 25 mg dimyristoylphosphatidylcholine (PC), TMCL or TLCL (Avanti Polar Lipids) was dissolved in 1 mL CHCl3:CH3OH (3:1 v/v). Two hundred µL aliquots (5 mg) were transferred to glass tubes and dried under a stream of N2 gas. The samples were lyophilized overnight and stored at −20 °C until use. For CL-ND formulation, 750 µL 20 mM Tris HCl pH 7.4 was added to 5 mg dried CL. The sample was vortexed, resulting in an opaque aqueous lipid dispersion. Subsequently, 2 mg recombinant human apolipoprotein (apo) A-I [22] in 20 mM Tris HCl was added. The mixture was brought to a final volume = 1.25 mL and bath sonicated at 48 °C until the solution cleared (< 10 min). PC-ND and TLCL-ND were formed in a similar manner, except that bath sonication was conducted at 25 °C. TLCL-ND samples were sonicated under an N2 atmosphere. DOX was purchased from Cayman Chemical Company and solubilized in a) 20 mM Tris HCl buffer (1 mM solution for dialysis studies) or b) DMSO (42 mM stock solution for agarose gel studies). DOX in Tris HCl buffer was prepared immediately prior to use while DOX in DMSO was stored at −20 °C until use.

DOX binding studies

To investigate DOX binding to different ND, 100 nmol DOX was incubated with PC-ND (1090 nmol PC), TMCL-ND (622 nmol CL) or TLCL ND (622 nmol CL) at 22 °C for 30 min in Tris HCl, pH 7.4 (1.0 mL total volume). Following incubation, each sample was dialyzed against 1.66 L buffer. To examine the effect of pH on this binding interaction, samples were prepared as above, followed by dialysis

against 1.66 L 25 mM $B_4Na_2O_7$ (sodium tetraborate), pH 9.5, or 20 mM Tris HCl, pH 7.4. To test the effect of ionic strength on this binding interaction, samples were prepared as above, then dialyzed against 1.66 L 20 mM Tris HCl pH 7.4, in the presence or absence of 250 mM NaCl. At indicated time points, absorbance spectra from 650 nm to 400 nm were collected for all samples on a Shimadzu UV-1800 spectrophotometer.

DNA samples

DOX binding experiments employed a 636 bp DNA gene amplification product generated from a plasmid encoding human glutaryl CoA dehydrogenase, using sequence specific forward and reverse primers. The amplification product was employed in gel-based DOX binding studies.

Competition binding studies

One µg aliquots of the 636 bp gene amplification product were electrophoresed on 0.8% agarose gels (w/v). A 16 tooth comb was used for all experiments, and sample volumes were 8 µL per well. Samples were electrophoresed at 100 V in 1× TAE buffer for 70 min. Where indicated, the DNA template was pre-incubated with specified reagents. Following electrophoresis, gels were stained with 3× GelRed (Biotium) dye for 30 min and destained in deionized H_2O for 2 h. Experiments were conducted a minimum of 3 times and gel data shown is representative of patterns observed between replicates.

Quantitative analysis

Gel imaging was performed using a Typhoon FLA7000 (GE Life Sciences) or a Bio-Rad ChemiDoc MP (Bio-Rad). Typhoon images were obtained using a pixel size of 50 µm, power output of 450 V, blue laser (488 nm) and red filter (610/30). ChemiDoc images were obtained using the native GelRed protocol; transilluminator excitation 302 nm and red filter (630/30). Densitometric analysis was performed using tools native to Image Lab software (Bio-Rad, version 5.2.1). Band intensities were quantified on the basis of pixel volume and area (mm2) of individual bands.

Statistical analysis

Statistical analysis was performed by two-way ANOVA followed by Tukey multiple comparison test to compare samples from the same time point (**Figures 4.1 and 4.2**). Statistical analysis was performed on agarose gel densitometry data by one-way ANOVA followed by Tukey test to compare control bands with unknown sample bands (**Figures 4.4–4.7**). Statistical tests were performed using GraphPad Prism version 8.2.1 for Windows (GraphPad Software, San Diego, CA).

4.4 Results

Cardiolipin ND

CL-ND have a diameter in the range of 20–30 nm [23], corresponding to a particle molecular weight>200,000 Da. The CL component of CL-ND exists as a

miniature bilayer membrane, similar to its organizational state in the inner mitochondrial membrane [10]. Surrounding the edge of this disk-shaped CL bilayer is apoA-I. Amphipathic α-helices of this scaffold protein contact otherwise exposed CL fatty acyl chains. This interaction serves to stabilize the CL bilayer while the polar face of apoA-I amphipathic α-helices project toward the aqueous environment.

DOX binding to CL-ND

DOX has a characteristic absorbance spectrum with a main peak centered around 480 nm (**Figure 4.1B**). In contrast, CL-ND absorbance in this spectral region is negligible. Taking advantage of the unique spectral properties of DOX and large size difference versus CL-ND, a dialysis-based assay was used to investigate DOX interaction with CL. To determine the specificity of DOX binding to CL, indicated amounts of DOX were incubated in buffer alone (20 mM Tris HCl buffer, pH 7.4) and buffer containing PC-ND, TMCL-ND or TLCL-ND. After 30 min incubation at 22 °C, the samples were dialyzed against Tris HCl buffer for 2 h. DOX content in the retentate of each sample was measured spectrophotometrically (**Figure 4.1C**). Compared to pre-dialysis absorbance values, following 2 h dialysis the sample containing DOX in buffer only, as well as the DOX plus PC-ND sample, lost >90% of the original DOX content. Given its molecular weight (543 Da), it is evident that free DOX rapidly escapes the dialysis bag and moreover, PC-ND had no significant effect on the rate of DOX dialysis. On the other hand, upon incubation of DOX with either TMCL-ND or

TLCL-ND, similar levels (~60–65%) of the added DOX were retained following dialysis.

Factors affecting DOX affinity for CL-ND

To investigate the nature of the binding interaction between DOX and TMCL-ND, free DOX was incubated with TMCL-ND in 20 mM Tris HCl, pH 7.4. Following incubation, the samples were dialyzed against 20 mM Tris HCl buffer or 25 mM sodium tetraborate buffer, pH 9.5, and DOX content in the retentate determined spectrophotometrically as a function of time (**Figure 4.2A**). After 2 h dialysis, ~60% of the original absorbance intensity was retained in the DOX-CL-ND sample that was dialyzed against pH 7.4 buffer while the sample dialyzed against pH 9.5 buffer retained ~20%. To further investigate the binding interaction between DOX and TMCL-ND, free DOX, in 20 mM Tris buffer, was incubated with TMCL-ND to promote a binding interaction. The samples were then dialyzed against 20 mM Tris HCl buffer, in the presence or absence of 250 mM NaCl. DOX content in each retentate was then determined as a function of time (**Figure 4.2B**). Whereas ~60% of original absorbance intensity was retained in samples dialyzed against buffer in the absence of 250 mM NaCl, when DOX plus TMCL-ND was dialyzed against 20 mM Tris HCl buffer containing 250 mM NaCl, ~18% of the starting DOX was recovered in the retentate.

Effect of DOX on GelRed DNA staining intensity

Having established that TMCL-ND constitute a useful platform for studies of DOX-CL interactions, a method was sought to determine whether DOX has a binding preference for DNA versus CL. To address this, an agarose gel-based assay was developed by taking advantage of the unique fluorescence properties of the commercial DNA binding dye, GelRed, versus those of DOX. GelRed is a nontoxic ethidium-based dye commonly used to visualize DNA following agarose gel electrophoresis [24]. When 1 µg of a 636 bp DNA template was electrophoresed on a 0.8% agarose gel and stained with GelRed, a strong positive band was observed (**Figure 4.3A, left**). However, pre-incubation of the DNA template with increasing amounts of DOX resulted in a DOX concentration-dependent attenuation of GelRed staining intensity (**Figure 4.3A**). Moreover, when pre-incubated with high concentrations of DOX, migration of the template DNA slowed and the band broadened. In control experiments (**Figure 4.3B**), when the template DNA was electrophoresed and stained directly with DOX, no band was visible under conditions used for optimal GelRed staining (excitation 302 nm) or when excited at 488 nm, the wavelength of maximum DOX fluorescence excitation [25]. On the other hand, when the DNA template was stained with GelRed, a band was visible under both conditions. These data confirm that DOX does not contribute to visualization of the DNA template band under GelRed imaging conditions. The apparent reduced electrophoretic mobility of the DNA template following pre-incubation with higher concentrations of DOX supports the interpretation that DOX intercalates base pairs in the DNA template and remains bound during electrophoresis [26]. The ability of DOX pre-incubation

to attenuate GelRed-specific DNA staining intensity indicates that GelRed does not displace DOX from DNA. Moreover, DOX-dependent attenuation of GelRed staining intensity can be used as the basis for an assay to assess the relative binding affinity of DOX for DNA versus CL.

Effect of CL-ND on DOX binding to DNA

To investigate the relative binding affinity of DOX for DNA versus CL, the gel-based dye binding assay described above was employed in conjunction with CL-ND comprised of either TMCL or TLCL. One μg of template DNA was incubated with free DOX or pre-formed DOX-CL-ND for 30 min. If prior association with CL prevents DOX binding to DNA, then it is expected that free DOX will result in a greater attenuation of GelRed staining intensity than that achieved by DOX-CL-ND. Additionally, by comparing ND formulated with TMCL versus TLCL in this assay, the effect of CL acyl chain saturation on DOX binding can be assessed. Following incubation, samples were subjected to agarose gel electrophoresis and stained with GelRed (**Figure 4.4A**). Densitometric analysis of the pixel intensity of the gel bands is depicted in **Figure 4.4B**. Compared to control DNA (no DOX incubation), the free DOX, DOX-TMCL-ND and DOX-TLCL-ND samples gave rise to a statistically significant attenuation of GelRed staining intensity. However, no differences were observed in the relative ability of free DOX, DOX-TMCL-ND or DOX-TLCL-ND to attenuate GelRed staining intensity of the template DNA band. Thus, it may be concluded that DOX displays preferential binding for DNA

versus CL and prior association with CL does not affect DOX's ability to bind DNA.

Effect of prior DNA binding on DOX affinity for CL-ND

To further investigate the binding preference of DOX for DNA versus TMCL, the gel-based dye binding assay was adapted to assess whether pre-incubation of DOX with DNA is affected by subsequent incubation with TMCL-ND. Following incubation of free DOX with the template DNA, 1 µg aliquots (as DNA) were incubated for 30 min in Tris HCl buffer or Tris HCl buffer containing TMCL-ND. Following incubation, the samples were subjected to agarose gel electrophoresis and stained with GelRed (**Figure 4.5A**). Compared to a control DNA sample (no DOX), both the DNA-DOX alone and DNA-DOX plus TMCL-ND samples showed statistically significant attenuation in GelRed staining intensity. Densitometric analysis of the template DNA band pixel intensity revealed that incubation with TMCL-ND did not affect GelRed staining attenuation of the template DNA induced by pre-incubation with DOX (**Figure 4.5B**). These data indicate that, when bound to DNA, DOX is not available for interaction with CL-ND.

Effect of apoA-I on DOX binding to DNA

To investigate whether lipid free apoA-I influences the interaction of DOX with DNA, the gel-based dye binding assay described above was employed. Samples of lipid free apoA-I were incubated with DOX for 30 min. One µg of template DNA was then incubated for an additional 30 min in buffer alone, in buffer containing

free DOX or in buffer containing free DOX plus apoA-I. Following incubation, the samples were subjected to agarose gel electrophoresis and stained with GelRed (**Figure 4.6A**). Densitometric analysis of the pixel intensity of the gel bands is depicted in **Figure 4.6B**. Compared to the DNA only sample (no DOX incubation), both the free DOX and free DOX plus apoA-I samples gave rise to a statistically significant attenuation of GelRed staining intensity. At the same time, there was no statistically significant difference between the DNA plus DOX samples and the DNA plus DOX plus apoA-I samples in terms of their ability to attenuate GelRed staining intensity of the template DNA band. Thus, it may be concluded that lipid free apoA-I has no effect on the interaction of DOX with DNA.

DOX competition binding assay for DNA versus CL

To further investigate the relative binding affinity of DOX for DNA versus CL, samples containing TMCL-ND and template DNA were incubated for 30 min. Following this, free DOX was added and the sample incubated a further 30 min. Control incubations, including DNA plus TMCL-ND (no DOX) and DNA plus DOX (no TMCL-ND) were run in parallel. Following incubation, the samples were subjected to agarose gel electrophoresis and stained with GelRed (**Figure 4.7A**). Band intensities were then analyzed by densitometry and the results depicted in **Figure 4.7B**. As expected, the DNA plus TMCL-ND (no DOX) control sample showed the strongest GelRed staining intensity, indicating that inclusion of TMCL-ND does not affect GelRed staining intensity. Compared to this sample,

both DOX-containing samples (DNA alone and DNA plus TMCLND) gave rise to a statistically significant, DOX-dependent attenuation of GelRed staining intensity. At the same time, however, the extent of DOX-induced GelRed staining intensity attenuation observed in the sample containing DNA plus TMCL-ND was not statistically different from the sample containing DNA alone. One difference noted in this sample, however, was band broadening in incubations containing DNA and TMCL-ND, possibly due to the presence of excess TMCL-ND in the sample. Regardless, the data show that DOX displays preferential binding to DNA versus CL.

4.5 Discussion

CL-ND provide a versatile model membrane system to investigate the CL interactome. For example, recent studies provided insight into the effect of calcium binding on CL dependent membrane phase transitions [20]. This system is also amenable to studies of the interaction between cytochrome c and CL [27]. In the present study, the binding interaction between the fluorescent anthracycline, DOX, and the mitochondrial phospholipid, CL, were examined. DOX was shown to bind to CL-ND but not to PC-ND. This difference may be due to the fact that CL is an anionic phospholipid while PC is zwitterionic. The more exposed phosphate groups on CL may promote binding via electrostatic attraction with DOX's single cationic amino group (see **Figure 4.1A**). Consistent with this interpretation, DOX binding to CL-ND was decreased at pH 9.5 (deprotonated, uncharged amino group) [28] versus pH 7.4 (protonated,

positively charged amino group). The binding interaction between DOX and CL-ND was also reduced when solution ionic strength was increased from 0 mM to 250 mM NaCl (in 20 mM Tris HCl, pH 7.4). One possibility is that electrostatic attraction accounts for an initial step in DOX binding to CL containing membranes that is followed by a second step wherein the anthraquinone portion of the molecule integrates into the hydrophobic portion of the bilayer [14–16]. Despite these reports of a second step in DOX association with CL containing membranes, we observed no difference between TMCL- and TLCL containing ND in terms of their relative ability to bind DOX or retain DOX upon incubation with DNA. If membrane insertion of the anthraquinone moiety occurred in the case of TLCL but not with TMCL, then a measurable difference in DOX binding behavior may be anticipated. Given that no effect of acyl chain saturation was observed, it may be that membrane insertion plays a less prominent role in DOX binding to membranes than previously reported or that some aspect of the ND particle structure, such as the presence of apoA-I as a scaffold protein, affects the ability of DOX to insert into the bilayer. This interpretation, however, does not align with the fact that numerous other hydrophobic molecules have been shown to intercalate between phospholipids in ND particles [21].

With regard to DOX-mediated membrane effects, it is conceivable that, when the drug binds to CL containing membranes, DOX may undergo conversion to a semiquinone radical that exerts pro-oxidant effects, leading to reactive oxygen species production, lipid peroxidation, membrane disruption and apoptosis. In fact, such a scenario may explain the well documented

phenomenon of DOX-induced cardiotoxicity associated with DOX use as an anti-cancer agent [7]. Of interest to this concept is the fact that CL found in mitochondria from cardiac tissue is highly enriched in linoleic acid [29]. As such, DOX binding to endogenous CL containing membranes could elicit a direct effect on CL oxidation, promoting a transition from bilayer to non-bilayer phase, an event that is capable of triggering an apoptotic cascade [30].

Given that DOX-induced cardiotoxicity arises from a mechanism that is distinct from its DNA intercalation activity, we sought to employ CL-ND in studies designed to examine the intrinsic preference of DOX for DNA versus CL. To address this, a novel agarose gel-based competition binding assay was developed. Both DOX and GelRed function as DNA intercalating agents, such that upon incubation with a fixed amount of DNA, DOX reduces the intensity of GelRed staining intensity in a concentration-dependent manner (**Figure 4.3A**). Furthermore, due to differences in fluorescence emission properties and imaging conditions, it is possible to visualize GelRed stained DNA bands without any contribution from DOX, despite the fact that it is present (**Figure 4.3B**). The results presented show that pre-incubation of a 636 bp template DNA with DOX induces a concentration-dependent attenuation of GelRed staining intensity following electrophoresis. These data indicate that DOX interaction with DNA effectively prevents subsequent GelRed binding. Decreased GelRed binding under these conditions reduces GelRed-based signal intensity, which allows for the extent of DOX binding to be inferred.

When the ability of DNA to bind DOX, presented as free DOX or DOX-CL-ND, was investigated, no significant differences in GelRed signal intensity were observed. This indicates that DOX preference for DNA is greater than that for CL-ND and is consistent with results reported by Mustonen and Kinnunen [31] wherein the addition of DNA was shown to relieve DOX-induced quenching of liposomes that contain CL and a pyrene labeled phosphatidylcholine analog. When the ability of CL-ND to remove DOX pre-bound to DNA was investigated, no significant differences in GelRed signal intensity were observed, as compared to control incubations of DNA alone. These data indicate that, once DOX is complexed to DNA, its affinity for CL-ND is not high enough to induce dissociation. In addition, prior incubation of free DOX with lipid-free apoA-I had no effect on the ability of DOX to attenuate GelRed signal intensity of the DNA template. Lastly, upon comparison of DOX's binding preference for DNA versus CL-ND in a direct competition binding assay, no significant difference in signal intensity was observed, as compared to control incubations of DNA without CL-ND. Overall, these data indicate DOX has a higher binding affinity for DNA than for CL-ND.

Given the prevalence of cardiotoxicity associated with DOX use in cancer chemotherapy, and evidence that interactions between DOX and CL may be responsible [32], the finding that DOX displays a strong binding preference for DNA versus CL-ND may be of key importance. For example, it is conceivable that administration of DOX as DOX-CLND may lead to a reduced incidence of cardiotoxicity because administered DOX will not be attracted to endogenous CL

since it is already associated with this lipid. By the same token, given that DOX has a stronger affinity for DNA, its ability to intercalate DNA and, thereby, inhibit DNA replication, should be unaffected. While validation of this concept will require in vivo investigations, studies to date have revealed that CL-ND are well tolerated when injected into mice [33].

4.6 References

[1] R.B. Weiss, The anthracyclines: will we ever find a better doxorubicin? Semin. Oncol. 19 (1992) 670–686.

[2] C.F. Thorn, C. Oshiro, S. Marsh, T. Hernandez-Boussard, H. McLeod, T.E. Klein, R.B. Altman, Doxorubicin pathways: pharmacodynamics and adverse effects, Pharmacogenetics Genom. 21 (2011) 440–446.

[3] K. Chatterjee, J. Zhang, N. Honbo, J.S. Karliner, Doxorubicin cardiomyopathy, Cardiology 115 (2010) 155–162.

[4] H.S. Al-Malky, S.E. Al Harthi, A.M. Osman, Major obstacles to doxorubicin therapy: cardiotoxicity and drug resistance, J. Oncol. Pharm. Pract. (2019), https://doi.org/10.1177/1078155219877931 Oct 9 Epub ahead of print.

[5] G. Takemura, H. Fujiwara, Doxorubicin-induced cardiomyopathy from the cardiotoxic mechanisms to management, Prog. Cardiovasc. Dis. 49 (2007) 330–352.

[6] S.M. Swain, F.S. Whaley, M.S. Ewer, Congestive heart failure in patients treated with doxorubicin, Cancer 97 (2003) 2869–2879.

[7] F.S. Carvalho, A. Burgeiro, R. Garcia, A.J. Moreno, R.A. Carvalho, P.J. Oliveira, Doxorubicin-induced cardiotoxicity: from bioenergetics failure and cell death to cardiomyopathy, Med. Res. Rev. 34 (2014) 106–135.

[8] Y. Octavia, C.G. Tocchetti, K.L. Gabrielson, S. Janssens, H.J. Crijns, A.L. Moens, Doxorubicin-induced cardiomyopathy: from molecular mechanisms to therapeutic strategies, J. Mol. Cell. Cardiol. 52 (2012) 1213–1225.

[9] G. Paradies, V. Paradies, F.M. Ruggiero, G. Petrosillo, Role of cardiolipin in mitochondrial function and dynamics in health and disease: molecular and pharmacological aspects, Cells 8 (2019) 728.

[10] N. Ikon, R.O. Ryan, Cardiolipin and mitochondrial cristae organization, Biochim. Biophys. Acta Biomembr. 1859 (2017) 1156–1163.

[11] F.A. de Wolf, Binding of doxorubicin to cardiolipin as compared to other anionic phospholipids? An evaluation of electrostatic effects, Biosci. Rep. 11 (1991) 275–284.

[12] M.A. Parker, V. King, K.P. Howard, Nuclear magnetic resonance study of doxorubicin binding to cardiolipin containing magnetically oriented phospholipid bilayers, Biochem. Biophys. Acta. 1514 (2001) 206–216.

[13] T.G. Burke, A.C. Sartorelli, T.R. Tritton, Selectivity of the anthracyclines for negatively charged model membranes: role of the amino group, Canc. Chemother. Pharmacol. 21 (1988) 274–280.

[14] N. Henry, E.O. Fantine, J. Bolard, A. Garnier-Suillerot, Interaction of Adriamycin with negatively charged model membranes: evidence of two types of binding sites, Biochemistry 24 (1985) 7085–7092.

[15] E. Goormaghtigh, R. Brasseur, P. Huart, J.M. Ruysschaert, Study of the Adriamycincardiolipin complex structure using attenuated total reflection infrared spectroscopy, Biochemistry 26 (1987) 1789–1794.

[16] E. Goormaghtigh, P. Huart, M. Praet, R. Brasseur, J.M. Ruysschaert, Structure of the adriamycin-cardiolipin complex. Role in mitochondrial toxicity, Biophys. Chem. 35 (1990) 247–257.

[17] A. Rahman, A. Joher, J.R. Neefe, Immunotoxicity of multiple dosing regimens of free doxorubicin and doxorubicin entrapped in cardiolipin liposomes, Br. J. Canc. 54 (1986) 401–408.

[18] K.G. Cheung, L.K. Cole, B. Xiang, K. Chen, X. Ma, Y. Myal, G.M. Hatch, Q. Tong, V.W. Dolinsky, Sirtuin-3 (SIRT3) protein attenuates doxorubicin-induced oxidative stress and improves mitochondrial respiration in H9c2 cardiomyocytes, J. Biol. Chem. 290 (2015) 10981–10993.

[19] S. Gorini, A. De Angelis, L. Berrino, N. Malara, G. Rosano, E. Ferraro, Chemotherapeutic drugs and mitochondrial dysfunction: focus on doxorubicin, trastuzumab, and sunitinib, Oxid Med. Cell Longev. 2018 (2018) 7582730, https://doi.org/10.1155/2018/7582730.

[20] C.A. Fox, P. Ellison, N. Ikon, R.O. Ryan, Calcium-induced transformation of cardiolipin nanodisks, Biochim. Biophys. Acta Biomembr. 1861 (2019) 1030–1036.

[21] R.O. Ryan, Nanobiotechnology applications of reconstituted high density lipoprotein, J. Nanobiotechnol. 8 (2010) 28.

[22] R.O. Ryan, T.M. Forte, M.N. Oda, Optimized bacterial expression of human apolipoprotein A-I, Protein Expr. Purif. 27 (2003) 98–103.

[23] N. Ikon, B. Su, F.F. Hsu, T.M. Forte, R.O. Ryan, Exogenous cardiolipin localizes to mitochondria and prevents TAZ knockdown-induced apoptosis in myeloid progenitor cells, Biochem. Biophys. Res. Commun. 464 (2015) 580–585.

[24] Q. Huang, L. Baum, W.L. Fu, Simple and practical staining of DNA with GelRed in agarose gel electrophoresis, Clin. Lab. 56 (2010) 149–152.

[25] P. Mohan, N. Rapoport, Doxorubicin as a molecular nanotheranostic agent: effect of doxorubicin encapsulation in micelles or nanoemulsions on the ultrasound-mediated intracellular delivery and nuclear trafficking, Mol. Pharm. 7 (2011) 1959–1973.

[26] J. Sigmon, L.L. Larcom, The effect of ethidium bromide on mobility of DNA fragments in agarose gel electrophoresis, Electrophoresis 17 (1996) 1524–1527.

[27] J. Muenzner, E.V. Pletneva, Structural transformations of cytochrome c upon interaction with cardiolipin, Chem. Phys. Lipids 179 (2014) 57–63.

[28] M. Liang, K. Fan, M. Zhou, D. Duan, J. Zheng, D. Yang, J. Feng, X. Yan, H-ferritinnanocaged doxorubicin nanoparticles specifically target and kill tumors with a single dose injection, Proc. Natl. Acad. Sci. U.S.A. 111 (2014) 14900–14905.

[29] R.H. Houtkooper, F.M. Vaz, Cardiolipin, the heart of mitochondrial metabolism, Cell. Mol. Life Sci. 65 (2008) 2493–2506.

[30] M.E. Clementi, B. Giardina, E. Di Stasio, A. Mordente, F. Misiti, Doxorubicin-derived metabolites induce release of cytochrome C and inhibition of respiration on cardiac isolated mitochondria, Anticancer Res. 23 (2003) 2445–2450.

[31] P. Mustonen, P.K. Kinnunen, On the reversal by deoxyribonucleic acid of the binding of Adriamycin to cardiolipin-containing liposomes, J. Biol. Chem. 268 (1993) 1074–1080.

[32] E. Goormaghtigh, P. Chatelain, J. Caspers, J.M. Ruysschaert, Evidence of a complex between adriamycin derivatives and cardiolipin: possible role in cardiotoxicity, Biochem. Pharmacol. 29 (1980) 3003–3010.

[33] N. Ikon, F.F. Hsu, J. Shearer, T.M. Forte, R.O. Ryan, Evaluation of cardiolipin nanodisks as lipid replacement therapy for Barth syndrome, J. Biomed. Res. 32 (2018) 107–112.

4.7 Figures and Figure Legends

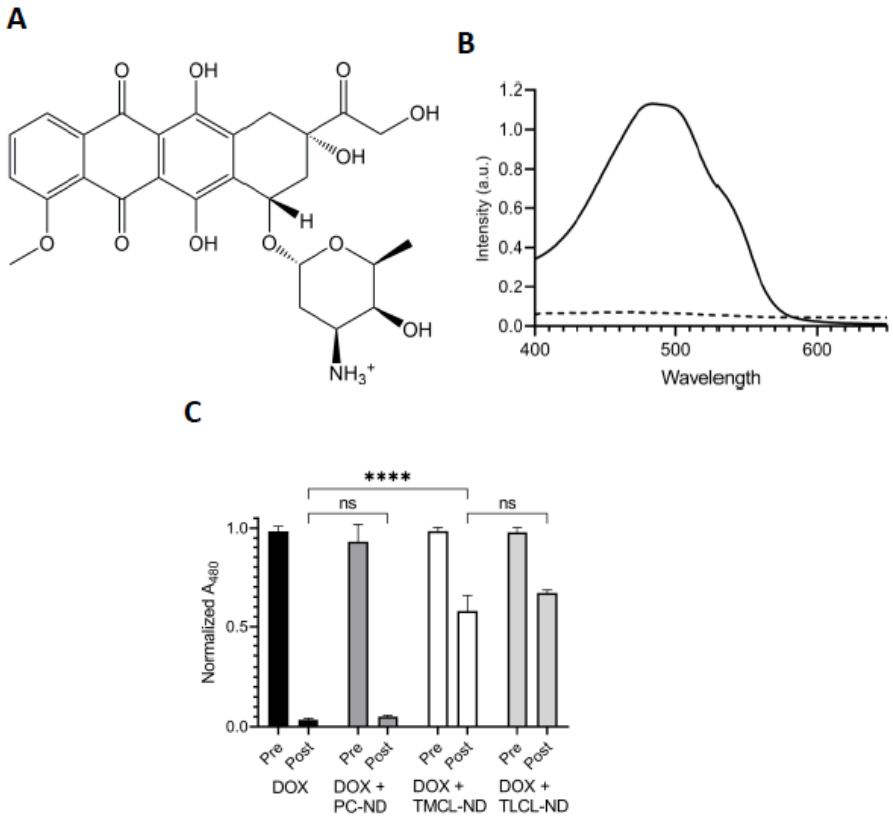

Figure 4.1 Effect of ND on DOX dialysis. A) Structure of doxorubicin at physiological pH. B) Visible absorption spectra of 0.1 μmol free DOX (solid line) and 0.6 μmol CL-ND (dashed line) in 20 mM Tris HCl, pH 7.4, were collected on a Shimadzu UV-1800 spectrophotometer. C) Effect of dialysis on DOX sample absorbance. Samples containing free DOX, DOX plus PC-ND, DOX plus TMCLND and DOX+TLCL-ND were incubated for 30 min prior to 2 h dialysis against Tris HCl buffer. Sample absorbance at 480 nm was measured before and after dialysis. Data reported as normalized A480. Values reported are the mean ± standard error (n = 3) ns, not significant; ****, $p < .0001$ versus free DOX control.

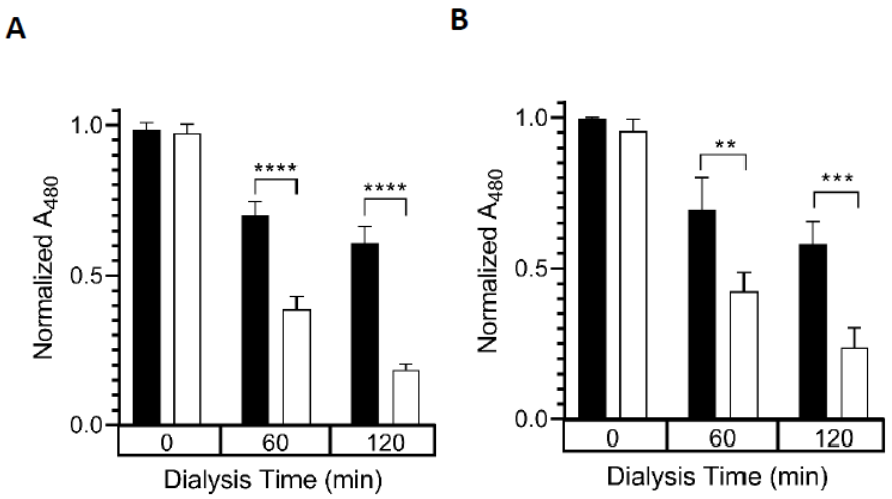

Figure 4.2 Effect of solution pH and ionic strength on DOX binding to CL-ND. A) TMCL-ND were formulated and 0.6 μmol aliquots (as CL) were incubated with DOX (0.1 μmol DOX) in Tris HCl buffer (final volume = 1 mL). After 30 min incubation, the samples were dialyzed against 20 mM Tris, pH 7.4 (filled bars), or 25 mM sodium tetraborate, pH 9.5 (open bars). Dialysis was performed at 22 °C for 2 h against 1.66 L buffer per sample. Sample absorbance was measured before dialysis, after 60 min dialysis and after 120 min dialysis. Data reported as normalized A480. Values reported are the mean ± standard error (n = 3) ****, $p < .0001$ versus pH 7.4 samples; B) Aliquots of TMCL-ND (0.6 μmol CL) were incubated with DOX (0.1 μmol) in 20 mM Tris HCl, pH 7.4. After 30 min incubation, samples were dialyzed for 2 h at 22 °C against 20 mM Tris HCl, pH 7.4 (filled bars) or 20 mM Tris HCl, pH 7.4, 250 mM NaCl (open bars). Sample absorbance was measured before dialysis, after 60 min dialysis and 120 min dialysis. Data reported as normalized A480. Values reported are the mean ± standard error (n = 3) **, $p < .01$ versus no NaCl control; ***, $p < .001$ versus no NaCl control.

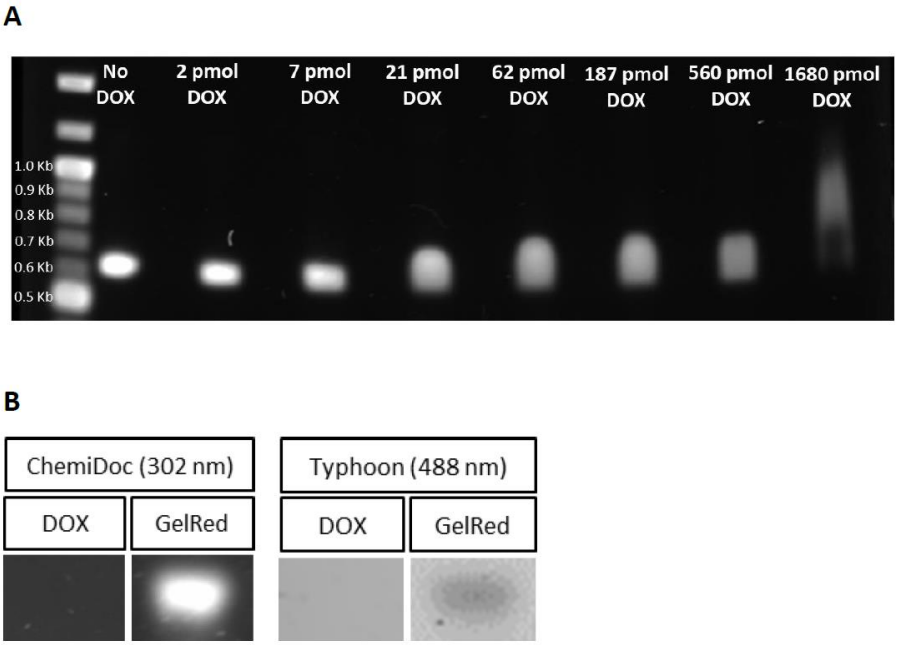

Figure 4.3 Effect of DOX preincubation on GelRed staining intensity of a DNA template. A) One µg aliquots of a 636 bp DNA template were incubated with indicated amounts of DOX for 30 min. Following incubation, samples were added to the wells of a 0.8% (w/v) agarose gel and electrophoresed at 100 V for 70 min. Following electrophoresis, the gel was stained with GelRed for 30 min and destained in deionized H2O for 2 h. The stained gel was imaged on a Bio-Rad ChemiDoc unit using the GelRed detection protocol. B) One µg aliquots of the 636 bp DNA template were applied to wells of a 0.8% (w/v) agarose gel and electrophoresed at 100 V for 70 min. Following electrophoresis, the gel was cut in half, and one half stained with GelRed while the other half was stained with DOX (50 µg/mL). Gels were then imaged using GelRed imaging conditions (302 nm excitation) on a Bio-Rad ChemiDoc and using DOX imaging conditions (488 nm excitation) on a GE Typhoon.

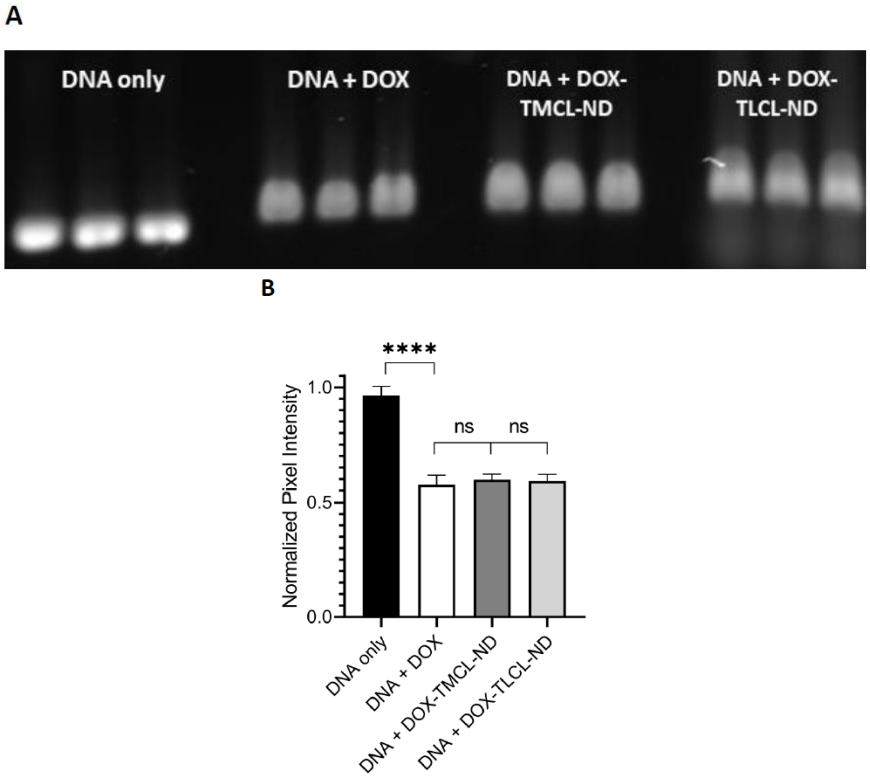

Figure 4.4 Effect of CL-ND on DOX binding to DNA. A) One µg aliquots of the 636 bp DNA template was incubated for 30 min in a) buffer alone; b) buffer containing 0.19 nmol free DOX; c) buffer containing 0.19 nmol DOX plus TMCL-ND and d) buffer containing 0.19 nmol free DOX plus TLCL-ND. Following incubation, the samples were applied to wells of a 0.8% agarose gel (w/v) and electrophoresed at 100 V for 70 min. Following electrophoresis, the gel was stained with GelRed for 30 min and destained for 2 h in deionized H2O. The gel was then imaged on a Bio-Rad ChemiDoc unit using the GelRed detection protocol; B) Densitometric analysis of gel bands from Panel A. Gel band pixel intensity was quantitated using ImageLab software analysis and defined as band pixel volume per band area (in mm^2). Data were normalized to the “no DOX” control samples and presented as normalized pixel intensity. Values reported are

the mean ± standard error (n = 3) ns, not significant; ****, $p < .0001$ versus no DOX control.

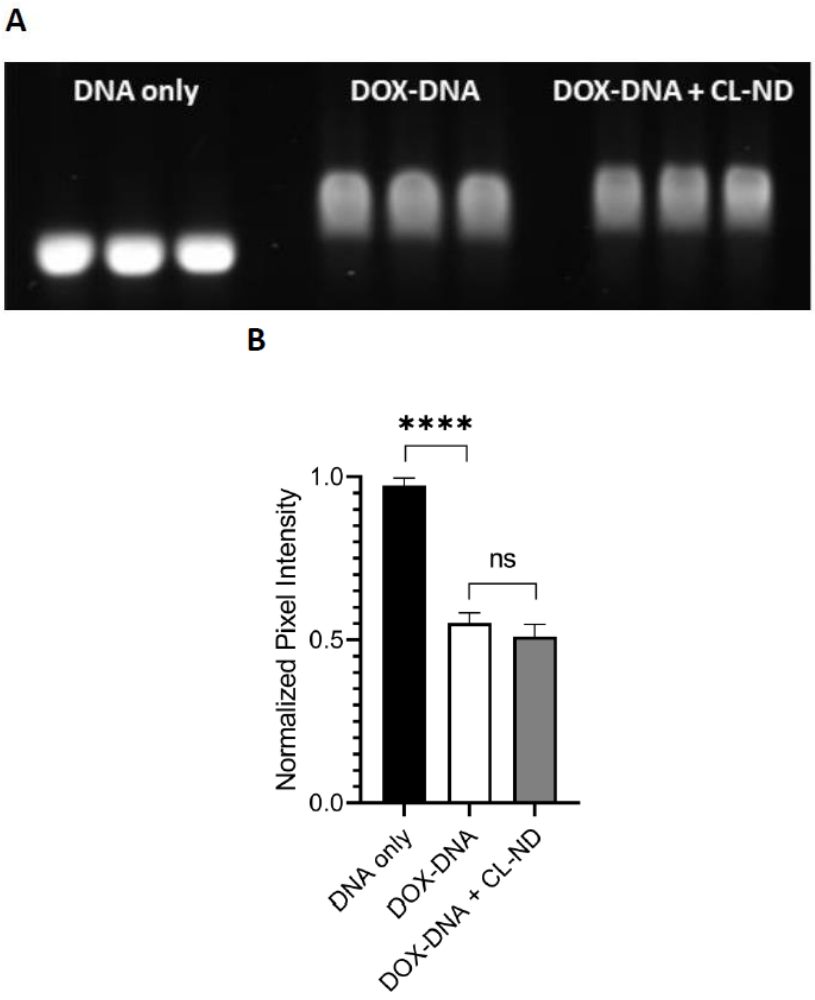

Figure 4.5 Ability of CL-ND to extract DOX from DNA.

A) One µg aliquots of the 636 bp DNA template were incubated for 30 min in deionized H2O (n = 3) or deionized H2O containing 0.19 nmol DOX (n = 6). Following incubation, TMCL-ND (1.6 nmol CL) was added to 3 of the 6 DOX-treated DNA samples. After a further 30 min incubation, the samples were subjected to agarose gel electrophoresis and stained with GelRed. After destaining, the gel was imaged on a Bio-Rad ChemiDoc unit using the GelRed detection protocol. B) Densitometric analysis of gel bands from panel A. Gel band pixel intensity was quantitated using ImageLab software analysis and

defined as band pixel volume per band area (in mm2). Data were normalized to the “no DOX” control samples and presented as normalized pixel intensity. Values reported are the mean ± standard error (n = 3) ns, not significant; ****, p < .0001 versus no DOX control.

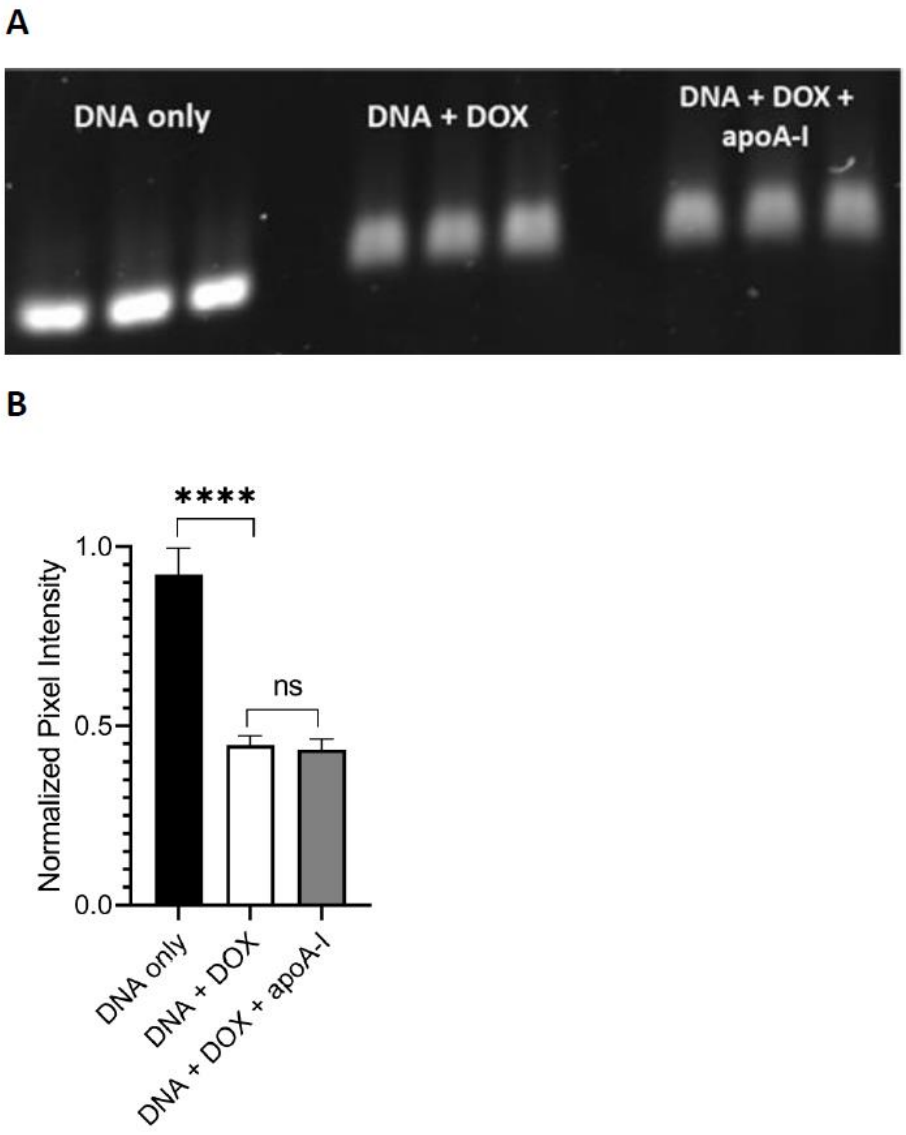

Figure 4.6 Effect of apoA-I on DOX binding to DNA.

One µg aliquots of the 636 bp DNA template were incubated for 30 min in a) buffer alone, b) buffer containing 0.19 nmol free DOX (DNA + DOX) and c) buffer containing 0.19 nmol DOX plus 2.4 µg apoA-I (DNA + DOX + apoA-I). Following incubation, the samples were applied to wells of a 0.8% agarose gel (w/v) and electrophoresed at 100 V for 70 min (Panel A). The gel was stained with GelRed for 30 min, destained for 2 h in deionized H2O and imaged on a Bio-Rad

ChemiDoc unit using the GelRed detection protocol; Panel B) Densitometric analysis of gel bands from Panel A. Gel band pixel intensity was quantitated using ImageLab software analysis and defined as band pixel volume per band area (in mm2). Data were normalized to the “DNA only” control samples and presented as normalized pixel intensity. Values reported are the mean ± standard error (n = 3) ns, not significant; ****, $p < .0001$ versus no DOX control.

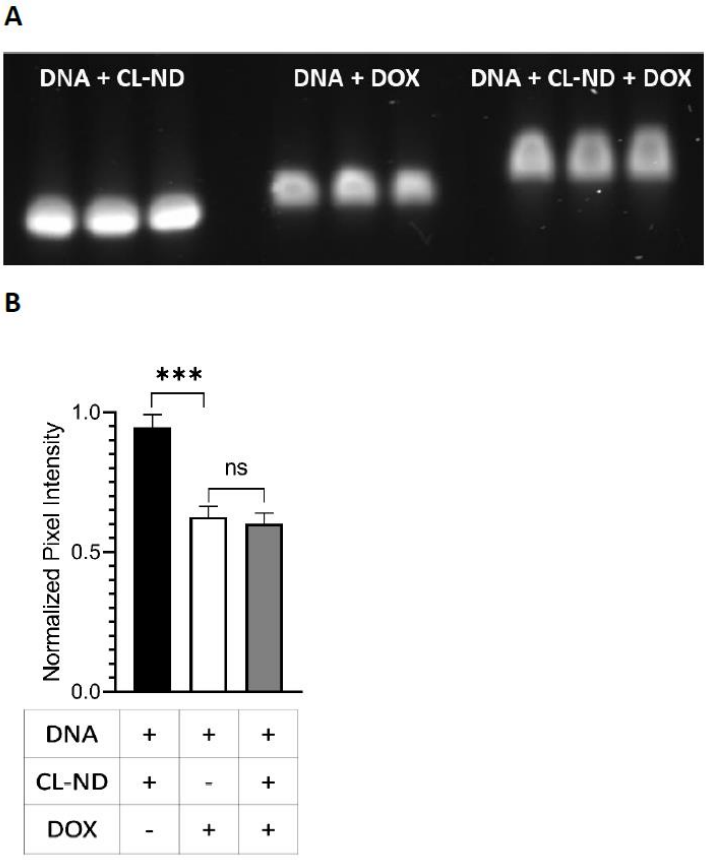

Figure 4.7 DOX competition binding assay for DNA versus CL.

A) One µg aliquots of the 636 bp DNA template were incubated for 30 min in the absence (n = 3) or presence (n = 6) of TMCL-ND (1.6 nmol CL). DOX (0.19 nmol) was then added to the 3 DNA only samples and 3 of the DNA + CL-ND samples. Following a further 30 min incubation, the samples were subjected to agarose gel electrophoresis and stained with GelRed. After destaining, the gel was imaged on a Bio-Rad ChemiDoc unit using the GelRed detection protocol. B) Densitometric analysis of gel bands from Panel A. Gel band pixel intensity was quantitated using ImageLab software analysis and defined as band pixel volume per band area (in mm2). Data were normalized to the “no DOX” control

lanes and presented as normalized pixel intensity. Values reported are the mean ± standard error (n = 3) ns, not significant; ***, $p < .0001$ versus no DOX control.

Chapter 5

Mitigation of doxorubicin-induced mitochondrial dysfunction by cardiolipin nanodisks

This chapter is based on a manuscript in preparation:

Fox CA, Romenskaia IR, Dagda RK, Ryan RO (2021). Mitigation of doxorubicin-induced mitochondrial dysfunction by cardiolipin nanodisks. In prep.

5.1 Abstract

Doxorubicin (DOX) is a clinically significant DNA intercalation agent used to treat a wide variety of cancers. Although DOX anti-cancer activity is dose-dependent, increased dosage enhances risk of cardiotoxicity, a potentially lethal side effect. The mechanism underlying this phenomenon has been extensively studied but remains enigmatic. DOX is known to bind to the mitochondrial phospholipid, cardiolipin (CL), which plays important roles in mitochondrial structure and bioenergetics. To study the interaction between DOX and CL, aqueous soluble nanoparticles, termed nanodisks (ND), comprised solely of CL and an apolipoprotein (apo) scaffold, were formulated and investigated as a potential DOX delivery vehicle. When DOX was incubated with CL ND, but not phosphatidylcholine (PC) ND, a 40% decrease in maximal fluorescence emission intensity was observed. In cultured hepatocarcinoma (HepG2) cells, uptake of DOX was similar when administered as free DOX or DOX CL ND. In two model cancer cell lines, DOX CL ND were as effective as free DOX in growth inhibition assays and more effective than liposomal DOX at all but one concentration tested. However, as compared to free DOX, incubation with DOX CL ND led to increased cell viability in rat cardiomyocytes. When incubated with DOX CL ND, cardiomyocytes also showed increased maximal mitochondrial respiration, as compared to cells treated with free DOX. Association of DOX with preformed CL ND reduces the decline in oxygen consumption rate observed with free DOX incubation, suggesting that interaction of free DOX with endogenous CL may contribute to DOX-induced cardiotoxicity.

5.2 Introduction

Doxorubicin (DOX) is a fluorescent anthracycline compound (**Figure 5.1A**) that is clinically significant due to its efficacy in treatment of a wide variety of cancers, including hepatocellular carcinoma, leukemia, Hodgkin's lymphoma and breast cancer [1,2]. Mechanistically, DOX inhibits cell division through intercalation of DNA base pairs. DOX binding to DNA is nonspecific, although effects are more pronounced in rapidly dividing tumor cells than normal somatic cells. Lack of specificity in the DOX mechanism of action is consistent with its broad efficacy against an assortment of cancer types. At the same time, this lack of specificity is postulated to result in undesirable off target effects. For example, at concentrations required for optimal therapeutic benefit, between 10-36% of patients exhibit symptoms of DOX-induced cardiotoxicity [3,4].

DOX-induced cardiotoxicity is dose dependent. Symptoms include changes in myocardial structure, cardiomyopathy and congestive heart failure. Symptom presentation is erratic, sometimes presenting 2-3 days after DOX administration or even years later [5,6]. Once symptoms develop, DOX-induced cardiotoxicity has a 50% mortality rate [7]. Consequently, dosage limits for DOX are highly restrictive [4]. Despite adherence to current dosage limitations, between 4-10% of patients will develop cardiotoxicity [5]. Although the mechanism underlying DOX-induced cardiotoxicity has been extensively studied, it remains poorly understood and heavily debated [3,4,7].

Interestingly, antioxidant enzymes known to combat mitochondrial damage are upregulated in response to DOX administration [8-10]. DOX

treatment also increases cardiomyocyte apoptosis rates [11,12]. These data suggest that DOX induces mitochondrial distress, adversely affecting mitochondrial function and viability. Furthermore, DOX incubation with cardiolipin (CL)-deficient cells results in lower levels of lipid peroxidation and protein carbonylation compared to DOX-treated control cells [13]. These observations raise important questions with respect to how DOX treatment relates to mitochondrial dysfunction and whether DOX interactions with CL play a role in DOX-induced cardiotoxicity.

CL is a uniquely structured anionic glycerophospholipid (**Figure 5.1B**) that localizes to the inner mitochondrial membrane [14]. In addition to its structural role in mitochondria, CL is an important component of the electron transport chain (ETC), through its ability to interact with cytochrome c [15,16]. Binding of cytochrome c to CL is specific, stoichiometric, and, under normal physiological conditions, cytochrome c remains anchored to CL molecules [17]. CL has also been shown to be a necessary component for the proper function of Complexes I, III, IV and V of the ETC [18]. These functions ultimately promote efficient aerobic respiration and ATP production.

It is well established that DOX displays strong, preferential binding for CL relative to other phospholipids [19,20]. However, the exact nature of this interaction remains enigmatic and underexplored [21]. Available DOX formulations do not target tumor cells exclusively such that DOX can potentially access cardiac tissue mitochondria and bind to endogenous CL therein. The binding interaction between DOX and CL has been proposed to be a root cause

of DOX-induced cardiotoxicity [19,22,23]. DOX binding to CL is postulated to reduce CL's normal functions, thereby affecting the efficiency of aerobic respiration, in turn reducing ATP production and cardiac muscle contraction. These effects are hypothesized to contribute to DOX-induced cardiotoxicity. However, experimental data supporting this hypothesis has remained elusive.

Encapsulating DOX in liposomes has led to improved targeting, and therefore, decreased off target effects [24,25]. However, individual doses of liposomal DOX (e.g. DOXIL) are limited by mucocutaneous toxicity [26,27]. Substitution of liposomal DOX for free DOX has not led to a reduction in maximal lifetime dosage restrictions [28,29]. Commercially available liposomal DOX formulations also suffer from limited stability and slow drug release [30,31]. While advances in PEGylation have begun to address some of these concerns, liposome stability and slow drug release remain important considerations. Given its DNA intercalation-based mechanism of action, slow release of DOX hampers efforts to use this drug clinically. Despite evidence illustrating that the lipid content of liposomes affects DOX uptake, release rate and cytotoxicity [32], commercially available liposomal formulations of DOX (e.g. DOXIL, Myocet) do not contain CL [30,33].

Aqueous-soluble lipid nanoparticles, termed nanodisks (ND), comprised of CL and apolipoprotein A-I (apoA-I), have been developed and characterized. ND represent a valuable tool that has been used previously to study transmembrane proteins, deliver hydrophobic bioactive compounds and myriad other applications [34,35]. ND are comprised of two essential components: phospholipids that form

a discoidal bilayer, and apolipoproteins that serve as a “scaffold”, stabilizing the bilayer perimeter. ND have proven to be a valuable tool due to their ease of formulation, high replicability, and nanometer-scale size [34-36]. ND comprised solely of CL and apolipoprotein have been formulated, characterized and used as a model membrane to investigate the CL interactome [37-39]. DOX CL ND have previously been formulated and were found to be capable of withstanding dialysis, suggesting a binding interaction. DOX incubated with phosphatidylcholine (PC) ND did not show evidence of a similar binding interaction [38]. Understanding the molecular mechanisms underlying DOX-induced cardiotoxicity, as it relates to mitochondrial damage, has the potential to impact DOX usage, reduce dosage restrictions and lead to development of therapeutic strategies to decrease the severity of DOX-induced cardiotoxicity.

Given the propensity of DOX to bind to CL, it is hypothesized that association of DOX with exogenous CL will limit interaction between DOX and endogenous CL, thereby reducing mitochondrial dysfunction induced as a result of DOX treatment. Free DOX and DOX CL ND were readily taken up by cultured cells localized to the nucleus within 2 h. Cancer cells treated with free DOX and DOX CL ND showed similar reductions in cell viability rates following 72 h incubation. By contrast, liposomal DOX was found to have higher cancer cell viability rates at all but one condition tested. Rat cardiomyocyte cells incubated with DOX CL ND show a significant increase in cell viability compared to cells treated with free DOX. Cardiomyocytes also show increased maximal respiration following DOX CL ND treatment, as compared to cells treated with free DOX.

These data suggest DOX CL ND are a potentially useful DOX formulation, capable of reducing cardiomyocyte apoptosis rates and preventing mitochondrial dysfunction while retaining the anti-cancer properties of DOX.

5.3 Materials and Methods

Nanodisk formulation. ND were formulated as described previously [37]. Briefly, 5 mg tetramyristoyl CL (Avanti Polar Lipids) was dissolved in 200 µL $CHCl_3$:CH_3OH (3:1 v/v) then dried under a stream of N_2 gas. The lipid appeared as a semi-opaque layer equally distributed on the bottom of the glass vial. The samples were stored at −20 °C until use. For ND formulation, 750 µL 20 mM Tris HCl pH 7.4 was added to 5 mg dried lipid. The sample was vortexed, resulting in an opaque aqueous lipid dispersion. Subsequently, 2 mg recombinant human apoA-I in 20 mM Tris HCl was added [40]. The mixture was brought to a final volume of 1250 µL and bath sonicated at 48 °C until the solution cleared (< 10 min). DOX (Cayman Chemical Company) was solubilized in 20 mM Tris HCl buffer as a 10 mM stock, and stored at −20 °C until use.

Fluorescence spectroscopy. To characterize DOX binding to ND, the following samples were prepared in 20 mM Tris HCl buffer, pH 7.4: free DOX (18 µM), CL ND (100 µM), DOX + CL ND (18 µM : 100 µM DOX:CL), PC ND (200 µM) and DOX + PC ND (18 µM : 200 µM DOX:PC). Samples were prepared and allowed to incubate for 30 min at 24 °C before being placed in a quartz cuvette. Samples were then loaded onto a Shimadzu RF-6000 Fluorimeter and the fluorescence

analyzed. Samples were excited at 488 nm and emission measured from 520-700 nm.

Fluorescence Microscopy. To investigate intracellular uptake and distribution of free DOX and DOX CL ND, HepG2 cells were seeded on a glass slide, treated with fibronectin (Sigma) diluted 1:40 in PBS, and allowed to adhere overnight. The following day, free DOX or DOX CL ND were added to a final concentration of 1 µM and incubated for 2 h. Following incubation, samples were fixed with 4% formaldehyde in PBS for 10 min then washed in PBS 3 times. Following fixation, cells were stained with 1 µg/mL 4′,6-diamidino-2-phenylindole (DAPI) for 2 min followed by an additional 2 washes in PBS. Prolong Diamond Antifade Mountant (Thermo-Fisher) was used to prevent photo bleaching. Slides were then examined via BZ-X 700 Keyence Microscope at 40x magnification. Slides were examined using excitation wavelengths from 340-380 nm and 450-490 nm (DAPI and DOX, respectively), while the emission was observed from 435-485 nm and 500-550 nm.

Cell Culture. HepG2 and MCF7 cells were purchased from Bioscience Divisional Services at UC Berkley. HepG2 cells were cultured in Eagle's Minimal Essential Medium (MEM, Caisson Labs) supplemented with 10% FBS (Peak Serum), 50 U/mL penicillin, 50 µg/mL streptomycin, 1:100 dilution Glutamax, 1:100 dilution MEM non-essential amino acids and 1:100 dilution sodium pyruvate. MCF7 cells were cultured in Dulbecco's Modified Eagle Medium (DMEM, Caisson Labs) supplemented with 10% FBS (Peak Serum), 50 U/mL penicillin, 50 µg/mL

streptomycin, 1:100 dilution Glutamax, 1:100 dilution MEM non-essential amino acids and 1:100 dilution sodium pyruvate. H9C2 cells were a generous gift from Dr. Bradley Ferguson (University of Nevada, Reno). Cells were cultured in DMEM media supplemented with 10% FBS (Peak Serum), 50 U/mL penicillin, 50 µg/mL streptomycin, 1:100 dilution Glutamax, and 1:100 dilution sodium pyruvate. Cells were incubated in a humidified incubator with 5% CO_2 at 37 °C. All reagents were purchased from Gibco if not stated otherwise.

Cell Viability Assays. HepG2, MCF7, or H9C2 cells were plated in a 96 well plates at a density of 10,000 cells/well with a final volume of 100 µL media. Cells were allowed to adhere overnight. The following day, samples were treated with the indicated concentrations of Tris buffer pH 7.4, empty CL ND, free DOX, DOX CL ND, or liposomal DOX, to a final volume of 120 µL. Samples were incubated for 72 h or 24 h at 37 °C before addition of CellQuanti Blue (BioAssay Systems) according to manufacturer's protocol. Samples were incubated an additional 2 h then the fluorescence (excitation 590 nm; emission 544 nm) read on a Spectramax Plate Reader.

Mitochondrial Oxygen Consumption Rate Analysis. In order to assess whether association with CL ND reduces DOX-induced mitochondrial dysfunction, oxygen consumption rates (OCR) in H9C2 cardiomyocytes were experimentally determined. H9C2 cardiomyocytes were cultured in 24-well XF24 microplates at a density of 40,000 cells/well. Media volume was kept at 400 µL. Cells were allowed to adhere to the plate for a minimum of 36 h. Following

adherence of cells to the plate, cells were incubated under specified conditions for 4 h. Wells A1 and D6 of the XF24 cell culture microplate were not seeded with cells in order to determine background OCR. A calibration plate was prepared by adding 1 mL calibrant fluid (Seahorse Bioscience) into wells of the plate 24 h prior to conducting the mitochondrial stress assay and incubated at 37 °C in the absence of CO_2. On the day of the assay, the cells were washed with XF Media (Seahorse Bioscience), glucose (4.5 g/L), 1 mM sodium pyruvate, and 1 mM glutamine. OCRs were analyzed at baseline for at least three cycles, after which 1.5 µM oligomycin, 7.5 µM FCCP, and 0.5 µM rotenone/antimycin A were sequentially injected into each well to assess ATP-linked OCR, maximal OCR, and mitochondrially-derived OCR, respectively [41]. In the present study, at the end of each assay, cells in the XF24 cell culture microplate were washed in PBS before being fixed in 4% paraformaldehyde for 10 min and washed sequentially with PBS and 1.25 µg/mL DAPI to stain nuclei. The DAPI-stained nuclei were washed 2 times in PBS for 10 min then visualized and imaged using an Image Express Nano, at a magnification of 20x, adapted from a procedure previously described [42]. Wells were separated into a 12x12 grid and sequentially scanned. The raw OCR values for each parameter were analyzed and normalized to the average number of nuclei per well.

Statistical Analysis. Statistical analysis was performed by one-way or two-way ANOVA followed by Tukey multiple comparison test to compare samples against the buffer treated control as well as against the same DOX concentration across

formulations **(Figures 5.4, 5.5, 5.6, 5.7)**. Statistical tests were performed using GraphPad Prism version 9.0.0 for Windows (GraphPad Software, San Diego, CA).

5.4 Results

Fluorescence and DOX binding to ND. DOX displays a characteristic fluorescence emission spectrum between 520-700 nm (excitation 488 nm). In contrast, both PC ND and CL ND have negligible fluorescence under these conditions (**Figure 5.2**). To determine the specificity of DOX binding to CL, DOX was incubated in buffer alone (20 mM Tris HCl buffer, pH 7.4) or buffer containing PC ND or CL ND. Following 30 min incubation at 22 °C, sample fluorescence spectra were collected. As expected, both CL ND and PC ND alone had negligible fluorescence, whereas DOX in buffer alone gave rise to a fluorescence spectrum with 3 maxima at 559, 594 and 628 nm. When DOX was incubated with PC ND, negligible changes in fluorescence were detected versus free DOX. However, when DOX was incubated with CL ND, a 40% reduction in maximal fluorescence intensity was observed. This loss in fluorescence intensity indicates that DOX interacts with the CL bilayer, likely via intercalation, thereby decreasing accessibility of the DOX ring structure to the exterior environment.

Fluorescence Microscopy and DOX intracellular trafficking. It has previously been documented that DOX has greater affinity for DNA than CL, even when DOX is presented as DOX CL ND [38]. As such, it is worth investigating whether

DOX CL ND retain a similar capacity to enter cancer cells and localize to the nuclei as free DOX. To test this, HepG2 cells were incubated with DOX or DOX CL ND for 2 h. Following incubation, cells were fixed, stained with DAPI and then imaged using fluorescence microscopy (**Figure 5.3**). Both free DOX and DOX CL ND treated samples show a co-localization of DOX fluorescence to the DAPI stained nuclei following this brief incubation. This suggests that DOX entry into the cell is not hampered by its prior association with preformed CL ND and, as a result, DOX retains the capacity to enter cancer cells and bind to nuclear DNA.

Effect of DOX CL ND on cancer cell viability. The ability of DOX CL ND to not only enter cells but to manifest a preference for DNA intercalation suggests DOX CL ND and free DOX possess a similar capacity to reduce cancer cell viability. Both HepG2 hepatocarcinoma and MCF-7 breast cancer cells were incubated with buffer, empty CL ND, free DOX, DOX CL ND or liposomal DOX for 72 h. Following incubation, cell viability was measured. Of interest, there was no statistically significant difference between buffer treated controls and empty CL ND controls in either cancer cell line, suggesting empty CL ND are well tolerated. In HepG2 cells, DOX CL ND were equally effective at reducing cancer cell viability as free DOX at both concentrations while showing a statistically significant reduction in cancer cell viability when compared to liposomal formulations (**Figure 5.4**). In MCF-7 cells, free DOX and DOX CL ND again showed similar reductions in cancer cell viability following incubation. Interestingly, however, incubation with liposomal DOX elicited a similar decrease in cancer cell viability as free DOX and DOX CL ND at the higher concentration

of DOX (5 μM). However, cells treated with the lower concentration of DOX (1 μM) did not elicit a similar reduction, resulting in a statistically significant increase in cancer cell viability (**Figure 5.5**) when compared to other formulations. These data indicate that DOX, when presented as DOX CL ND, possesses growth inhibition properties similar to free DOX, and more robust growth inhibition activity than liposomal DOX.

DOX CL ND and cardiomyocyte cell viability. To assess the effect of DOX formulation on cultured somatic cells, cell viability assays were performed following incubation with different DOX formulations. H9C2 rat cardiomyocytes were incubated with Tris buffer, empty CL ND, free DOX or DOX CL ND at 4 different concentrations followed by 24 h incubation. Subsequently, cell viability assays (**Figure 5.6**) revealed that, at all 4 concentrations tested, a statistically significant increase in cell viability occurred in cells treated with DOX CL ND, as compared those treated with free DOX alone.

DOX CL ND and the mitochondrial oxygen consumption rate of H9C2 cardiomyocytes. Having shown that incubation with DOX CL ND induces less toxicity relative to free DOX, further investigation into the underlying cause was warranted. H9C2 cells were incubated with free DOX or DOX CL ND and subjected to an assessment of OCR test, a proxy of mitochondrial function, via an XF24^{e} Seahorse Analyzer (**Figure 5.7A**). Basal respiration rates did not show a statistically significant difference between samples, either in treated or control cells (**Figure 5.7B**). In contrast, maximal respiration was drastically reduced in

cells treated with free DOX as compared to both buffer and control (empty) ND cells (**Figure 5.7C**). Treatment with free DOX showed a statistically significant reduction in maximal respiration compared to DOX CL ND treated cells, while no difference was noted between DOX CL ND and buffer treated control cells. These data suggest that DOX CL ND reduce mitochondrial dysfunction associated with DOX incubation.

5.5 Discussion

ND technology has been applied as bioactive agent delivery vehicles, miniature bilayers for transmembrane protein structure studies and model membranes to study ligand interactions [35]. Likewise, specialized nanoparticles such as CL ND have been used to study the interaction between calcium and CL that induces a bilayer to non-bilayer transformation [37]. CL ND have also been used to study how the binding interaction between CL and cytochrome c is disrupted by calcium, providing novel insight into the release of cytochrome c from mitochondria during cell mediated apoptosis [39]. Both examples illustrate the utility of CL ND, and how they can serve as a useful model for understanding interactions CL may encounter in mitochondria.

DOX is a fluorescent anthracycline anti-cancer agent that intercalates DNA. This binding reduces the ability of cells to divide, disproportionally affecting rapidly dividing cells. As this mechanism is non-specific, it allows treatment for a wide range of cancers. However, DOX-induced cardiotoxicity remains an

important issue for clinicians and patients utilizing DOX for its anti-cancer properties. Higher DOX doses are more efficacious but, as DOX dose is increased, so too do rates of DOX-induced cardiotoxicity, a potentially lethal side effect [7]. Despite decades of study, the mechanism underlying DOX induced cardiotoxicity remains enigmatic. Modern DOX formulations have not proven to be sufficiently safe to increase dosages of this life saving medication [29].

An important finding regarding DOX is that DOX binds more readily to CL than other phospholipids [20]. A second important finding is that DOX incubation results in mitochondrial dysfunction [44,45]. These two observations have led to the hypothesis that the interaction between DOX and mitochondrial CL induces mitochondrial dysfunction that ultimately presents as DOX-induced cardiotoxicity [19]. There are a variety of mechanisms that may be implicated but, ultimately, this interaction is postulated to affect ATP production. Tissues that are rich in mitochondria (liver, skeletal muscle and cardiac) and utilize large amounts of ATP are more likely to be affected than other tissues. Skeletal muscle tissue, and cardiac tissue in particular, are among the most affected type of tissue for these reasons [11,23]. However, experimental evidence supporting this hypothesis has proven elusive. One increasingly widely used method for studying the effect of DOX incubation on mitochondria is through the use of an XF24^{e} Seahorse Metabolic Bioanalyzer (Agilent Technologies) to study cell culture or tissue samples. This system creates a closed system wherein oxygen consumed by cells seeded to the bottom of tissue culture plates can be measured. This system, in conjunction with a variety of compounds known to induce specific

effects on mitochondrial function (oligomycin, FCCP, rotenone and antimycin A), can be used to assess mitochondrial “health” in cultured cell or tissue preparations. DOX incubation has previously been shown to induce mitochondrial dysfunction, further supporting the concept that cardiotoxicity may be the result of mitochondrial dysfunction [43,44]. If true, analysis of aerobic respiration via Seahorse Analyzer could prove enlightening and a valuable tool for investigating the link between DOX-induced cardiotoxicity and CL or to determine the mitochondrial toxicity and disruption in bioenergetics of other pharmacological compounds (anti-cancer drugs or statins) bound to ND as a drug delivery vehicle [45].

CL ND present an opportunity to study the interaction between DOX and CL in a novel way. It has previously been shown that CL ND retain key characteristics of CL, including an ability to bind DOX [38]. The retention of binding affinity in addition to full aqueous solubility and lack of an enclosed aqueous interior, as opposed to liposomes or vesicles, offer a preferred experimental model to study this important, yet understudied, interaction between DOX and CL.

In the present study, the interaction between DOX and exogenous CL was investigated as a potential method to reduce mitochondrial stress and dysfunction previously observed as a side effect of DOX treatment [43,46]. The binding interaction between DOX and CL ND has previously been characterized and shown to withstand dialysis to a much greater degree than PC ND [38]. However, this work did not further investigate the mechanism of interaction

between DOX and CL ND. Using the native fluorescence of DOX, it was observed that when DOX is incubated with CL ND, a 40% reduction in maximal fluorescence signal intensity results (**Figure 5.2**). This is surprising, as CL ND alone has no fluorescence in this region, and DOX incubated with PC ND does not show this phenomenon. One possible explanation lies with the binding interaction between DOX and CL ND. It has previously been hypothesized that DOX has a two stage binding interaction with CL enriched membranes. Initially, the positive charge on the DOX molecule initiates an electrostatic interaction with the negatively charged phosphate moieties on CL. In the second step, DOX inserts its anthraquinone portion into the bilayer via a hydrophobic interaction, further increasing the stability of the binding interaction [19]. This secondary interaction would decrease accessibility of DOX's aromatic ring structures to the exterior aqueous environment. As a result, this interaction would likely lead to the reduced fluorescence signal observed. This phenomenon has previously been reported in studies utilizing vesicles and liposomes binding to the most common molecular species of CL found in the mitochondria, tetralinoleoyl CL (18:2) [19]. These data suggest that tetramyristoyl (14:0) CL is capable of a similar binding interaction and that this interaction can be replicated in CL ND.

This study set out to determine whether CL ND might serve as a useful delivery vehicle for DOX. Determination of the viability of these nanoparticles required looking into a number of different characteristics. These can be broken down into three main categories: the binding interaction between DOX and CL ND, the ability of DOX CL ND to inhibit cancer cell growth and whether DOX CL

ND show a protective effect as compared to free DOX treatment. The binding interaction has been reported previously and has been shown to be resistant to dialysis [38]. The fluorescence studies presented in **Figure 5.2** further add to this point, suggesting that tetramyristoyl CL ND may behave similarly to TLCL vesicles and liposomes in engaging in a two-step binding interaction consisting of an electrostatic interaction followed by the insertion of DOX's hydrophobic anthraquinone portion into the ND bilayer, although further investigation is warranted.

The ability of DOX CL ND to inhibit cancer cell growth was also investigated and compared to both free DOX and liposomal DOX in two different cancer cells types: HepG2 hepatocarcinoma cells and MCF7 breast cancer cells. These cell lines were chosen as both hepatic and breast cancers are frequently treated by DOX in a clinical setting. DOX CL ND and free DOX reduced cancer cell viability to a similar extent, both performed better than liposomal DOX in all but one condition tested. This suggests that DOX CL ND retain the anti-cancer properties characteristic of DOX.

To determine whether the pre-binding of DOX to exogenous CL has a protective effect against symptoms characteristic of DOX induced cardiotoxicity, effect on both cell viability and mitochondrial function were tested in a rat cardiomyocyte cell line. H9C2 cardiomyocyte cells incubated with DOX CL ND show a statistically significant increase in both cell viability and mitochondrial function, notably maximal respiration, as compared to cells incubated with free DOX. The observed increase in cell viability and maximal mitochondrial

respiration suggest that DOX CL ND do have a protective effect on cardiac cells. The statistically significant protection from DOX toxicity observed in **Figure 5.6** and **Figure 5.7** supports the hypothesis that delivering DOX via DOX CL ND will diminish or prevent DOX-induced cardiotoxicity.

CL ND may prove to be not only an effective delivery vehicle, but could also serve as a model membrane for understanding the underlying relationship between DOX treatment and mitochondrial dysfunction. Further *in vitro* study is warranted in order to better understand not only how DOX enters the mitochondria and binds to endogenous CL, but also the nature of the underlying mechanism relating CL and DOX induced cardiotoxicity. Studies reveal a path to *in vivo* studies of DOX mediated cardiotoxicity, employing DOX CL ND as both delivery vehicle and model system. While studies designed to change the composition of endogenous CL by injecting CL ND into mice were ultimately unsuccessful, it was shown that CL ND are well tolerated in mice [47]. Similar studies utilizing DOX CL ND would be beneficial in determining whether the protection observed in cells occurs in an animal model as well. These studies will clear a way to a better understanding of the underlying mechanisms involved as well as allowing clinicians to utilize this life saving drug to its true potential, saving lives without fear of DOX induced cardiotoxicity.

5.6 References

[1] Weiss RB (1992). The anthracyclines: will we ever find a better doxorubicin? *Seminars in Oncolology*, 19, 670-686.

[2] Shi J, Kantoff PW, Wooster R, Farokhzad OC (2017). Cancer nanomedicine: progress, challenges and opportunities. *Nat Rev Cancer*, 17, 20–37.

[3] Swain SM, Whaley FS, Ewer MS (2003). Congestive heart failure in patients treated with doxorubicin. *Cancer*, 97, 2869–2879.

[4] Takemura G, Fujiwara H (2007). Doxorubicin-induced cardiomyopathy from the cardiotoxic mechanisms to management. *Prog Cardiovasc Dis*, 49, 330–352.

[5] Octavia Y, Tochetti CG, Gabrielson KL, Janssens S, Crijns HJ, Moens AL (2012). Doxorubicin-induced cardiomyopathy: From molecular mechanisms to therapeutic strategies. *J. Mol. Cell Cardiol* 52 1213-1225.

[6] Zhao L, Zhang B (2017). Doxorubicin induces cardiotoxicity through upregulation of death receptors mediated apoptosis in cardiomyocytes. *Sci Rep*, 7:44735, doi: 10.1038/srep44735.

[7] Chatterjee K, Zhang J, Honbo N, Karliner JS (2010). Doxorubicin Cardiomyopathy. *Cardiology*, 115, 155–162.

[8] Gilliam LAA, St. Clair DK (2011). Chemotherapy-induced weakness and fatigue in skeletal muscle: the role of oxidative stress. Antioxidants & Redox Signaling, 15, 2543–2563.

[9] Green PS, Leeuwenburgh C (2002). Mitochondrial dysfunction is an early indicator of doxorubicin-induced apoptosis. *Biochim Biophys Acta*, 1588, 94–101.

[10] Carvalho FS, Burgeiro A, Garcia R, Moreno AJ, Carvalho RA, Oliveira PJ (2013). Doxorubicin-Induced Cardiotoxicity: From Bioenergetic Failure and Cell Death to Cardiomyopathy. *Med Res Rev*, 34, 106–135.

[11] Arola OJ, Saraste A, Pulkki K, Kallajoki M, Parvinem M, Volpio-Pullki LM (2000). Acute doxorubicin cardiotoxicity involves cardiomyocyte apoptosis. *Cancer Res*, 60, 1789-1792.

[12] Kalyanaraman B, Joseph J, Kalivendi S, Wang S, Konorev E, Kotamraju S (2002). Doxorubicin-induced apoptosis: implications in cardiotoxicity. *Mol Cell Biochem*, 234-235, 119-124.

[13] Aryal B, Rao VA (2016). Deficiency in Cardiolipin Reduces Doxorubicin-Induced Oxidative Stress and Mitochondrial Damage in Human B-Lymphocytes. *PLoS One*, 11, doi: 10.1371/journal.pone.0158376

[14] Ikon N, Ryan RO (2017). Cardiolipin and mitochondrial cristae organization. *Biochim Biophys Acta Biomembr*, 1859, 1156–1163.

[15] Mattson MP, Chan SL (2003). Calcium orchestrates apoptosis. *Nat Cell Biol*, 5, 1041–1043.

[16] Brand MD, Nicholls DG (2011). Assessing mitochondrial dysfunction in cells. *Biochem J*, 435, 297-312.

[17] Iverson SL, Orrenius S (2004). The cardiolipin–cytochrome c interaction and the mitochondrial regulation of apoptosis. *Arch Biochem Biophys*, 423, 37–46.

[18] Paradies G, Paradies V, De Benedictis, Ruggiero FM, Petrosillo G (2014). Functional role of cardiolipin in mitochondrial bioenergetics. *Biochim Biophys Acta Bioenerg,* 1837, 408-417.

[19] Parker MA, King V, Howard KP (2001). Nuclear magnetic resonance study of doxorubicin binding to cardiolipin containing magnetically oriented phospholipid bilayers. *Biochim Biophys Acta Biomembr*, 1514, 206–216.

[20] Wolf FA (1991). Binding of doxorubicin to cardiolipin as compared to other anionic Phospholipids-- An evaluation of electrostatic effects. *Biosci Rep,* 11, 275–284.

[21] Clapham DE (2007). Calcium Signaling. *Cell*, 131, 1047–1058.

[22] Rahman A, Joher A, Neefe JR (1986). Immunotoxicity of multiple dosing regimens of free doxorubicin and doxorubicin entrapped in cardiolipin liposomes. *Br J Cancer*, 54, 401–408.

[23] Cheung KG, Cole LK, Xiang B, Chen K, Ma X, Myal Y, Hatch GM, Tong Q, Dolinsky VW (2015). Sirtuin-3 (SIRT3) Protein Attenuates Doxorubicin-induced Oxidative Stress and Improves Mitochondrial Respiration in H9c2 Cardiomyocytes. *J Biol Chem*, 290, 10981–10993.

[24] Daemen T, Regts J, Meesters M, Kate MTT, Bakker-Woudenberg IA, Scherphof GL (1997). Toxicity of doxorubicin entrapped within long-circulating liposomes. *J Control Release*, 44, 1–9.

[25] Rahman AM, Yusuf SW, Ewer MS (2007). Anthracycline-induced cardiotoxicity and the cardiac-sparing effect of liposomal formulation. *Int J Nanomed*, 2, 567-583.

[26] Daemen T, Regts J, Meesters M, Kate MTT, Bakker-Woudenberg IA, Scherphof GL (1997). Toxicity of doxorubicin entrapped within long-circulating liposomes. J Control Release, 44(1), 1–9.

[27] Rahman AM, Yusuf SW, Ewer MS (2007). Anthracycline-induced cardiotoxicity and the cardiac-sparing effect of liposomal formulation. Int J Nanomed, 2(4), 567-583.

[28] “DOXIL Label - FDA.” Federal Drug Agency, May 2007, www.accessdata.fda.gov/drugsatfda_docs/label/2007/050718s029lbl.pdf.

[29] Safra T (2003). Cardiac Safety of Liposomal Anthracyclines. *Oncologist*, 8, 17–24.

[30] Chang H-I, Yeh M-K (2012). Clinical development of liposome based drugs: formulation, characterization, and therapeutic efficacy. *Int J Nanomedicine*, 7, 49-60.

[31] Gabizon A, Shmeeda H, Barenholz Y (2003). Pharmacokinetics of pegylated liposomal Doxorubicin: review of animal and human studies. *Clin Pharmacokinet*, 42, 419-436.

[32] Sakai-Kato K, Nanjo K, Kawanishi T, Okuda H, Goda Y (2015). Effects of lipid composition on the properties of doxorubicin-loaded liposomes. *Ther Deliv*, 6, 785-794.

[33] Bulbake U, Doppalapudi, S, Kommineni N, Khan W (2017). Liposomal Formulations in Clinical Use: An Updated Review. *Pharmaceutics* 9, doi:10.3390/pharmaceutics9020012.

[34] Ryan RO (2010). Nanobiotechnology applications of reconstituted high density lipoprotein. *J Nanobiotechnology*, 8(28), doi: 10.1186/1477-3155-8-28.

[35] Fox CA, Moschetti A, Ryan RO (2021). Reconstituted HDL as a therapeutic delivery device. *Biochim Biophys Acta Mol Cell Biol Lipids,* 1866, epub before publication.

[36] Denisov IG, Sligar SG (2017). Nanodiscs in Membrane Biochemistry and Biophysics. *Chem Rev* 117, 4669–4713.

[37] Fox CA, Ellison P, Ikon N, Ryan RO (2019). Calcium-induced transformation of cardiolipin nanodisks. *Biochim Biophys Acta Biomembr*, 1861, 1030-1036.

[38] Fox CA, Ryan RO (2020). Dye binding assay reveals doxorubicin preference for DNA versus cardiolipin. *Anal Biochem* 594, 113617.

[39] Fox CA, Lethcoe K, Ryan RO (2021). Calcium-induced release of cytochrome c from cardiolipin nanodisks: implications for apoptosis. *Biochim Biophys Acta Biomembr* 1863, epub before publication.

[40] Ryan RO, Forte TM, Oda MN (2003). Optimized bacterial expression of human apolipoprotein A-I. *Protein Expr Purif* 27, 98-103.

[41] Smolina N, Bruton J, Kostareva A, Sejersen T (2017). Assaying Mitochondrial Respiration as an Indicator of Cellular Metabolism and Fitness. Methods Mol Biol, 1601, 79-87.

[42] Banerjee TD, Reihl K, Swain M, Torres M, Dagda RK (2021). Mitochondrial PKA is neuroprotective in a cell culture model of Alzheimer's Disease. Mol Neurobiol, 58, 3071-3083.

[43] Wallace KB, Sardao VA, Oliveira PJ (2020). Mitochondrial Determinants of Doxorubicin-Induced Cardiomyopathy. *Circ Res,* 126, 926-941.

[44] Gorini S, De Angelis A, Berrino L, Malara N, Rosano G, Ferraro E (2018). Chemotherapeutic drugs and mitochondrial dysfunction: Focus on Doxorubicin, Trastuzumab, and Sunitinib. Oxid Med Cell Longev.

[45] Moschetti A, Dagda RK, Ryan RO (2021). Coenzyme Q nanodisks counteract the effect of statins on C2C12 myotubes. Nanomed 37.

[46] Abdullah CS, Alam S, Aishwarya R. *et al.* (2019). Doxorubicin-induced cardiomyopathy associated with inhibition of autophagic degradation process and defects in mitochondrial respiration. *Sci Rep* **9,** 2002.

[47] Ikon N, Hsu FF, Sheare J, Forte TM, Ryan RO (2018). Evaluation of cardiolipin nanodisks as lipid replacement therapy for Barth syndrome. J Biomed Res 32, 107-112.

5.7 Figures and Figure Legends

A

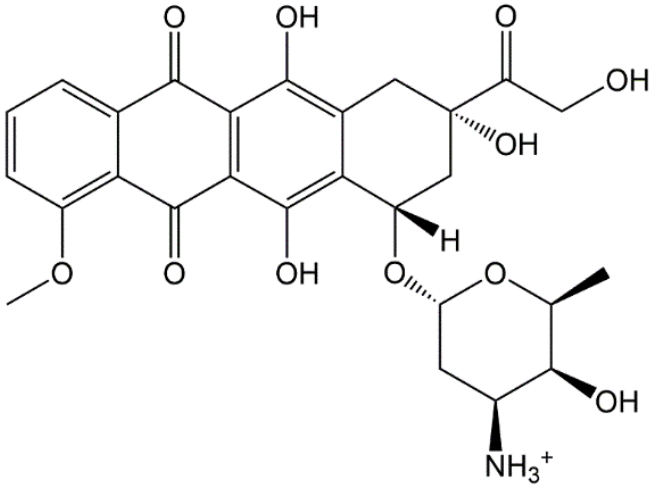

B

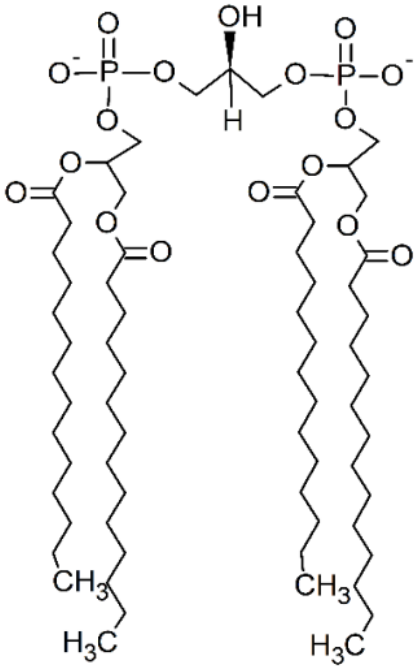

Figure 5.1 Structures of Doxorubicin and Cardiolipin. A) Structure of Doxorubicin (DOX) at physiological pH; B) Structure of tetramyristoyl cardiolipin at physiological pH.

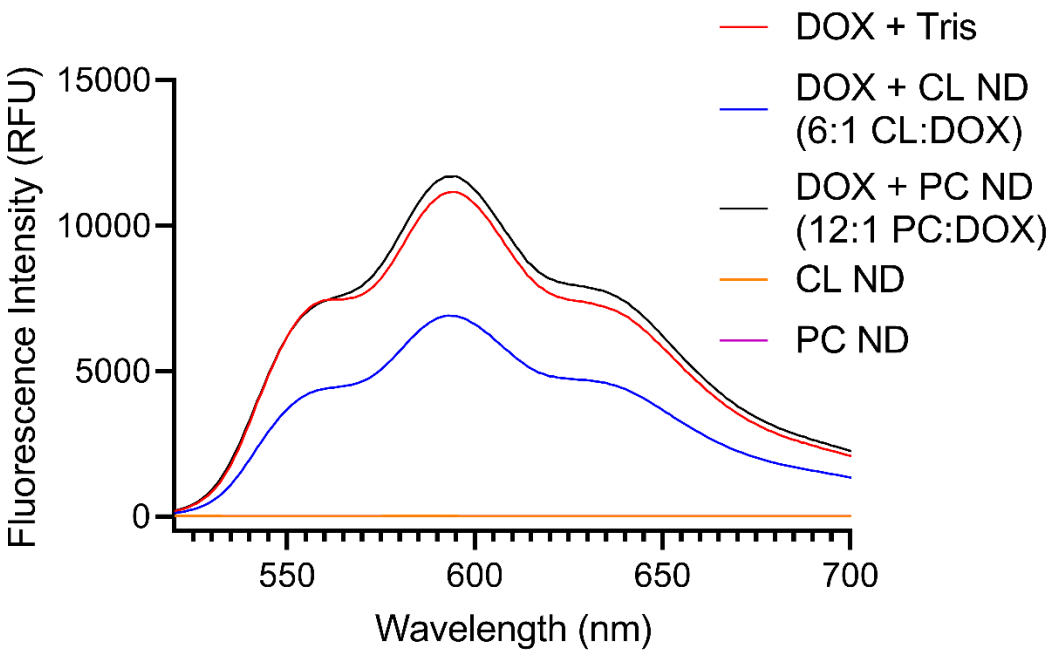

Figure 5.2 Fluorescence spectra of DOX and ND formulations. Fluorescence emission spectra of DOX (18 µM) in 20 mM Tris buffer, pH 7.4, CL ND in buffer, PC ND in buffer, DOX incubated with CL ND (6:1 CL:DOX mol/mol), and DOX incubated with PC ND (12:1 PC:DOX mol/mol). Samples were allowed to incubate for 30 min prior to excitation at 488 nm. Fluorescence was read from 520-700 nm on a Shimadzu RF 6000.

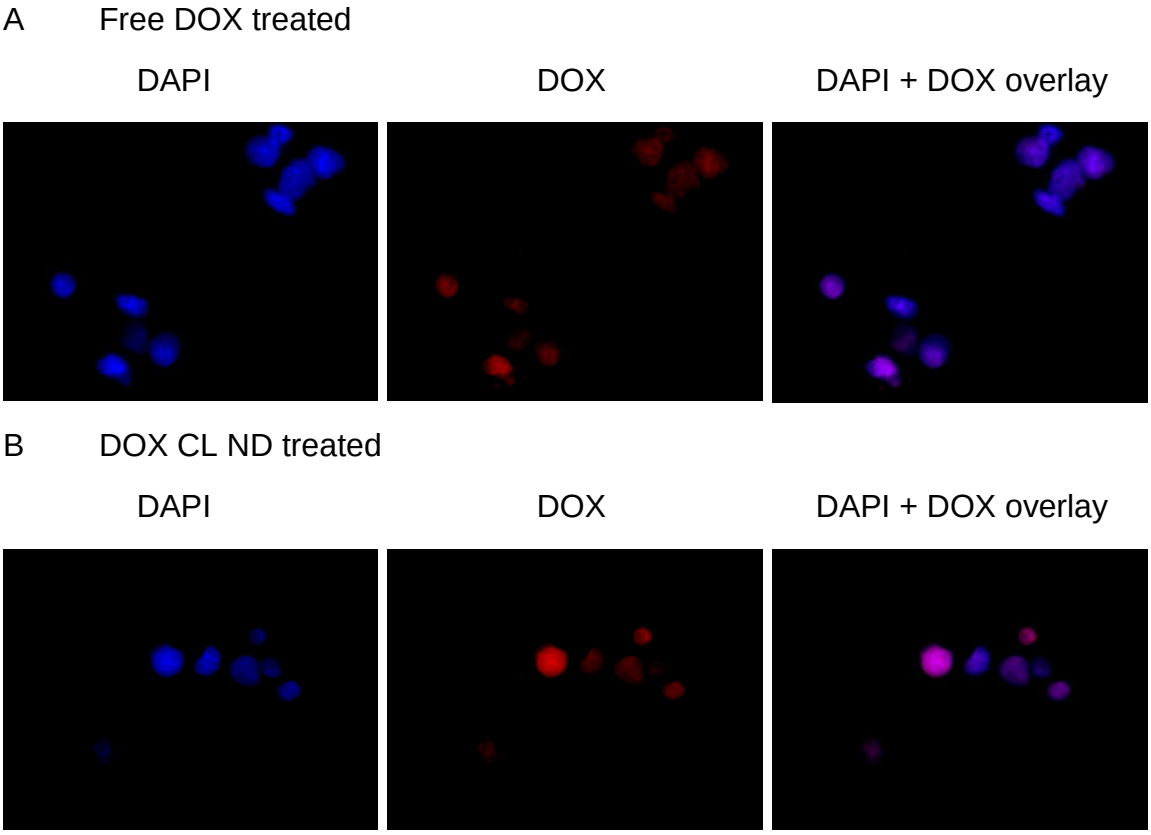

Figure 5.3 Intracellular trafficking of DOX and DOX CL ND into HepG2 cells. HepG2 cells were seeded on a glass slide with A) DOX (1 µM) or B) DOX CL ND (1 µM as DOX) for 2 h. Following incubation, cells were fixed with formaldehyde and stained with DAPI for 2 min. Samples were imaged at an excitation wavelength range from 340-380 nm (left) and 450-490 nm (middle). The emission wavelength was read from 435-485 nm (left) and 500-550 nm (middle). The images taken were then superimposed (right). Images were taken on a Keyence BZ-X 700 Fluorescence Microscope.

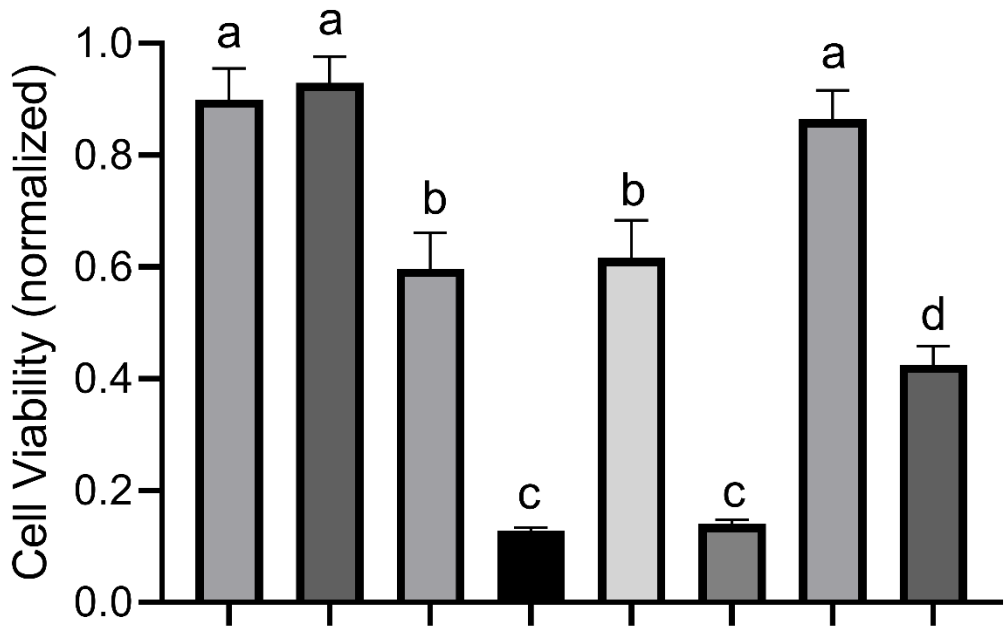

DOX (μM)	0	0	1	5	0	0	0	0
DOX CLND (μM DOX)	0	0	0	0	1	5	0	0
Liposomal DOX (μM DOX)	0	0	0	0	0	0	1	5
Empty ND (μM CL)	0	15	0	0	0	0	0	0

Figure 5.4 Comparison of DOX formulation efficacy on HepG2 cancer cell viability. HepG2 cells were incubated with media supplemented with Tris buffer, CL ND, or indicated concentrations of free DOX, DOX CL ND or liposomal DOX for 72 h. Following incubation, cell viability assays were performed using a fluorimetric assay. Sample fluorescence emission was measured at 590 nm (excitation 544 nm). Significance determined through two-way ANOVA multiple comparison with a Tukey's post hoc test. Values reported are the mean +/- standard error (n = 6 wells, representative of three independent experiments).

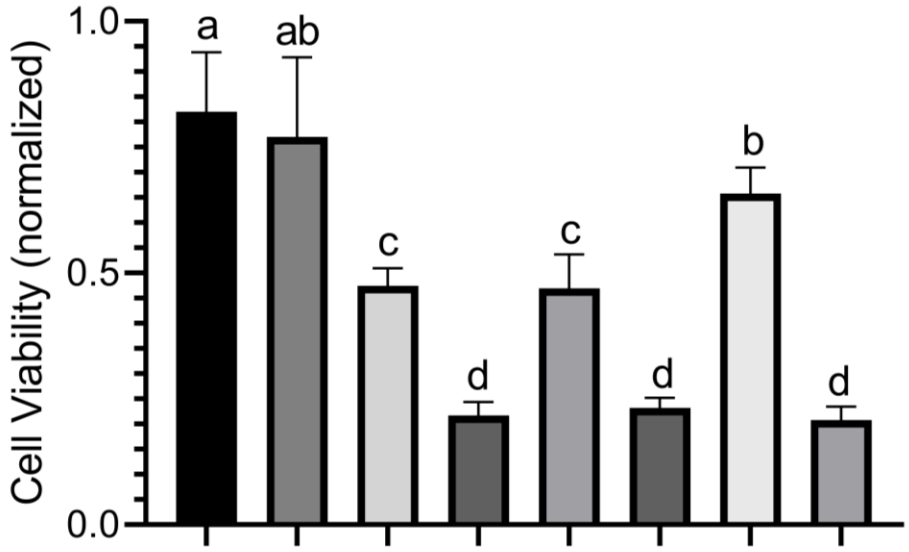

DOX (μM)	0	0	1	5	0	0	0	0
DOX CLND (μM DOX)	0	0	0	0	1	5	0	0
Liposomal DOX (μM DOX)	0	0	0	0	0	0	1	5
Empty ND (μM CL)	0	15	0	0	0	0	0	0

Figure 5.5 Comparison of DOX formulation efficacy on MCF7 cancer cell viability. MCF7 cells were incubated with media supplemented with Tris buffer, CL ND, or indicated concentrations of free DOX, DOX CL ND or liposomal DOX for 72 h. Following incubation, cell viability assays were performed using a fluorimetric assay. Sample fluorescence emission was measured at 590 nm (excitation 544 nm). Significance determined through two-way ANOVA multiple comparison with a Tukey's post hoc test. Values reported are the mean +/- standard error (n = 6 wells, representative of three independent experiments).

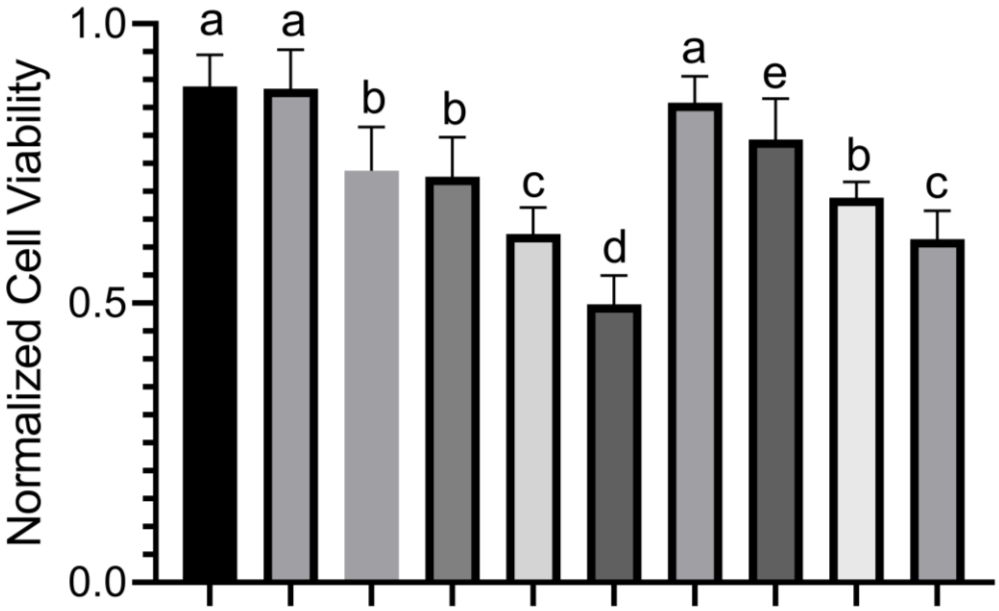

DOX (μM)	0	0	0.25	0.5	1	2	0	0	0	0
DOX CLND (μM DOX)	0	0	0	0	0	0	0.25	0.5	1	2
Empty ND (μM CL)	0	6	0	0	0	0	0	0	0	0

Figure 5.6 Comparison of DOX formulation efficacy on H9C2 cardiomyocyte cell viability. H9C2 cells were incubated with media supplemented with Tris buffer, CL ND, indicated concentrations of free DOX or DOX CL ND for 24 h. Following incubation, cell viability assays were performed using a fluorimetric assay. Sample fluorescence emission was measured at 590 nm (excitation 544 nm). Significance determined through two-way ANOVA multiple comparison with a Tukey's post hoc test. Values reported are the mean +/- standard error (n = 18 wells, result of three independent experiments).

A

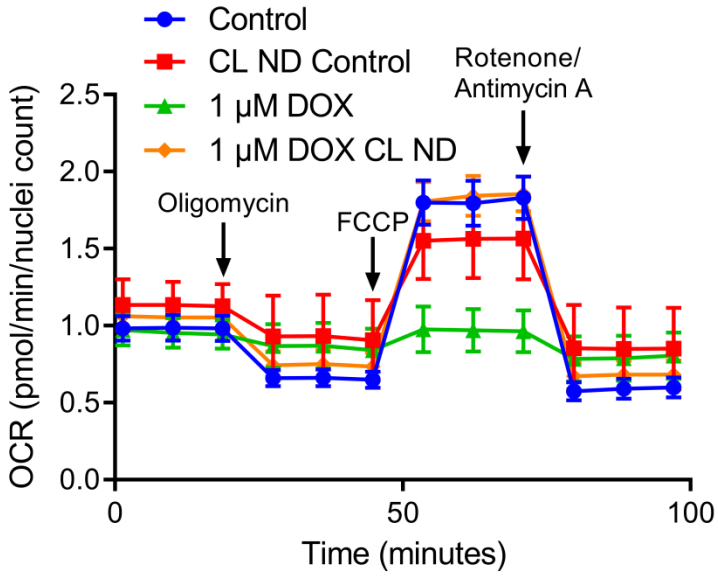

B

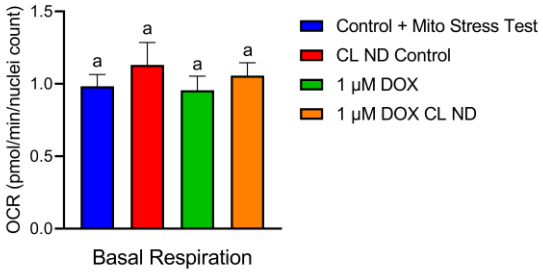

C

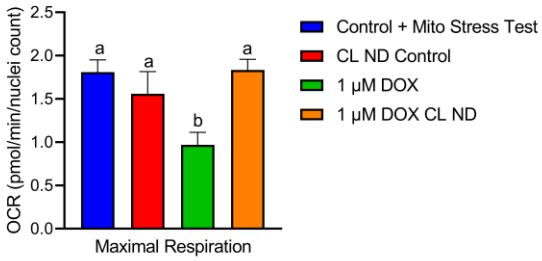

Figure 5.7 Effect of DOX formulation on H9C2 cardiomyocyte oxygen consumption rate (OCR). H9C2 cells were incubated for 4 h in media supplemented with Tris HCl, empty CL ND, free DOX or DOX CL ND. Following incubation, cells were subjected to a mitochondrial stress test assay on a Seahorse XF24 analyzer with intervals of drug additions (1.5 μM Oligomycin, 7.5 μM FCCP, and 0.5 μM Rotenone + Antimycin A). The OCR was measured for each incubation condition and normalized to a nuclei count, as visualized by DAPI stain. A) OCR traces for each incubation condition; B) histogram for mean basal OCR; C) histogram depicting maximal respiration for each treatment condition. Significance determined through one-way ANOVA multiple comparison with a Tukey's post hoc test. Values reported are the mean ± standard error (n = 4 wells, results are indicative of three separate experiments).

Chapter 6

Summary, Conclusions and Future Directions

Portions of this chapter are based on the following manuscripts:

Fox CA, Moschetti A, Ryan RO (2021), Reconstituted HDL as a therapeutic delivery device. Biochim. Biophys. Acta Mol. Cell Biol. Lipids.

Lethcoe K, Fox CA, Ryan RO (2021), Foam fractionation of a recombinant biosurfactant apolipoprotein. J Biotech. *In rev.*

Moschetti A, Fox CA, McGowen S, Ryan RO (2021), Lutein nanodisks protect human retinal pigment epithelial cells from UV light-induced damage. *In prep.*

6.1 Summary of Presented Work

This work presents the formulation of novel cardiolipin nanodisks (CL ND) which were used to test numerous hypotheses regarding the interaction of the mitochondrial phospholipid CL with several of its ligands including calcium, cytochrome c and doxorubicin (DOX) [1-4].

CL studies have historically been conducted using liposomes. An interesting phenomenon was noted wherein liposomes containing CL undergo a bilayer to non-bilayer transformation upon addition of calcium [5,6]. Liposomes with a similar lipid composition in the absence of CL do not undergo this transformation. This phenomenon was replicated and studied using CL ND and the results of these experiments presented in Chapter 2 [1]. As a result of these studies a novel mechanism was proposed wherein the two negatively charged phosphate moieties of CL shift to better bind to the divalent positively charged calcium ion. This shift induces strain on the CL molecule, ultimately forcing the fatty acyl chains to re-orient and push outward, thereby accentuating the overall “cone shape” of the CL molecule. As a result, the ability of calcium bound CL molecules to remain stably incorporated into a planar bilayer is reduced. Once sufficient CL molecules undergo this change, the stabilizing force of the apolipoprotein scaffold is exceeded and the bilayer transitions to a non-bilayer, reverse hexagonal state.

The ability of calcium to induce a bilayer to non-bilayer state has previously been hypothesized to play a role in the release of cytochrome c from CL enriched cristae membranes during cell mediated apoptosis [7,8]. As

presented in Chapter 3, cytochrome c was found to stably bind to CL ND, allowing for investigation into the interaction between cytochrome c and a CL enriched membrane [3]. Surprisingly, cytochrome c CL ND were found to be more susceptible to calcium induced disruption than empty CL ND. When cytochrome c CL ND were treated with sufficient calcium to induce a non-bilayer transformation, it was found that cytochrome c did not fully dissociate from the bilayer and become a soluble component of the supernatant. However, addition of calcium just below the threshold required to induce a non-bilayer disruption resulted in complete dissociation of cytochrome c from the CL bilayer. Pre-incubating CL ND with the same concentration of calcium had a similar effect, wherein the cytochrome c was no longer able to bind to the presumably calcium bound CL bilayer of the ND [3]. These data suggest a competition exists between calcium and cytochrome c for CL binding sites. This project presents the first direct experimental evidence that calcium alone can liberate cytochrome c from a CL enriched membrane, a finding which may have major implications in the study of cell mediated apoptosis.

DOX is an important anti-cancer drug that functions as an intercalation agent, binding to DNA and thereby reducing replication of rapidly dividing cells. This non-specific anti-replication mechanism means DOX is useful against a wide range of cancer types and increasing the drug concentration given to a patient will increase anti-cancer efficacy. However, patients treated with DOX frequently suffer from a series of heart related disorders that have drastically reduced clinicians' ability to use this important medication. These disorders,

collectively termed DOX induced cardiotoxicity, are a major issue facing clinicians. Of significant scientific interest is that despite decades of study, the underlying mechanism remains enigmatic [9,10].

In Chapter 5, CL ND were investigated as a delivery vehicle for DOX and as a model for studying whether CL plays a role in DOX induced mitochondrial dysfunction and cardiotoxicity. DOX CL ND have proven to be a capable DOX delivery vehicle *in vitro* [4]. As presented in Chapter 4, DOX will bind to CL ND, but readily dissociate to preferentially bind DNA [2]. Furthermore, DOX CL ND retain similar anti-cancer efficacy to free DOX while being more effective at killing two different cancer cell lines than liposomal DOX under all but one condition tested. Furthermore, incubation of DOX CL ND with cardiomyocytes leads to a statistically significant increase in both cell viability and maximal mitochondrial respiration as compared to cells incubated with free DOX [4]. In summary, DOX CL ND show a great deal of promise in inhibiting growth of cancer cells while ameliorating cardiomyocyte cell death and mitochondrial dysfunction that is characteristic of DOX treatment. Further studies may lead to a better understanding of the mechanism underlying the relationship between DOX induced cardiotoxicity, CL and mitochondrial dysfunction.

6.2 Future Research Directions

Despite the relatively short history of this technology, ND have been utilized in a number of diverse and interesting delivery strategies. Incorporation of atypical glycerophospholipids, natural lipid adjuvants, synthetic nickel chelating

lipids and cationic lipids are but a few of the myriad ways in which ND technology has been applied [11]. There are, however, still many interesting directions in which to take this technology.

One promising avenue of research is the utilization of alternate apolipoproteins as the scaffold component of the ND. As described in Chapter 3, apolipophorin-III (apoLp-III) was used in lieu of apolipoprotein A-I (apoA-I) as the scaffold protein for production of CL ND [3]. ApoLp-III is a member of the exchangeable apolipoprotein family that originates from insects. This protein shares many similarities with mammalian apolipoproteins, including apoA-I, but, as described in Lethcoe *et al* is significantly easier to produce in vast quantities through a novel bioreactor based expression and purification system [12].

An important aspect of the findings reported by Lethcoe *et al.* is the possibility that other members of the amphipathic exchangeable apolipoprotein class are also amenable to this production method. There are a dozen or more unique exchangeable apolipoproteins, many of which have been investigated in detail [13]. Collectively, members of the apolipoprotein class perform biological functions related to lipoprotein metabolism. Moreover, in the case of apoA-I and apolipoprotein E (apoE), they are known to form rHDL for use in specific medical or biotechnological applications. The fact that the N terminal 22 kDa fragment of human apoE3 [14], when expressed as a pelB fusion protein, is also secreted into the culture media [15], suggests this protein is amenable to foam fractionation [12].

A project is currently underway to test whether this bioreactor based approach is applicable to apoE. This project has the potential to advance the study of Alzheimer's disease and may result in the production of sufficient ApoE to produce ND with the ability to readily pass through the blood brain barrier. Either of these outcomes have the potential to drastically affect the study of their respective fields, advancing scientific knowledge in a way that may ultimately revolutionize patient care.

Another promising avenue of research is the incorporation and solubilization of additional hydrophobic bioactive compounds. Poor oral bioavailability of hydrophobic compounds is an area of great interest in the fields of both nutrition and pharmacology. Incorporation of hydrophobic bioactive compounds into ND results in complete aqueous solubility, which has been shown to assist with cellular uptake [11,16]. This, in turn, allows for better availability of medication, phytochemicals and nutrients for patients and consumers. While a wide variety of compounds have already been investigated, numerous compounds remain to be studied. For example, as described in Moschetti *et al*, lutein, a key phytochemical implicated in age related macular degeneration, has been incorporated and found to be effective at reducing damage to cells treated with UV light [17]. This study lends credence to the idea that there remains a wide variety of novel bioactive compounds that can be incorporated into ND, thereby further increasing the utility of the ND system.

As detailed in Chapter 3, cytochrome c was found to stably bind to CL ND. The addition of calcium under the proper conditions can induce complete

release of this cytochrome c. However, there is some disagreement amongst the scientific community in regards to the nature of the binding interaction between cytochrome c and CL. It is largely agreed that the binding interaction consists of two different interactions. The first is a relatively weak electrostatic interaction. The second is a stronger hydrophobic interaction. However, the relative number of these interactions under normal circumstances remains enigmatic and, thus, is controversial. Interestingly, it has been reported that only at extremely high ratios of cytochrome c to CL (5:1 cyt c:CL) do hydrophobic interactions occur [18]. At lower ratios, such as those presented in Chapter 3, the binding is postulated to be entirely electrostatic. However, all published data was collected through the use of vesicles and liposomes, which differ significantly both in composition and in structure from CL ND. As such, these results are unlikely to translate directly. Additional research into the interaction between cytochrome c and CL ND would be prudent, in order to better understand how the results presented herein translate relative to existing literature.

In addition to binding cytochrome c, CL has been shown to bind at least 60 additional proteins [19]. The interactions between CL and these proteins could prove to be an area of great scientific interest. These proteins are also unlikely to be the only proteins with the capacity to bind CL. CL ND offer a novel tool for binding to, and allowing study into the functions of, this wide array of proteins.

As detailed in Chapters 4 and 5, studies of CL ND as a delivery vehicle for DOX have shown great promise *in vitro*. Further *in vitro* studies are warranted to better understand the underlying mechanism relating DOX induced cardiotoxicity,

CL and mitochondrial dysfunction. Additionally, DOX CL ND have proven to be a potentially powerful delivery vehicle, retaining important anti-cancer properties while reducing toxicity in cardiomyocytes and mitochondria. To further investigate the merits of DOX CL ND as a delivery vehicle, *in vivo* studies utilizing a mouse or rat model are warranted.

6.3 Concluding Remarks

With the completion of the projects described herein, several important mechanisms and a new pharmaceutical delivery vehicle have been investigated, characterized and discussed in detail. These works serve to further our understanding of a number of pathways including cell mediated apoptosis and DOX induced cardiotoxicity. These data contained herein will undoubtedly lead to further discoveries in these realms of study.

6.4 References

[1] Fox CA, Ellison P, Ikon N, Ryan RO (2019). Calcium-induced transformation of cardiolipin nanodisks. *Biochim Biophys Acta Biomembr*, 1861, 1030-1036.

[2] Fox CA, Ryan RO (2020). Dye binding assay reveals doxorubicin preference for DNA versus cardiolipin. *Anal Biochem* 594, 113617.

[3] Fox CA, Lethcoe K, Ryan RO (2021). Calcium-induced release of cytochrome c from cardiolipin nanodisks: implications for apoptosis. *Biochim Biophys Acta Biomembr* 1863, epub before publication.

[4] Fox CA, Romenskaia IR, Dagda RK, Ryan RO (2021). Mitigation of doxorubicin-induced mitochondrial dysfunction by cardiolipin nanodisks. In prep.

[5] Rand RP, Sengupta S (1972) Cardiolipin forms hexagonal structures with divalent cations. Biochim Biophys Acta. 255, 484–492. [PubMed: 4333431]

[6] De Kruijff B, Verkleij AJ, Leunissen-Bijvelt J, Van Echteld CJA, Hille J, Rijnbout H (1982) Further aspects of the calcium dependent polymorphism of bovine heart cardiolipin. Biochim Biophys Acta 693, 1–12. [PubMed: 7150583]

[7] Huang Y, Liu L, Shi C, Huang J, Li G, Electrochemical analysis of the effect of Ca^{2+} on cardiolipin-cytochrome c interaction. Biochim. Biophys. Acta. 1760 (2006) 1827-1830.

[8] Hwang MS, Schwall CT, Pazarentzos E, Datler E, Alder NN, Grimm S, Mitochondrial Ca(2+) influx targets cardiolipin to disintegrate respiratory chain complex II for cell death induction. Cell Death Differ. 21 (2014) 1733-1745.

[9] G. Takemura, H. Fujiwara, Doxorubicin-induced cardiomyopathy from the cardiotoxic mechanisms to management, Prog. Cardiovasc. Dis. 49 (2007) 330–352.

[10] Chatterjee K, Zhang J, Honbo N, Karliner JS (2010). Doxorubicin Cardiomyopathy. *Cardiology*, 115, 155–162.

[11] Fox CA, Moschetti A, Ryan RO (2021), Reconstituted HDL as a therapeutic delivery device. Biochim. Biophys. Acta Mol. Cell Biol. Lipids.

[12] Lethcoe K, Fox CA, Ryan RO (2021), Foam fractionation of a recombinant biosurfactant apolipoprotein. J Biotech. *In rev.*

[13] Mahley RW, Innerarity TL, Rall SC Jr, Weisgraber KH (1984). Plasma

lipoproteins: apolipoprotein structure and function. *J. Lipid Res*. 25, 1277-1294.

[14] Wilson C, Wardell MR, Weisgraber KH, Mahley RW, Agard DA (1991). Three dimensional structure of the LDL receptor-binding domain of human apolipoprotein E. *Science* 252, 1817–182

[15] Fischer NO, Blanchette CD, Segelke BW, Corzett M, Chromy BA, Kuhn EA, Bench G, Hoeprich PD (2010). Isolation, characterization, and stability of discretelysized nanolipoprotein particles assembled with apolipophorin-III. *PLoS One*. 5, e11643.

[16] Ryan RO (2010) Nanobiotechnology applications of reconstituted high density lipoprotein. J. Nanobiotech 8, 8–28.

[17] Moschetti A, Fox CA, McGowen S, Ryan RO (2021), Lutein nanodisks protect human retinal pigment epithelial cells from UV light-induced damage. *In prep.*

[18] Schweitzer-Stenner R (2018). Relating the multi-functionality of cytochrome c to membrane binding and structural conversion. Biophys Rev. 10, 1151-1185.

[19] Planas-Iglesias J, Dwarakanath H, Mohammadyani D, Yanamala N, Kagan VE and Klein-Seetharaman J (2015), Cardiolipin Interactions with Proteins. Biophys J. 109, 1282-1294.